Analysis and Numerical Simulation of Electrokinetic Models for the Evolution of Charged Droplets

Lucía Belén Gamboa Salazar

A thesis submitted in partial fulfillment of the requirements for the degree of Doctor of Philosophy in Mathematics

Advisor

Marco Antonio Fontelos López

September, 2014

A mi familia, amigos y maestros.

Agradecimientos

A Dios, quien me abrió una puerta que yo no había imaginado que traería tanta gente, aprendizajes, experiencias y vivencias tan geniales a mi vida.

A mi familia: mis papás mexicanos y españoles, mi hermano, mi cuñada, mis abuelos, mis primos, tíos, padrinos y madrinas, quienes siempre me han apoyado, motivado, comprendido, aconsejado, cuidado, sostenido y quienes son una parte muy importante y muy valiosa en mi vida, nada que pueda decir o hacer es suficiente para hacer mérito a todo lo que han dado y hecho por mí.

A mis compañeros de despacho de la UAM y del ICMAT, a quienes considero mis amigos para toda la vida, el trato con ustedes ha sido una motivación para mí, el verlos y saberles trabajando y tomarse en serio lo que hacen, verlos transitar de trabajar muy duro a trabajar mejor, de manera más eficiente, disfrutando la ciencia y la vida a pesar de todas las adversidades, los admiro profundamente, quiero poner en práctica lo bueno que he visto en ustedes, lo he hecho en la medida de lo posible en este tiempo. Por otro lado, sin la ayuda, consejos, ideas, sugerencias, intuición y visión de mi director, este trabajo hubiera sido imposible o eternizado. A todos mis amigos entre ellos mi director Marco A. Fontelos, a todos aquellos a quienes ahora llamo amigos y que aparecieron o reaparecieron en esta aventura, afortunadamente son tantos que no puedo poner a todos sin dejarme a alguno, gracias por su paciencia, sinceridad, apoyo, aliento, compañía, comprensión, tolerancia, oraciones, regaños, confrontaciones, inconformidades, juegos, bromas, risas y carcajadas, por las comidas, los cafés, las cañas, tequilas y licores exóticos, los helados, los bailes, por su hombro para llorar, por los tacos, su escucha atenta, su mano amiga, sus abrazos fuertes y llenos de aceptación, por todo el amor que me dieron sin que yo tuviera que hacer algo en particular por merecerlo, gracias! ha sido un descanso y una dicha saberme amada sólo porque sí, confío haber aprendido de ustedes a hacer lo mismo y hacerlo sentir. Los tengo y me tienen.

A los mexicanos, porque gracias al dinero de sus impuestos he tenido la oportunidad de llegar donde estoy, espero haberlo usado con responsabilidad e integridad.

A los maestros de las escuelas rurales en las que tuve la oportunidad de iniciar mis estudios en Sinanché y Dzidzantún, a los de la Universidad Autónoma de Yucatán, a los de la Universidad Nacional Autónoma de México Unidad Cuernavaca, del Instituto Politécnico Nacional Unidad Azcapotzalco, a la gente del ICMAT, de la Universidad Autónoma de Madrid, del Centro de Supercomputación de Galicia, de la Universidad Complutense de Madrid, de la Universidad Politécnica de Madrid, del Instituto Isaac Newton de Cambridge y a la gente de todas las demás instituciones que han sido parte de mi formación de manera directa o indirecta. Gracias por haber compartido conmigo lo que tienen, haré lo mismo.

Contents

Prefacio

El propósito de esta tesis es el desarrollo de herramientas para el estudio de algunos problemas en la intersección entre la microfluídica y electrocinética. En esta introducción ofrecemos una visión general de estas áreas e introducimos el problema específico que vamos a estar tratando: la evolución de gotas cargadas de soluciones iónicas.

Motivación

Las gotas electrificadas están presentes en las nubes de tormenta [20], así como en aplicaciones tecnológicas como electrospray [8] (utilizado, por ejemplo, para producir pequeñas muestras de soluciones iónicas adecuadas para espectrometría, una aplicación que se mereció el Premio Nobel de 2002 en Química por J. Fenn), microencapsulación [48], impresión de chorro de tinta [53], Propulsión por Emisión de Campo Eléctrico (FEEP por sus siglas en inglés) [68], papel electrónico [40], chips microfluídicos [21], [18], [29], [65], etc.

Figure 1: Papel electrónico

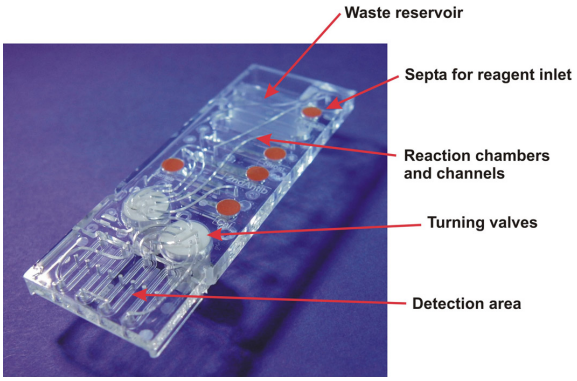

Figure 2: Lab-on-a-chip

A fin de traducir los conceptos a dispositivos prácticos, tenemos que aprender a controlar fluidos con gran precisión y velocidad a veces a escalas muy pequeñas. De las gotas cargadas de líquido, se sabe que se vuelven inestables cuando se cargan más allá de un número llamado límite de Rayleigh y después se desarrollan singularidades (cf. [6], [7] y [20] para resultados experimentales y [26], [12] para simulaciones numéricas). Cuando el fluido es un conductor perfecto y se modela bajo aproximación de Stokes, se demostró que se desarrollan puntas cónicas en tiempo finito (ver [26], [12]). En observaciones experimentales, se producen chorros muy rápidos y finos a partir de las puntas cónicas (ver figuras en 3). Este es un

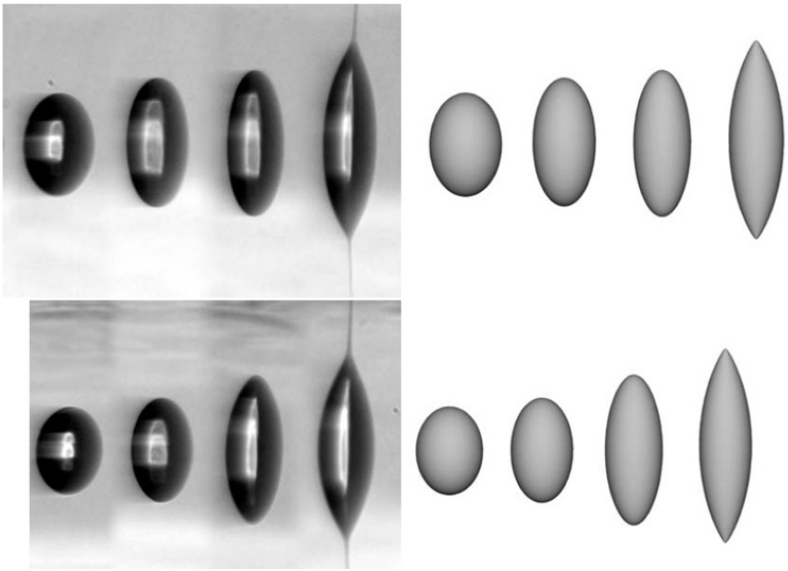

Figure 3: Formación de jets de Rayleigh bajo la acción de un campo eléctrico externo de [7] y comparación con las simulación numérica en [26]

hecho que no puede ser reproducido en [26], [12] bajo el supuesto de Stokes y conductores perfectos. Para fluidos perfectos, se ha informado de chorros recientemente en [34]. Sin embargo, para gotas muy pequeñas (del orden de los 100 μm o inferior), el número de Reynolds puede ser muy pequeño (del orden de 10^{-4} o inferior), por lo que parece necesario investigar la formación de chorros bajo aproximación de Stokes. Nuestra hipótesis es que la conductividad eléctrica finita y la presencia de capas de Debye en soluciones electrolíticas son las que inducen la producción de chorros de Rayleigh. La formación de chorros de puntas cónicas bajo la acción de campos eléctricos se encuentra en el corazón de algunas de las aplicaciones mencionadas arriba: el electrospray se origina a partir de la desintegración de los jets de Rayleigh en gotas, la fuerza de propulsión de los propulsores tienen lugar como una reacción a los chorros de Rayleigh y la microencapsulación tiene lugar cuando dos chorros coaxiales de Rayleigh se rompen en gotas (con el fluido interno encapsulado por el fluido exterior).

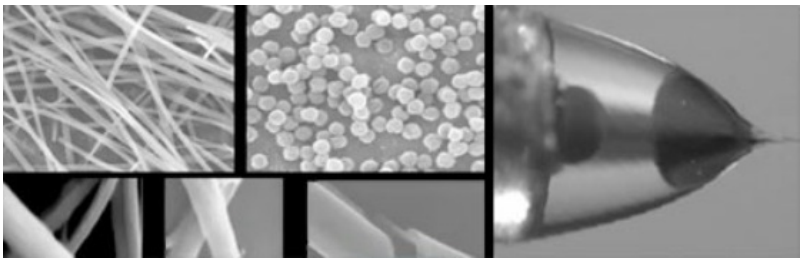

Figure 4: Microencapsulación de un fluido interno por uno externo

Una visión general de la microfluídica y electrocinética

Primero vamos a echar un vistazo sobre los contextos más generales a las que nuestro problema puede estar relacionado. En primer lugar vamos a dar una rápida visión general de la microfluídica (véase [65], [35] para una introducción general) que produce hoy en día miles de publicaciones científicas y patentes cada año y representa un negocio de billones de dólares en la electrónica y sectores médicos. Entonces, vamos a considerar más específicamente el mecanismo para manipular fluidos a pequeña escala: el uso de campos eléctricos y la respuesta del flujo electrocinético a ellos.

Microfluídica

Una rica variedad de sistemas de microfluidos han surgido en el mundo natural a través de millones de años de evolución y la selección natural (véase [2], [16], [52]). Sin embargo, la historia de la microfluídica como un área de la actividad humana se puede medir en décadas. Por ello no es de extrañar que dispositivos prácticos de microfluidos sean relativamente pocos, muchas ideas, como "Lab on a chip" exista sobre todo en concepto y el más útil de los dispositivos de microfluidos está probablemente aún por ser concebido. La microfluídica se refiere a dispositivos y métodos para controlar y manipular flujos de fluidos con una longitud de escala de menos de un milímetro. Los estudios de tales fenómenos relacionados con fluidos han sido durante mucho tiempo parte de la componente mecánica de fluidos de la ciencia coloidal [60] y biología vegetal [17] y viene en muchas características clásicas de la dinámica de los flujos viscosos (por ejemplo, [39], [5],). Sin embargo, el tema ha recibido una enorme atención reciente debido a la disponibilidad de métodos para la fabricación individual y configuraciones de flujo integrados con escalas de longitud del orden de decenas y cientos de micras y más pequeña (por ejemplo, [42], [64], [66]), y rápidos avances en la biología y la biotecnología para manipulaciones en la escala de longitud celular (y más pequeña) y la capacidad de detectar pequeñas cantidades y manipular volúmenes muy pequeños (típicamente menos de 1 microlitro) ofrece ventajas ([70], [44], [9]), también la búsqueda de dispositivos portátiles económicos capaces de realizar tareas analíticas simples, y el potencial uso de microsistemas de gotas cargadas para realizar estudios fundamentales de física, química y procesos biológicos. Esta tendencia se mantiene; además, el término nanofluídica hace hincapié en el deseo de manipular fluídos a la escala de las cadenas de ADN, otros biopolímeros, y proteínas grandes. Flujos de microfluidos son fácilmente manipulados utilizando muchos tipos de campos externos (presión, eléctricidad, magnétismo, capilaridad, y así). Como las dimensiones se reducen, la importancia relativa de las fuerzas de superficie con respecto a las de volumen aumenta. Tales manipulaciones de flujo pueden lograrse ya sea por fuerzas aplicadas macroscópicamente, por ejemplo, en la apropiada entrada y salida, o se pueden generar a nivel local dentro del microcanal por componentes integrados. La tabla 1 de [65] resume las fuerzas impulsoras mencionadas con frecuencia para controlar microflujos.

Alternativamente, electrocinética ahora es estudiado en una variedad de formas para controlar microflujos. Electro-ósmosis, donde el fluido se mueve en relación a fronteras cargadas estacionarias; dielectrofóresis, que se mueve de una interfaz (a menudo una partícula) en un gradiente de campo eléctrico; y electrohumectación, donde el campo eléctrico modifica

Fuerza impulsora	Subcategorización
Gradiente de Presión ∇p	
Efectos de capilaridad	Tension superficial γ
	Térmica
	Eléctrical (electrocapilaridad)
	Gradientes de tensión superficial $\nabla\gamma$
	Química
	Térmica
	Eléctrica
	Optica
Campos Eléctricos **E**	DC electro-osmosis
	AC electro-osmosis
	Dielectrofóresis
Campo Magnetico/Fuerzas de Lorentz	Agitación magnetohydrodynamica
Rotación	Fuerzas Centrífugas
Sonido	Transmisión acústica

Table 1: Fuerzas y campos externos con los cuales manipular flujos en configuraciones de microfluidos. También es posible utilizar medios externos para manipular partículas inmersas en los flujos, como en electrofóresis o el uso de fuerzas magnéticas [3]

propiedades humectantes, todos han sido explotados. Se pueden considerar campos AC y CC, y la respuesta del sistema a continuación depende de la frecuencia y la amplitud del campo.

Otros medios pueden ser utilizados para controlar los flujos. En particular, campos externos pueden usarse para inducir movimiento de los objetos incrustados en el, o las paredes del canal de fluido pueden estar distorsionados sistemáticamente: los campos magnéticos pueden influir en los flujos directamente o manipular partículas magnéticas dispersas, campos de sonido pueden producir movimientos por transmisiones acústicas, la deformación cíclica de una pared puede inducir bombeo peristáltico, etc. Para cada forma de conducir movimiento de fluido, las características de la superficie del dispositivo también pueden ser explotada para proporcionar control adicional. Por ejemplo, las características geométricas, químicas y mecánicas del canal y la red de canales se puede alterar o que cumpla con algún patrón, como se resume en la tabla 2 de [65].

Electrocinética

La electrocinética se refiere a los efectos mecánicos que surgen debido al movimiento de iones en líquidos. El fluido que trabaja en los sistemas de microfluidos es normalmente agua que contienen iones de ambos signos, debido a las moléculas disociadas de agua u otros componentes iónicos: ácidos, sales, y moléculas con grupos cargados disociables. Normalmente, un elemento de volumen de un fluido considerado infinitesimal desde el punto de vista continuo todavía contiene un número suficientemente grande de iones de uno u otro signo para que

Geometría	Características Químicas	Propiedades mecánicas
Conectividad de la red	Mojabilidad	Materiales duros
Sección transversal del canal y curvatura	Carga superficial	Materiales elásticos
Topografía de la superficie	Afinidad Química	Geles
Porosidad (e.g., en lechos de relleno)	Sensibilidad de Ph/Fuerza iónica	Materiales porosos

Table 2: Las consideraciones de diseño para el control de flujo y transporte en un canal de microfluidos puede incluir la influencia de la geometría, la química, y características mecánicas. Además, los electrodos, la actuación de calentadores piezoeléctricos, etc se puede incrustar en las fronteras del canal.

las fluctuaciones estadísticas no sean importantes y para que el elemento de fluido sea considerado con carga neutra. Por lo tanto, la transferencia neta algebraica de impulso debido a cualquier campo eléctrico ambiental también es cero (a pesar de que una corriente eléctrica distinta de cero pueda existir en el líquido debido al movimiento ordenado de estos iones). Surgen efectos electrocinéticos cuando este balance de cargas positivas y cargas negativas se altera debido a factores externos. Por ejemplo, en el interfase de agua de sílice, la sílice hidratada a menudo deprotona resultando en una carga superficial neta negativa fija sobre la superficie de la sílice. Estas cargas fijas atraen una capa de iones de signo contrario (y repelen los iones del mismo signo) lo que resulta en la creación de una capa de fluido con una carga neta positiva junto a la interfaz. Efectos similares se presentan en la superficie de las grandes macromoléculas, partículas coloidales o micelas surfactantes.

Vamos a describir a continuación algunos de los efectos electrocinéticos más relevantes desde el punto de vista de la aplicaciones: electroósmosis, electrofóresis, dielectrofóresis y electrowetting.

Electroósmosis. Cuando un electrolito es adyacente a una superficie, el estado químico de la superficie es generalmente alterado, ya sea por ionización de grupos superficiales de enlaces covalentes o por absorción de iones. El efecto neto es que la superficie hereda una carga mientras son liberados contraiones en el líquido. En el equilibrio, un balance entre las interacciones electrostáticas y la agitación térmica se establece en una capa delgada cerca de la sólida (la llamada capa de Debye, que será discutida profusamente en esta tesis). Cuando un campo eléctrico se aplica a lo largo de un canal, una corriente conductora y el correspondiente campo local $\mathbf{E}$ se establecen a través del líquido. Típicamente, la mayor parte del líquido permanece eléctricamente neutro y por lo tanto no actúa sobre él una fuerza neta. Por el contrario, en la capa de Debye hay una densidad de carga eléctrica neta, por lo que el campo eléctrico local que es tangente a la superficie del canal genera una body force sobre el fluido y por lo tanto induce una fuerza de cizalla y un flujo (el flujo electroosmótico) en el interior del canal. Por lo tanto, una fluido neutral se pone en movimiento debido al desequilibrio local en la capa de Debye.

Electrofóresis. La electrofóresis se refiere al transporte de pequeños objetos cargados en un fluido debido a un campo eléctrico aplicado. Un cuerpo sólido rodeado por una solución iónica presenta una capa de Debye, que es, en general, no uniforme. La distribución de carga en la capa cambia a lo largo de la superficie del cuerpo. Cuando se establece un

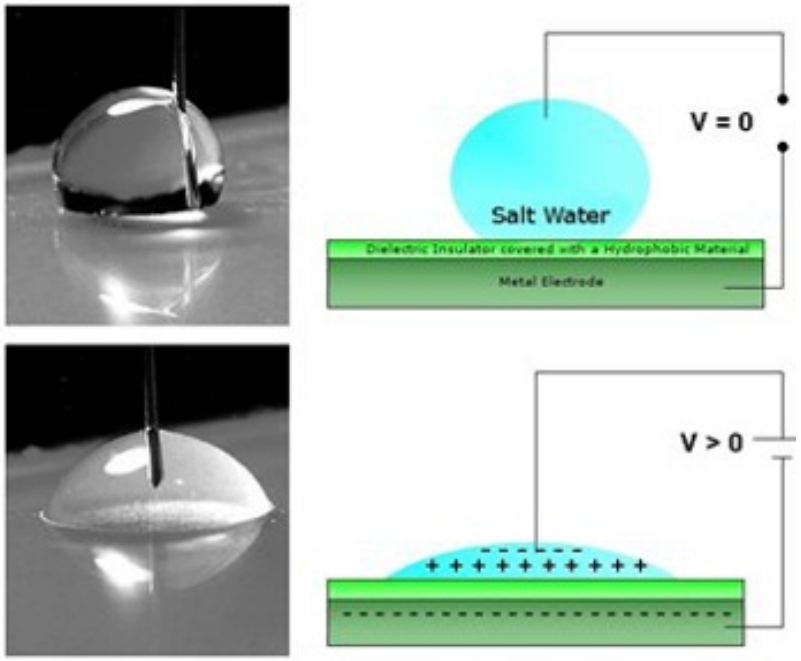

Figure 5: El fenómeno de electrowetting básico

campo eléctrico uniforme, la fuerza originada en diferentes sectores de la capa de Debye podrían ser no uniformes, de modo que aparece una fuerza neta capaz de mover el cuerpo. Muchas macromoléculas contienen grupos de carga disociables en su superficie, y por lo tanto, adquieren espontáneamente una carga en solución acuosa. Por lo tanto, se mueven en respuesta a un campo eléctrico aplicado, y este movimiento es la base para la separación de macromoléculas de solución utilizando estas técnicas de bioanálisis como electrofóresis capilar (EC), electroforesis en gel (SGE por sus siglas en inglés) y el electroenfoque (IEF por sus siglas en inglés), en particular en los procesos de secuenciación de ADN.

Dielectrofóresis. Las partículas que están sin carga pero polarizables experimentan una fuerza en un campo eléctrico no uniforme, el movimiento resultante es conocido como di-electrofóresis. En la dielectrofóresis a diferencia de la electrofóresis, el efecto no desaparece si el campo eléctrico constante se sustituye por uno oscilante. Por lo tanto, la fuerza dielectroforética se puede ajustar con precisión por ajuste de la frecuencia.

Electrowetting. Electrowetting es esencialmente el fenómeno por el cual un campo eléctrico puede modificar el comportamiento de humectación de una gota en contacto con un electrodo aislado (véase la figura para un dibujo del experimento más simple de electrowetting).

Cuando se aplica un voltaje entre una gota eléctricamente conductora y un sustrato hidrófobo o parcialmente humectable, el ángulo de contacto aparente se reduce y la gota comienza a extenderse. Este efecto ha sido descubierto por Lippmann hace más de un siglo [47]. Además de estas cuestiones fundamentales de la investigación básica, el fenómeno de electrowetting es de gran interés para aplicaciones tecnológicas relacionadas con la microfluídica, de manera más precisa, la posibilidad de manipular el movimiento y la forma de pequeñas cantidades de líquido. Una ventaja particular en comparación con otros métodos

estudiados recientemente es una mayor flexibilidad de electrowetting, no son necesarias válvulas, bombas o incluso canales fijos.

Ejemplos importantes de las aplicaciones tecnológicas son filtros ópticos pixelados [57], lentes adaptativos [45], [11], y recubrimiento de páneles [13]. Del mismo modo, displays de cambio rápido -patentado por Philips recientemente (vea también [**?**]) -toman ventaja de la observación de que films estables de aceite de color intercalados entre agua y aisladores hidrofóbicos inmediatamente se contraen en gotas cuando se aplica un campo eléctrico externo.

Modelación matemática de Electrohidrodinámica

En esta sección presentamos los modelos generales de fenómenos electrocinética en los medios fluidos (o electrohidrodinámica). Necesitan combinar ecuaciones generales para el movimiento de los fluidos (Navier-Stokes o, cuando el número de Reynolds es pequeño, el sistema de Stokes) con las ecuaciones para el movimiento de cargas eléctricas en un fluido (sistema de Nernst-Planck) y la ecuación satisfecha por el campo eléctrico en presencia de cargas eléctricas (ecuación de Poisson). Una descripción general junto con varias aproximaciones puede encontrarse en [62].

En primer lugar, los fenómenos que nos interesan, tienen lugar en un medio líquido. Por lo tanto, es conveniente introducir un campo vectorial para la velocidad $\vec{v}$ junto con un campo de presión. El fluido, normalmente un líquido viscoso y uno incompresible como el agua o glicerina, se puede modelar mediante Sistema de Navier-Stokes:

$$\rho_0 \left(\partial_t \mathbf{v} + \mathbf{v} \cdot \nabla \mathbf{v}\right) = -\nabla p + \mu \Delta \mathbf{v} + \mathbf{F}_e \tag{1}$$

$$\nabla \cdot \mathbf{v} = 0 \tag{2}$$

que expresa el equilibrio de momento y masa. ρ_0 y μ son la densidad y la viscosidad del fluido, respectivamente. La ecuación (1) se sigue de la segunda ley de Newton bajo body forces externas $\vec{F_e}$ que actúan por unidad de volumen (por ejemplo, gravedad, electricidad, fuerza electromagnética o fuerza centrífuga). En nuestro caso, vamos a considerar sólo las fuerzas de naturaleza eléctrica. Por lo tanto, $\mathbf{F}_e$ se puede expresar como la divergencia del tensor de esfuerzos de Maxwell

$$T_{M,ij} = \varepsilon_0 \varepsilon_r \left(E_i E_j - \frac{1}{2} \delta_{ij} \left|\mathbf{E}\right|^2 \right) \tag{3}$$

donde $\varepsilon_0 \varepsilon_r$ es la permitividad dieléctrica del medio y E_j representa el componente j del campo eléctrico. De ahí que

$$F_{e,i} = \left(T_{M,ij}\right)_i$$

Por otro lado, el campo eléctrico satisface las ecuaciones de Maxwell (cf. [37], [43]). Si despreciamos los efectos magnéticos (las velocidades del fluido y de las cargas son mucho

menores que la velocidad de la luz), el campo eléctrico es $\vec{E} = -\nabla V$ donde V es el potencial eléctrico. El potencial satisface entonces la ecuación de Poisson:

$$\nabla \cdot (\varepsilon_0 \varepsilon_r \nabla V) = -\rho \tag{4}$$

donde ρ representa la densidad de carga eléctrica.

Finalmente, las cargas eléctricas se mueven en respuesta a campos eléctricos, agitación térmica (difusión) y el campo de velocidades del fluido. Esto se expresa en la ecuación

$$\mathbf{j}_i = \mu_i e z_i n_i \mathbf{E} - D_i \nabla n_i + n_i \mathbf{v}, \tag{5}$$

que expresa el flujo neto de las especies cargadas i como la suma de tres flujos: el flujo convectivo $n_i\mathbf{v}$ debido al campo de velocidades $\mathbf{v}$ del fluido, el flujo difusivo $D_i \nabla n_i$, y el flujo electrocinético $\mu_i e z_i n_i \mathbf{E}$ debido al campo eléctrico. μ_i es la movilidad de los iones: la velocidad adquirida por el ion cuando actúa sobre una unidad de fuerza externa. D_i es el coeficiente de difusión de la especie i^{th}. La relación de Einstein establece que $\frac{D_i}{mu_i} = k_b T$, donde k_b es la constante de Boltzmann y T la temperatura absoluta. En general, podemos tener muchos tipos diferentes de especies cargadas: electrones, iones de diverso tipo y valencia(Na^+, Cl^-, K^+, Ca^{2+}, etc). Por lo tanto,

$$\rho(\mathbf{x}, t) = \sum_{i=0}^{N-1} e z_i n_i. \tag{6}$$

donde N es el número de especies, e es la carga del electrón, n_i es la concentración de la especie i, y z_i es su valencia. La continuidad de cada una de las especies cargadas conduce al sistema de Nernst-Planck:

$$\frac{\partial n_i}{\partial t} + \nabla \cdot \mathbf{j}_i = 0, \tag{7}$$

El sistema (1)-(7) contiene un gran número de ecuaciones y parámetros físicos. Su resolución representa entonces un enorme desafío teórico y computacional. En esta tesis, utilizaremos la pequeñez de algunas magnitudes adimensionales en el contexto de microfluidos con el fin de simplificar el sistema y que sea adecuado para el análisis y la simulación. En particular, el número de Reynolds será pequeño, por lo que vamos a aproximar el sistema de Navier-Stokes por el sistema de Stokes:

$$-\nabla p + \mu \Delta \mathbf{v} + \mathbf{F}_e = 0 \tag{8}$$

$$\nabla \cdot \mathbf{v} = 0 \tag{9}$$

Una segunda simplificación producirá a partir del sistema de Nernst-Planck combinado con Poisson, una ecuación diferencial parcial no lineal conocida como Ecuación de Poisson-Boltzmann.

Descripción de la disertación

Este trabajo se divide en tres partes. En la primera parte, que corresponde al Capítulo 2, comenzamos a estudiar las condiciones físicas que nos conducen más tarde un modelo para el potencial eléctrico dentro de la gotita, la ecuación de Poisson-Bolztmann ya mencionada.

En este capítulo se estudian las soluciones a la ecuación de Poisson-Boltzmann para soluciones electrolíticas en un dominio Ω, rodeado por un medio dieléctrico no cargado. Establecemos existencia, unicidad y regularidad de soluciones y estudiamos en detalle su comportamiento asintótico cerca de $\partial\Omega$ cuando una longitud característica, la llamada longitud de Debye, es suficientemente pequeña. Esta es una doble capa con un espesor que cambia de punto a punto a lo largo de $\partial\Omega$ en función de la derivada normal de una función armónica fuera de Ω y la curvatura media de $\partial\Omega$. También proporcionamos evidencia numérica de los resultados basados en una aproximación de Runge-Kutta y de elementos finitos para el problema. En la segunda parte, el capítulo 3, acoplamos la electrocinética descrito por la aproximación de Poisson-Boltzmann con el movimiento del fluídos descrita por las ecuaciones de Navier-Stokes (véase [46], [19]). Nosotros hallamos que el término de fuerza en la formulación de Stokes dado por el potencial descrito por la ecuación de Poisson-Boltzmann, se convierte en una condición de frontera. Usando este modelo establecimos una formulación integral formulación, el cual discretizado adecuadamente conduce a una formulación de Elementos de Contorno para dos tipos de ecuaciones diferenciales: Dirichlet para la condición de frontera relacionada con el potencial y Stokes con término de fuerza cero para la velocidad en la frontera. Una de nuestras principales motivaciones es describir los llamados Chorros de Rayleigh. Nuestra hipótesis es que es que la conductividad eléctrica finita y la presencia de capas de Debye en las soluciones electrolíticas inducen la producción de chorros de Rayleigh. En el último capítulo, el Capítulo 4, utilizamos armónicos esféricos y armónicos esféricos vectoriales para el estudio de la estabilidad de una gota viscosa llena con una solución electrolítica diluida usando un linealización de la ecuación de Poisson-Boltzmann conocida como linealización Debye-Hückel.

Conclusiones y trabajo futuro

En el capítulo 2 hemos deducido fórmulas asintóticas para la distribución de carga de una solución iónica cerca de su interfaz con un medio externo. Nuestras principales hipótesis fueron: 1) todas las especies iónicas están en equilibrio dinámico y 2) un parámetro adimensional ε que es inversamente proporcional a las movilidades de iones se muy pequeña. Nuestros expansiones contienen correcciones debidas a la geometría de la interfaz y por lo tanto describen posibles acumulaciones de carga en ciertas regiones de la interfaz en función de su curvatura.

Nuestra hipótesis es que la conductividad finita implica que las cargas eléctricas no se mueven infinitamente rápido dentro del medio líquido. La finitud de la capa de Debye, implica que las cargas positivas y negativas no se equilibran exactamente dentro de la gota sino que forman una capa delgada (la llamada capa de Debye), donde hay una carga neta diferente de cero. Mostramos en el capítulo 3 que esta hipótesis se encuentra de hecho en el corazón de la formación de chorros de Rayleigh y se puede utilizar para calcular características principales del chorro, tales como la velocidad y el tamaño. Se encontró que la carga crítica incrementa con ε. Este hecho está de acuerdo con la observación en [20] que las gotas de agua, que contiene siempre una cierta cantidad de iones, son capaces de mantener una cantidad de carga un poco más grande que el límite de Rayleigh.

En el capítulo 4 se calcula la corrección a un resultado clásico debido a Rayleigh que establece que una gota viscosa de un líquido perfectamente conductor debe convertirse en inestable para un valor suficientemente grande de la carga eléctrica neta contenida por la gota, pero suponiendo ahora un líquido dieléctrico con iones disueltos en lugar de un conductor perfecto. Llegamos a la conclusión de que el hecho de tener una solución electrolítica disminuye el valor crítico del parámetro de fisibilidad de Rayleigh. Este resultado está en contraste con el resultado obtenido en el capítulo anterior, el resultado q sólo es válido para κ pequeña (la condición de validez de la aproximación Debye-Hückel) que corresponde a una solución diluida, va en el dirección opuesta.

Como una aplicación, nos centraremos en futuros trabajos, en el caso de gotas de soluciones iónicas sometidas a campos eléctricos externos y en cómo la movilidad finita de los iones introduce correcciones en el comportamiento dinámico de la gota con respecto al caso ya estudiado de movilidad infinita de iones. Nuestras fórmulas asintóticas pueden, por supuesto, también ser aplicadas a los fenómenos electrocinéticos más generales. Otro tema interesante para futura investigación resulta de la eliminación de la hipótesis de estacionariedad en las distribuciones de iones (es decir, cuando la escala de tiempo para el movimiento de cargas es comparable con la escala el tiempo para el movimiento de la interfaz fluida). En ese caso, uno no puede trabajar directamente con la ecuación de Poisson-Boltzmann, sino utilizar el sistema original de Nernst-Planck.

Chapter 1

Introduction

The purpose of this thesis is to develop tools to study some problems in the intersection between microfluidics and electrokinetics. In this introduction we provide an overview of this areas and introduce the specific problem that we will be dealing with: the evolution of charged drops of ionic solutions.

1.1 Motivation

Electrified droplets are present in thunderstorms clouds [20] as well as in technological applications such as electrospraying [8] (used, for instance, to produce small samples of ionic solutions suitable for spectrometry, an application that deserved the 2002 Nobel Prize in Chemistry by J. Fenn), microencapsulation [48], ink-jet printing [53], Field Emission Electric Propulsion (FEEP) thrusters [68], Electronic paper [40], microfluidic chips [21], [18], [29], [65], etc.

Figure 1.1: Electronic paper

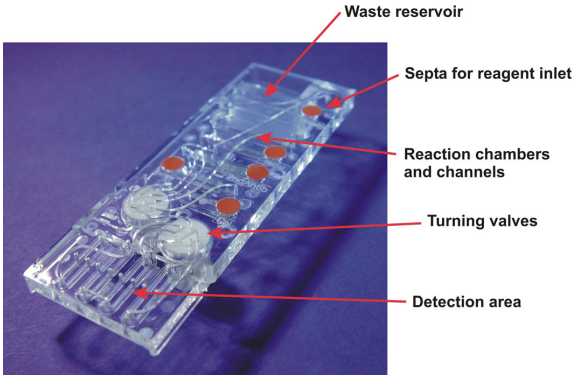

Figure 1.2: Lab-on-a-chip

In order to translate concepts into practical devices, we must learn to control fluids with great precision and speed at, sometimes, ultra small scales. About charged fluid droplets, it is known that they become unstable when charged beyond a number called the Rayleigh limit, and then they develop singularities (cf [6], [7] and [20] for experimental results and [26],

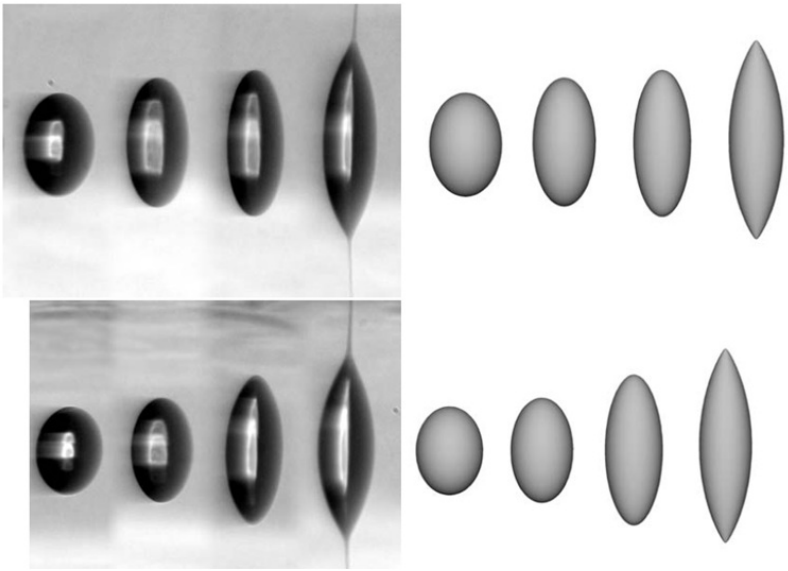

Figure 1.3: Formation of Rayleigh jets in drops under the action of an external electric field from [7] and comparison with the numerical simulation in [26]

[12] for numerical simulations). When the fluid is a perfect conductor and is modeled under Stokes approximation, it was shown that conical tips develop in finite time (see [26], [12]). In the experimental observations, very fast and thin jets are produced from the conical tips (see figures in 1.3). This is a fact that cannot be reproduced in [26], [12] under the Stokes and perfect conductor assumptions. For perfect fluids, jets have been reported recently in [34]. Nevertheless, for very small drops (of the order of 100 μm or smaller), Reynolds number can be very small (of the order of 10^{-4} or smaller), so that it seems necessary to investigate the formation of jets under Stokes approximation. Our hypothesis is that it is the finite electric conductivity and the presence of Debye layers in electrolyte solutions what induces the production of Rayleigh jets. The formation of jets from conical tips under the action of electric fields lies at the heart of some of the applications mentioned above: the electrospray originates from the breakup of Rayleigh jets into drops, the force from Propulsion thrusters is in reaction to Rayleigh jets and the microencapsulation takes place when two coaxial Rayleigh jets breakup into droplets (with the inner fluid encapsulated by the outer fluid).

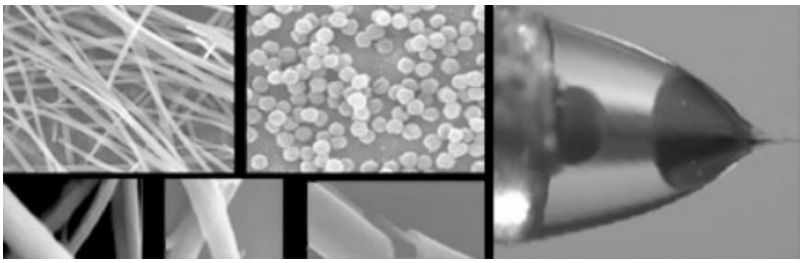

Figure 1.4: Microencapsulation of an inner fluid by an outer fluid

1.2 An overview of microfluidics and electrokinetics

Let us first take a look about more general contexts to which our problem can be somewhat related. First we will provide a quick overview of the bursting area of Microfluidics (see [65], [35] for a general introduction) which nowadays produces thousands of scientific publications and patents each year and represents a multibillion dollar business in the electronic and medical sectors. Then, we will more specifically consider a particular mechanism to manipulate fluids at small scale: the use of electric fields and electrokinetic response of the flow to them.

1.2.1 Microfluidics

A rich variety of microfluidic systems have arisen in the natural world through millions of years of evolution and natural selection (see [2], [16], [52]). However, the history of microfluidics as an area of human endeavor can be measured in decades. It is therefore not surprising that practical microfluidic devices are relatively few, many ideas such as the "Lab On a Chip" exist mostly in concept and the most useful of microfluidic devices are probably yet to be conceived. Microfluidics refers to devices and methods for controlling and manipulating fluid flows with length scales less than a millimeter. Studies of such fluid-related phenomena have long been part of the fluid mechanical component of colloid science [60] and plant biology [17] and draw on many classical features of the dynamics of viscous flows (e.g., [39], [5],). However, the subject has received enormous recent attention because of the availability of methods for fabricating individual and integrated flow configurations with length scales on the order of tens and hundreds of microns and smaller (e.g. [42], [64], [66]), and rapid developments in biology and biotechnology for which manipulations on the cellular length scale (and below) and the ability to detect small quantities and manipulate very small volumes (typically less than 1 microliter) offer advantages ([70], [44], [9]), also the quest for cheap portable devices able to perform simple analytical tasks, and the potential use of Charged droplets microsystems to perform fundamental studies of physical, chemical, and biological processes. This trend is continuing; moreover, the term nanofluidics emphasizes the desire to manipulate flows on the scale of DNA strands, other biopolymers, and large proteins.

Microfluidic flows are readily manipulated using many kinds of external fields (pressure, electric, magnetic, capillary, and so on). As dimensions shrink, the relative importance of surface to volume forces increases. Such manipulations of flow can be achieved either by forces applied macroscopically, e.g., at appropriate inlets and outlets, or can be generated locally within the microchannel by integrated components. Table 1.1 from [65] summarizes frequently mentioned driving forces for controlling microflows.

Alternatively, electrokinetics is now studied in a variety of forms for controlling microflows. Electro-osmosis, where the fluid moves relative to stationary charged boundaries; dielectrophoresis, which moves an interface (often a particle) in a gradient of electric field; and electrowetting, where the electric field modifies wetting properties, have all been exploited. AC and DC fields can be considered, and the system response then depends on frequency and amplitude of the field.

Driving force	Subcategorization
Pressure gradient ∇p	
Capillary effects	Surface tension γ
	Thermal
	Electrical (electrocapillarity)
	Surface tension gradients $\nabla\gamma$
	Chemical
	Thermal
	Electrical
	Optical
Electric Fields $\mathbf{E}$	DC electro-osmosis
	AC electro-osmosis
	Dielectrophoresis
Magnetic field/Lorentz forces	Magnetohydrodynamic stirring
Rotation	Centrifugal forces
Sound	Acoustic streaming

Table 1.1: Forces and external fields with which to manipulate flows in microfluidic configurations. It is also possible to use external means to manipulate particles embedded in flows, as in electrophoresis or the use of magnetic forces [3]

Other means can be used to control flows. In particular, external fields can be used to induce motion of objects embedded in the fluid, or the channel walls can be systematically distorted: magnetic fields can influence flows directly or manipulate dispersed magnetic particles, sound fields can produce acoustic streaming motions, cyclic deformation of a wall can induce peristaltic pumping, etc. For each manner of driving a fluid motion, the surface characteristics of the device can also be exploited to provide additional control. For example, the geometrical, chemical, and mechanical features of the channel and network of channels can be patterned or altered, as summarized in Table 1.2 from [65].

Geometry	Chemical Characteristics	Mechanical properties
Network connectivity	Wettability	Hard materials
Channel cross section and curvature	Surface charge	Elastic materials
Surface topography	Chemical affinity	Gels
Porosity (e.g., in packed beds)	Ph/ionic strength sensitivity	Porous materials

Table 1.2: Design considerations for controlling flow and transport in a microfluidic channel can include the influence of geometric, chemical, and mechanical characteristics. In addition, electrodes, heaters piezoelectric actuation, etc. can be embedded in the channel boundaries.

1.2.2 Electrokinetics

Electrokinetics refers to mechanical effects that arise due to the motion of ions in liquids. The working fluid in microfluidic systems is normally water which contain ions of both signs due to dissociated water molecules or other ionic components: acids, salts, and molecules with dissociable charged groups. Normally, a volume element of such a fluid considered infinitesimal in the continuum viewpoint still contains a sufficiently large number of ions of either sign for statistical fluctuations to be unimportant and for the fluid element to be considered charge neutral. Therefore, the net algebraic transfer of momentum due to any ambient electric field is also zero (even though a non-zero electric current may exist in the fluid due to the ordered motion of these ions). Electrokinetic effects arise when this balance of positive and negative charges is disturbed due to external factors. For example, at the silica water interface, the hydrated silica often deprotonates resulting in a net negative fixed surface charge on the silica surface. These fixed charges attract a layer of ions of the opposite sign (and repel ions of like sign) resulting in the creation of a fluid layer with a net positive charge next to the interface. Similar effects arise at the surface of large macromolecules, colloidal particles or surfactant micelles.

We will describe next some of the most relevant, from the point of view of applications, electrokinetic effects: Electroosmosis, Electrophoresis, Dielectrophoresis and Electrowetting.

Electroosmosis. When an electrolyte is adjacent to a surface, the chemical state of the surface is generally altered, either by ionization of covalently bound surface groups or by ion adsorption. The net effect is that the surface inherits a charge while counterions are released into the liquid. At equilibrium, a balance between electrostatic interactions and thermal agitation is established at a thin layer near the solid (the so-called Debye layer, which will be profusely discussed in this thesis). When an electric field is applied along a channel, a conductive current and the corresponding local field $\mathbf{E}$ are established throughout the liquid. Typically, the bulk of the liquid remains electrically neutral and so is not acted on by a net force. By contrast, in the Debye layer there is a net electrical charge density, so the local electric field that is tangent to the surface of the channel generates a body force on the fluid and thus induces a shear and a flow (the electroosmotic flow) inside the channel. Hence, a neutral fluid is set into motion due to the local imbalance at the Debye layer.

Electrophoresis. Electrophoresis refers to the transport of small charged objects in a fluid due to an applied electric field. A solid body surrounded by an ionic solution presents a Debye layer which is, in general, not uniform. The charge distribution at the layer changes along the body's surface. When a uniform electric field is established, the force originated at different sectors of the Debye layer might be not uniform so that a net force able to move the body appears. Many macromolecules contain dissociable charge groups on its surface, and therefore, spontaneously acquire a charge in aqueous solution. They therefore move in response to an applied electric field, and this motion is the basis for separating macromolecules from solution using such bioanalytical techniques as Capillary Electrophoresis (CE), Slab Gel Electrophoresis (SGE) and Isoelectric Focussing (IEF), most notably in DNA sequencing processes.

Dielectrophoresis. Particles that are uncharged but polarizable experience a force in a non-uniform electric field, the resulting motion is known as di-electrophoresis. Dielec-

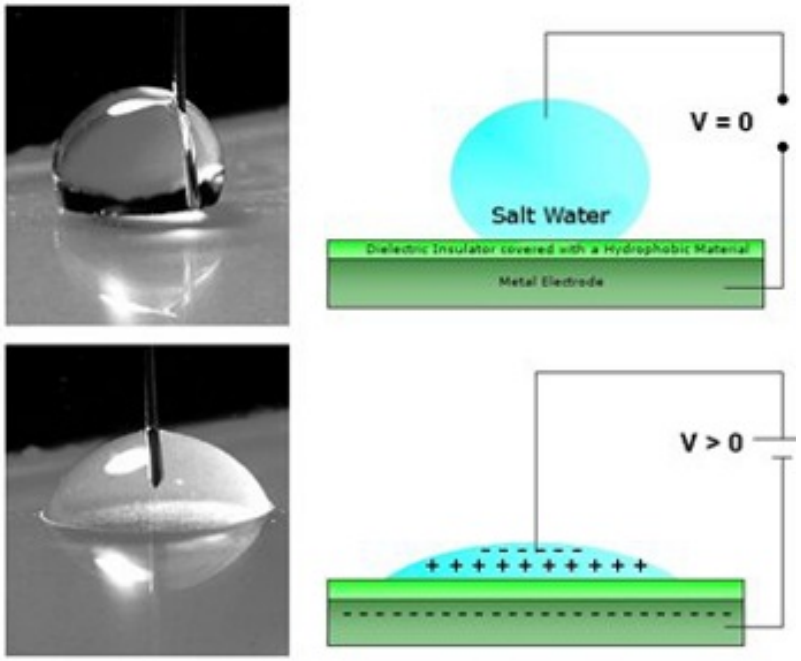

Figure 1.5: The basic electrowetting phenomena.

trophoresis is that unlike electrophoresis, the effect does not disappear if the constant electric field is replaced by an oscillating one. Thus, the dielectrophoretic force can be fine tuned by adjusting the frequency.

Electrowetting. Electrowetting is essentially the phenomenon whereby an electric field can modify the wetting behavior of a droplet in contact with an insulated electrode (see Figure 3.7.5 for a sketch of the simplest electrowetting experiment). When a voltage is applied between an electrically conductive droplet and an hydrophobic or partially wettable substrate, the apparent contact angle is reduced and the droplet starts to spread. This effect has been discovered by Lippmann more than a century ago [47]. Besides these fundamental questions of basic research, the phenomenon of electrowetting is of major interest for technological applications related to microfluidics, more precisely the possibility of manipulating motion and shape of small amounts of fluid. A particular advantage compared to other methods studied recently is the enhanced flexibility of electrowetting, as valves, pumps or even fixed channels are not needed.

Important examples of technological applications are pixelated optical filters [57], adaptive lenses [45], [11], and curtain coating [13]. Similarly, fast switching electrowetting displays – patented by Philips just recently (see also [**?**]) – take advantage of the observation that stable films of coloured oil sandwiched between water and hydrophobic insulators immediately contract to droplets when an external electric field is applied.

1.3 Mathematical modelling of Electrohydrodynamics

In this section we introduce the general models for electrokinetic phenomena in fluid media (or electrohydrodynamics). They need to combine the general equations for the motion of fluids (Navier-Stokes or, when Reynolds number is small, Stokes system) with the equations for the motion of electric charges in a fluid (Nernst-Planck system) and the equation satisfied by the electric field in presence of electric charges (Poisson equation). A general description together with various approximation can be found in [62].

First, the phenomena we are interested in, take place in a liquid environment. Hence, it is appropriate to introduce a velocity vector field $\mathbf{v}$ together with a pressure field. The fluid, ordinarily a viscous and incompressible one such as water or glycerine, can be modelled by means of Navier-Stokes system:

$$\rho_0 \left(\partial_t \mathbf{v} + \mathbf{v} \cdot \nabla \mathbf{v}\right) = -\nabla p + \mu \Delta \mathbf{v} + \mathbf{F}_e \tag{1.1}$$

$$\nabla \cdot \mathbf{v} = 0 \tag{1.2}$$

expressing balance of Momentum and mass. ρ_0 and μ are the density and viscosity of the fluid respectively. Equation (1.1) follows from Newton's second law under external body forces $\mathbf{F}_e$ acting per unit volume (e.g., gravity, electric, electromagnetic or centrifugal force). In our case, we will consider only forces of electric nature. Hence, $\mathbf{F}_e$ can be expressed as the divergence of Maxwell's stress tensor

$$T_{M,ij} = \varepsilon_0 \varepsilon_r \left(E_i E_j - \frac{1}{2} \delta_{ij} \left|\mathbf{E}\right|^2 \right) \tag{1.3}$$

where $\varepsilon_0 \varepsilon_r$ is the dielectric permitivity of the medium and E_j represents the j component of the electric field. Hence

$$F_{e,i} = \left(T_{M,ij}\right)_i$$

On the other hand, the electric field satisfies Maxwell equations (cf. [37], [43]). If we neglect magnetic effects (the fluid and charges velocities are much smaller than the velocity of light), the electric field is $\mathbf{E} = -\nabla V$ where V is the electric potential. The potential satisfies then Poisson's equation:

$$\nabla \cdot (\varepsilon_0 \varepsilon_r \nabla V) = -\rho \tag{1.4}$$

where ρ represents the electric charge density.

Finally, the electric charges will move in response to electric fields, thermal agitation (diffusion) and the fluid velocity field. This is expressed in the equation

$$\mathbf{j}_i = \mu_i e z_i n_i \mathbf{E} - D_i \nabla n_i + n_i \mathbf{v}, \tag{1.5}$$

which expresses the net flux of the charged species i as the sum of three fluxes: the convective flux $n_i \mathbf{v}$ due to the velocity field $\mathbf{v}$ of the fluid, the diffusive flux $D_i \nabla n_i$, and the electrokinetic flux $\mu_i e z_i n_i \mathbf{E}$ due to the electric field. μ_i is the ion mobility: the velocity acquired by the ion when acted upon by a unit of external force. D_i is the diffusion coefficient of the i^{th} species. Einstein's relation establishes that $\frac{D_i}{\mu_i} = k_b T$, where k_b is Boltzmann's constant

and T the absolute temperature. In general, we may have many different kinds of charged species: electrons, ions of diverse type and valencies (Na^+, Cl^-, K^+, Ca^{2+}, etc). Therefore,

$$\rho(\mathbf{x}, t) = \sum_{i=0}^{N-1} e z_i n_i. \tag{1.6}$$

where N is the number of species, e is the charge of the electron, n_i is the concentration of the species i, and z_i is its valency. Continuity of each of the charged species leads to the Nernst-Planck system:

$$\frac{\partial n_i}{\partial t} + \nabla \cdot \mathbf{j}_i = 0, \tag{1.7}$$

The system (1.1)-(1.7) contains a large number of equations and physical parameters. Its resolution represents then an enormous theoretical and computational challenge. In this thesis, we will use the smallness of some dimensionless quantities in the microfluidics context in order to simplify the system and make it suitable for analysis and simulation. In particular, Reynolds number will be small so that we will approximate Navier-Stokes system by Stokes system:

$$-\nabla p + \mu \Delta \mathbf{v} + \mathbf{F}_e = 0 \tag{1.8}$$

$$\nabla \cdot \mathbf{v} = 0 \tag{1.9}$$

A second simplification will lead from Nernst-Planck system combined with Poisson to a nonlinear Partial Differential Equation known as Poisson-Boltzmann equation.

1.4 Description of the dissertation

This work is divided in three parts. In the first part, which corresponds to Chapter 2, we start studying physical conditions that leads us latter to a model to the electric potential inside the droplet, the afore mentioned Poisson-Bolztmann equation.

In this chapter we study the solutions to Poisson-Boltzmann equation for electrolytic solutions in a domain Ω, surrounded by an uncharged dielectric medium. We establish existence, uniqueness and regularity of solutions and study in detail their asymptotic behaviour close to $\partial\Omega$ when a characteristic length, called the Debye length, is sufficiently small. This is a double layer with a thickness that changes from point to point along $\partial\Omega$ depending on the normal derivative of a harmonic function outside Ω and the mean curvature of $\partial\Omega$. We also provide numerical evidence of our results based on a Runge-Kutta and a finite elements approximation to the problem.

In the second part, the Chapter 3, we couple the electrokinetics as described by Poisson-Boltzmann approximation with the fluid motion described by Navier-Stokes equations (see [46], [19]). We obtain that the force term in the Stokes formulation given by the potential described by the Poisson-Boltzmann equation, becomes a boundary condition. Using this model we establish an integral formulation for the problem, that being properly discretized can lead to a Boundary Element formulation for two kinds of differential equations: Dirichlet

for the boundary condition related to the potential and Stokes with force term zero for the velocity in the drop. One of our main motivations is to describe the so-called Rayleigh jets. Our hypothesis is that it is the finite electric conductivity and the presence of Debye layers in electrolyte solutions what induces the production of Rayleigh jets.

In the last Chapter, the Chapter 4, we use spherical harmonics and vector spherical harmonics for studying the stability of a viscous drop filled with an diluted electrolytic solution using a linearization of the Poisson-Boltzmann equation known as Debye-Hückel linearization.

1.5 Conclusions and future work

In Chapter 2 we have deduced asymptotic formulae for the distribution of charge of an ionic solution near its interface with an external medium. Our main assumptions were 1) all ionic species are in dynamic equilibrium and 2) a dimensionless parameter ε which is inversely proportional to ion mobilities is very small. Our expansions contain corrections due to the geometry of the interface and hence describe possible accumulations of charge at certain regions of the interface depending on their curvature.

Our hypothesis was that finite conductivity implies electric charges do not move infinitely fast inside the liquid medium. The finiteness of Debye layer, implies that positive and negative charges do not balance exactly inside the drop but they form a thin layer (the so-called Debye layer) where there is a nonzero net charge. We show in Chapter 3 that this hypothesis does indeed lie at the heart of the formation of Rayleigh jets and can be used to compute the jet's main characteristics such as velocity and size. We found that the critical charge increases with ε. This fact agrees with the observation in [20] that water droplets, containing always a certain amount of ions, are able to hold an amount of charge slightly larger than Rayleigh's limit.

In Chapter 4 we compute the correction to a classical result due to Rayleigh that establishes that a viscous drop of a perfectly conducting liquid should become unstable for a large enough value of the net electric charge contained by the drop, but assuming now a dielectric liquid with ions dissolved instead of a perfect conductor. We conclude that the fact of having an electrolyte solution lowers down the critical value of Rayleigh fissibility parameter. This result is in contrast with the result obtained in the previous chapter, the result which is only valid for κ small (this is the condition of validity of Debye-Hückel approximation) that corresponds to a diluted solution, goes in the opposite direction.

As an application, we will focus in future works, on the case of drops of ionic solutions subject to external electric fields and on how the finite ion mobility introduces corrections on the dynamic behaviour of the drop with respect to the already studied case of infinite ion mobility. Our asymptotic formulae can, of course, be also applied to more general electrokinetic phenomena. Another interesting issue for future investigation results from removing the hypothesis of stationarity in the ion distributions (that is, when the time scale for the motion of charges is comparable with the time scale for the motion of the fluid interface). In that case one cannot directly work with Poisson-Boltzmann equation but

instead must use the original Nernst-Planck system.

Chapter 2

The structure of double layers in Poisson-Boltzmann equation

2.1 Introduction

Electrokinetic phenomena are mechanical effects caused by the presence and motion of ions in liquids. These ions can be dissociated water molecules or the result of dissociated acids, salts, etc. The result of ions dissolved in an ambient fluid is called an electrolyte. Since ions are electrically charged, they move in response to an applied electric field and therefore induce fluid flows. Hence electrolytes can be used to manipulate small masses of fluids by means of suitably applied electric fields. This is the reason why electrokinetic phenomena have an important connection to microfluidics, the science of manipulating fluids on spatial scales anywhere between one to a hundred micron. Fluids at such small scales appear both in various natural systems and in microdevices intended for applications ranging from gene sequencing and gene expression to micropixels in electronic paper. As we shall see below, the analysis of electrokinetic phenomena involves systems of partial differential equations with highly nontrivial couplings (see also [62]). Therefore, mathematical analysis is needed in order to improve our understanding of the subject.

Perhaps one of the most interesting applications of electrokinetic effects is electrowetting. Electrowetting has become one of the most widely used tools for manipulating tiny amounts of liquids on surfaces. Applications range from "lab-on-a-chip" devices [62] to adjustable lenses and new kinds of electronic displays [51], [10]. In the simplest configuration, a drop of conducting fluid rests over a solid substrate, and a potential difference V_0 is established between the drop and an electrode placed at a distance d from the substrate. Another important instance where electrokinetic equations appear is in the deformation and disintegration of charged drops in the presence of electric field when the fluid consists of an electrolyte solution instead of a perfect electric conductor fluid (as considered in [27], [12], see also [24] for a general review).

The electrokinetic equations. The main characteristic of an electrolyte is the presence of N species, whose concentrations we denote by $n_i(\mathbf{x}, t)$, $i = 0, \ldots, N-1$, carrying a charge $\rho_i = ez_i n_i$, where e is the charge of an electron, and z_i the valence of the i^{th} species.

Therefore, the total charge will be given by

$$\rho^e(\mathbf{x}, t) = \sum_{i=0}^{N-1} e z_i n_i.$$

Notice that some of the species might be neutral so that the corresponding z_j is zero. This happens, for instance, if the fluid contains neutral species that can dissociate to produce ions of different sign or be produced by recombination of two ionic species.

The presence of free charges creates or modifies an imposed electric field. This is expressed by means of Poisson's equation (cf. [43])

$$-\nabla \cdot (\varepsilon_0 \varepsilon_r \nabla V) = \rho^e,$$

where ε_0 is the electric permittivity of vacuum, ε_r the relative electric permittivity of the electrolyte medium, and V the electrostatic potential so that the electric field equals $\mathbf{E} = -\nabla V$.

In absence of dissociations or recombinations that modify the total mass of each of the species, ion and molecule concentrations satisfy the continuity equation

$$\frac{\partial n_i}{\partial t} + \nabla \cdot \mathbf{j}_i = 0, \tag{2.1}$$

where $\mathbf{j}_i$ is the mass flux of the i^{th} species. In response to an electric field, ions may modify their flux modelled by the Nernst-Planck law

$$\mathbf{j}_i = \mu_i e z_i n_i \mathbf{E} - D_i \nabla n_i + n_i \mathbf{v}, \tag{2.2}$$

which expresses the net flux as the sum of three fluxes: the convective flux $n_i\mathbf{v}$ due to the velocity field $\mathbf{v}$ of the fluid, the diffusive flux $D_i \nabla n_i$, and the electrokinetic flux $\mu_i e z_i n_i \mathbf{E}$ due to the electric field. μ_i is the ion mobility: the velocity acquired by the ion when acted upon by a unit of external force. D_i is the diffusion coefficient of the i^{th} species. Einstein's relation establishes that $\frac{D_i}{\mu_i} = k_b T$, where k_b is Boltzmann's constant and T the absolute temperature. In absence of externally imposed velocities, the condition that charge fluxes vanish leads, from (2.2), to

$$n_i = c_i e^{-\frac{\mu_i e z_i}{D_i} V} = c_i e^{-\frac{e z_i}{k_b T} V},$$

where $c_i > 0$ are to be determined from boundary conditions or the condition that the total amount of each ionic species is given. Poisson equation is then

$$-\nabla \cdot (\varepsilon_0 \varepsilon_r \nabla V) = \sum_{i=0}^{N-1} e z_i c_i e^{-\frac{e z_i}{k_b T} V}.$$

and in the case of constant electric permittivity $\varepsilon_0 \varepsilon_r$,

$$\Delta V = -\sum_{i=0}^{N-1} \frac{e z_i c_i}{\varepsilon_0 \varepsilon_r} e^{-\frac{e z_i}{k_b T} V}. \tag{2.3}$$

Equation (2.3) is known as Poisson–Boltzmann equation and defines the electric potential distribution in the diffuse ionic layer adjacent to a charged surface subject to appropriate boundary conditions. A simplified situation corresponds to the special case of a single salt dissociating into cationic and anionic species (i.e.,$N = 2$) with the added simplification of symmetric electrolyte solution (e.g., NaCl, $CuSO_4$, or AgI). In symmetric electrolytes, both the cations and anions have the same valences, $z_1 = -z_2 = z$. In the case of planar electric double layers defined for $x \geq 0$, assuming $n_1 = n_2 = n_\infty$ as x tends to ∞, one obtains the equation

$$\frac{d^2V}{dx^2} = \frac{ezn_\infty}{\varepsilon_0\varepsilon_r}\left(e^{\frac{ez}{k_bT}V} - e^{-\frac{ez}{k_bT}V}\right) = \frac{2ezn_\infty}{\varepsilon_0\varepsilon_r}\sinh\left(\frac{ez}{k_bT}V\right) \ , \tag{2.4}$$

and an analytical solution known as the Gouy–Chapman solution. It is obtained by assuming a given potential V_s at $x = 0$, and $V = 0$ as $x \to \infty$ so that

$$V = \frac{k_bT}{ze}\log\left(\frac{1 + e^{-\kappa x}\tanh\frac{k_bTV_s}{4ze}}{1 - e^{-\kappa x}\tanh\frac{k_bTV_s}{4ze}}\right) \ , \tag{2.5}$$

with

$$\kappa^{-1} = \left(\frac{\varepsilon_0\varepsilon_r k_bT}{2e^2z^2n_\infty}\right)^{\frac{1}{2}} \ .$$

The parameter κ^{-1} is called the Debye length and measures the electric double layer thickness. The solution (2.5) is such that the net electric charge, given by the right hand side of (2.4) with minus sign, is very small beyond the Debye length while it becomes large for $x \lesssim \kappa^{-1}$ if $\kappa^{-1} \ll 1$.

The formation of double layers with a nonzero net charge and their mechanical effects on the fluid solvent are of crucial importance in the field of electrohydrodynamics and electrokinetic phenomena (cf. [62], [50], [58] for instance). Despite its importance, the general solutions to (2.3) for general domains and boundary conditions are poorly understood due to its highly nonlinear character. Our goal will be to obtain a closed-form asymptotic representation of the solutions to (2.3) for general domains in the limit of very small Debye length.

In order to fix ideas, we will consider two electrolyte species (say Na^+ and Cl^- for instance) together with free charges of a third species (say electrons for instance) in a bounded domain Ω surrounded by a neutral (no charge) domain $\Omega^*\backslash\Omega$ with a given potential imposed at $\partial\Omega^*$. This situation might be viewed as a drop consisting of an electrolyte solution together with free electrons that have been introduced externally into the drop, surrounded by another fluid that is in contact with electrodes where a certain potential is imposed (we will take it as zero, for the sake of simplicity). Therefore, there will be a certain imbalance between positive and negative charges in the drop. If the valence of the ions is the same as the charge of the free carriers (as it is the case with the $NaCl$ ions and the electrons), then equation (2.3) becomes

$$\begin{aligned}\Delta V &= \frac{ezc_0}{\varepsilon_0\varepsilon_r}\left(e^{\frac{ez}{k_bT}V} - e^{-\frac{ez}{k_bT}V}\right) + \frac{ezc_1}{\varepsilon_0\varepsilon_r}e^{\frac{ez}{k_bT}V} \\ &= \frac{ez\left(c_0 + c_1\right)}{\varepsilon_0\varepsilon_r}e^{\frac{ez}{k_bT}V} - \frac{ezc_0}{\varepsilon_0\varepsilon_r}e^{-\frac{ez}{k_bT}V} \ ,\end{aligned} \tag{2.6}$$

where c_0 is the concentration of both positive and negative ions and c_1 the concentration of free carriers. One can write the problem in dimensionless form by introducing

$$\varepsilon = \frac{\varepsilon_0 \varepsilon_r k_b T l}{(ez)^2} \ ,$$

where l is a characteristic length associated to Ω that we can take, for instance, to be $l = |\Omega|^{1/n}$ with n being the space dimension, and reescaling variables and unknowns in the form

$$V = \frac{ez}{\varepsilon_0 \varepsilon_r l} u, \ \mathbf{x}' = \mathbf{x}/l \ , C_1 = (c_0 + c_1)\, l^3, \ C_2 = c_0 l^3 \ . \tag{2.7}$$

By denoting, for simplicity, the rescaled domains also by Ω, Ω^*, we arrive from (2.6) and (2.7) at the equation

$$\Delta u = C_1 e^{\frac{u}{\varepsilon}} - C_2 e^{-\frac{u}{\varepsilon}} \text{ in } \Omega \ , \tag{2.8}$$

with the condition that the total negative charge $M = C_1 \int_\Omega e^{\frac{u}{\varepsilon}}$ and the total positive charge $N = C_2 \int_\Omega e^{-\frac{u}{\varepsilon}}$ are given. We can then rewrite (2.8) in the form

$$\Delta u = M \frac{e^{\frac{u}{\varepsilon}}}{\int_\Omega e^{\frac{u}{\varepsilon}}} - N \frac{e^{-\frac{u}{\varepsilon}}}{\int_\Omega e^{-\frac{u}{\varepsilon}}} \text{ in } \Omega \ . \tag{2.9}$$

The absence of charge in $\Omega^* \backslash \Omega$ leads to

$$\Delta u = 0 \text{ in } \Omega^* \backslash \Omega \ , \tag{2.10}$$

with a given potential u at $\partial\Omega^*$ that we will take zero for simplicity

$$u = 0 \text{ at } \partial\Omega^* \tag{2.11}$$

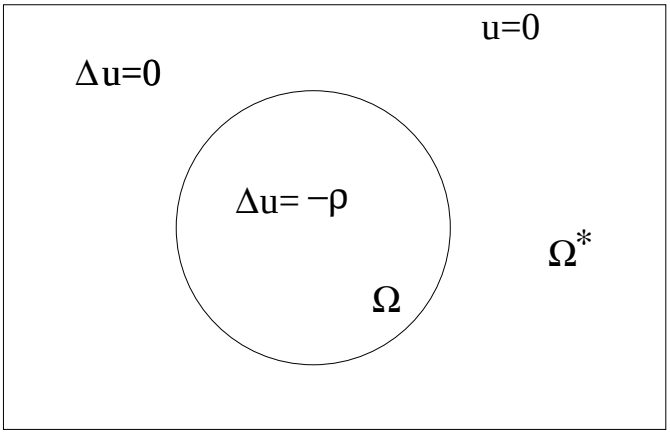

Figure 2.1: Geometrical setting of the problem with $-\rho$ given by the right hand side of equation (2.9)

In Figure 2.1 we represent the geometrical setting for problem (2.9)-(2.11). Our goal is to describe the solutions of (2.9)-(2.11) in the limit of very small Debye lengths $\varepsilon \ll 1$. As we will see, they consist of a boundary layer near $\partial\Omega$ with a variable thickness that depends

on geometrical properties of $\partial\Omega$. Moreover, the limit $\varepsilon \to 0$ corresponds, in some sense to the case of a perfect conductor with net charge $Q = N - M$. Hence one of the goals of this work is to study the convergence of solutions to Poisson-Boltzmann equation, when ion mobility $\varepsilon \to 0$, to the solution of a perfect conductor (formally corresponding to $\varepsilon \equiv 0$). More precisely, we consider two problems:

a) The problem of a perfect conductor in Ω surrounded by a dielectric uncharged media in $\Omega^* \backslash \Omega$. The electrostatic potential u satisfies

$$\Delta u = 0 \text{ in } \Omega^* \backslash \bar{\Omega} \ ,$$

with boundary conditions

$$\begin{aligned} u &= 0 \text{ in } \partial\Omega^* \ , \\ u &= C \text{ in } \partial\Omega \ , \end{aligned}$$

where C is a constant to be determined with the condition that the total charge is a given quantity $Q = N - M$. Namely, integrating (2.9) over Ω and using the divergence theorem,

$$-\int\limits_{\partial\Omega} \frac{\partial u}{\partial n} dS = Q \ .$$

Notice that $-\frac{\partial u}{\partial n}$ represents then the surface charge density that we will denote as

$$\sigma_0(x_S), \ x_S \in \partial\Omega \ .$$

The regularity of $\sigma_0(x_S)$ depends on the regularity of $\partial\Omega$ and is such that (cf. Theorem 6.19 in [36]):

$$\partial\Omega \in C^{k+2+\alpha} \Rightarrow \sigma_0(x_S) \in C^{k+1+\alpha} \ , \tag{2.12}$$

with $0 < \alpha < 1$, $k \in \mathbb{N}$. We will assume $\partial\Omega \in C^{3+\alpha}$, so that $\sigma_0(x_S) \in C^{2+\alpha}$.

b) The problem of an ionic solution with M units of negative charge and N units of positive charge in Ω. The medium Ω is supposed to have an ion mobility ε. This leads to the problem described by equations (2.9)-(2.11). In other words, we are solving

$$\Delta u = M(x) \frac{e^{\frac{u}{\varepsilon}}}{\int\limits_{\Omega} e^{\frac{u}{\varepsilon}}} - N(x) \frac{e^{-\frac{u}{\varepsilon}}}{\int\limits_{\Omega} e^{-\frac{u}{\varepsilon}}} \text{ in } \Omega^* \ , \tag{2.13}$$

$$u = 0 \text{ in } \partial\Omega^* \ , \tag{2.14}$$

with $M(x) = M$ in Ω, $M(x) = 0$ in $\Omega^* \backslash \Omega$, $N(x) = N$ in Ω, $N(x) = 0$ in $\Omega^* \backslash \Omega$.

Problem b) will have solutions u such that, when $\varepsilon \ll 1$, the quantity

$$\rho(x) = -M \frac{e^{\frac{u}{\varepsilon}}}{\int\limits_{\Omega} e^{\frac{u}{\varepsilon}}} + N \frac{e^{-\frac{u}{\varepsilon}}}{\int\limits_{\Omega} e^{-\frac{u}{\varepsilon}}} \ , \tag{2.15}$$

in Ω, representing the volumetric charge density, will be very small except for a thin boundary layer close to $\partial\Omega$ where the charge difference $\rho(x)$ will experience drastic changes. In fact, we expect

$$\rho(x) \to \sigma_0(x_S)\delta(\partial\Omega) \ ,$$

where $\delta(\partial\Omega)$ is the Dirac measure concentrated in the boundary of Ω and the kind of convergence will be precised below.

Our main result is the following Theorem:

Theorem 1. *For any $\varepsilon > 0$ there exists a unique solution to problem (2.9)-(2.11) in $H_0^1(\Omega^*)$. Such solution is $C^\infty(D)$ for any $D \subset\subset \Omega$ or $D \subset\subset \Omega^*\backslash\Omega$. Moreover, if ε is sufficiently small, then the net charge density defined by (2.15) where u is the solution to (2.9)-(2.11), admits the following representation in an $O(\varepsilon^{\frac{1}{2}+\nu})$ ($0 < \nu \ll 1$, ν independent of ε) neighborhood in Ω of $\partial\Omega$:*

$$\rho(x) = \sigma_0(x_S)\frac{|\sigma_0(x_S)|}{2\varepsilon}\frac{1}{\left[\frac{|\sigma_0(x_S)|}{2\varepsilon}dist(x,x_S)+1\right]^2} + \rho_1(x) \ ,$$

where x_S is the point of $\partial\Omega$ closest to x and with $\rho_1(x)$ uniformly bounded in ε.

At a more formal level, we will find the next order correction to $\rho(x)$ and show that, for x such that $dist(x,x_S) < C\varepsilon^{\frac{1}{2}+\nu}$,

$$\rho(x) = \sigma(x_S)\frac{|\sigma(x_S)|}{2\varepsilon}\frac{1}{\left[\frac{|\sigma(x_S)|}{2\varepsilon}dist(x,x_S)+1\right]^2} + \frac{1}{2}\frac{\sigma_0(x_S)\mathcal{H}(x_S)}{\left[\frac{|\sigma_0(x_S)|}{2\varepsilon}dist(x,x_S)+1\right]} + O(\varepsilon) \ ,$$

where $\mathcal{H}(x_S)$ denotes the mean curvature of $\partial\Omega$ at x_S and

$$\sigma(x_S) = \sigma_0(x_S) + \varepsilon\widetilde{\sigma}(x_S) \ ,$$

$\widetilde{\sigma}(x_S)$ being

$$\widetilde{\sigma}(x_S) = -\frac{2\int_{\partial\Omega}\mathcal{N}\left[\ln|\sigma_0(x_S)|\right]}{M-N}\sigma_0(x_S) + 2\mathcal{N}\left[\ln|\sigma_0(x_S)|\right] \ ,$$

where $\mathcal{N}[\cdot]$ is the Dirichlet to Neumann operator, restricted to $\partial\Omega$ and with zero Dirichlet data at $\partial\Omega^*$, for Laplace equation in $\Omega^*\backslash\Omega$. We will also compute quantities, such as the Maxwell stress, that are important in the electrokinetic context.

This chapter is organized as follows: in Section 2.2 we obtain general results concerning existence, uniqueness and regularity of the solutions to (2.13)-(2.14) for any value of ε. Section 2.3 is devoted to obtaining closed form expressions for the asymptotic values of the solutions to (2.13)-(2.14) near $\partial\Omega$ when $\varepsilon \ll 1$. Section 2.3 will be devoted to the formal deduction of higher order correction involving the curvature of $\partial\Omega$, as well as expression of the so-called Maxwell stress tensor (see [37] for the definition) which is relevant for applications in fluid mechanics. Finally section 2.4 is devoted to the numerical study of the problem in the cases of spherical symmetry (using a Runge-Kutta scheme) and general two dimensional domains (using an adaptive Finite Element Method).

2.2 Existence, uniqueness and regularity

In this section, we prove a theorem for the existence and uniqueness of weak solutions (in a sense to be defined below) to (2.13), (2.14). We also show that such solutions are $C^{1+\alpha}(\Omega^*)$ for any $0 < \alpha < 1$ and $C^\infty(D)$ for any $D \subset\subset \Omega$ or $D \subset\subset \Omega^* \backslash \Omega$.

As shown by Friedman & Tintarev [30] (see also [58]), the equation (2.13), in the particular case where $M(x)$ and $N(x)$ are constant and $\varepsilon = 1$, is the Euler-Lagrange equation for the variational problem of finding the critical points of the functional

$$J[\phi] = \frac{1}{2}||\nabla\phi||^2_{L^2(\Omega^*)} + M \ln\left(\int_{\Omega^*} e^{\phi} dx\right) + N \ln\left(\int_{\Omega^*} e^{-\phi} dx\right) .$$

For a general ε, (2.13) is the Euler-Lagrange equation for the following functional

$$J[\phi] = \frac{1}{2}||\nabla\phi||^2_{L^2(\Omega^*)} + \varepsilon M \ln\left(\int_{\Omega^*} e^{\phi/\varepsilon} dx\right) + \varepsilon N \ln\left(\int_{\Omega^*} e^{-\phi/\varepsilon} dx\right) .$$

It is simple to see that in our problem, where $M(x)$ and $N(x)$ present jump discontinuities along $\partial\Omega$, the energy functional can be chosen as

$$J[\phi] = \frac{1}{2}||\nabla\phi||^2_{L^2(\Omega^*)} + \varepsilon M \ln\left(\int_{\Omega} e^{\phi/\varepsilon} dx\right) + \varepsilon N \ln\left(\int_{\Omega} e^{-\phi/\varepsilon} dx\right) . \tag{2.16}$$

We will look for the critical points in $H^1_0(\Omega^*)$ and prove the following theorem:

Theorem 2. *There exists a unique minimum of $J[u]$ defined by (2.16) in $H^1_0(\Omega^*)$.*

Proof. Our proof follows essentially the steps of the proof of Ryham (cf. [61]) in the particular case of constant $M(x)$, $N(x)$ and $\varepsilon = 1$. It follows the steps of the direct method in the calculus of variations (see [23], for instance). First, notice that J is strictly convex since

$$J[\lambda\phi + (1-\lambda)\psi] \leq \lambda J[\phi] + (1-\lambda) J[\psi] , \tag{2.17}$$

for any $\phi, \psi \in H^1_0(\Omega^*)$, with strict inequality if $\phi \neq \psi$. This follows from the following inequalities:

$$||\nabla(\lambda\phi + (1-\lambda)\psi)||^2_{L^2(\Omega^*)} \leq \lambda||\nabla\phi||^2_{L^2(\Omega^*)} + (1-\lambda)||\nabla\psi||^2_{L^2(\Omega^*)} ,$$

which is strict except for $\phi = \psi$, and

$$\begin{aligned} \ln\left(\int_{\Omega} e^{\lambda\phi/\varepsilon + (1-\lambda)\psi/\varepsilon} dx\right) &\leq \ln\left(\left[\int_{\Omega} e^{\phi/\varepsilon} dx\right]^{\lambda}\left[\int_{\Omega} e^{\psi/\varepsilon} dx\right]^{1-\lambda}\right) \\ &= \lambda \ln\left[\int_{\Omega} e^{\phi/\varepsilon} dx\right] + (1-\lambda)\ln\left[\int_{\Omega} e^{\psi/\varepsilon} dx\right] , \end{aligned} \tag{2.18}$$

$$\ln\left(\int_\Omega e^{-\lambda\phi/\varepsilon-(1-\lambda)\psi/\varepsilon}dx\right) \le \ln\left(\left[\int_\Omega e^{-\phi/\varepsilon}dx\right]^\lambda\left[\int_\Omega e^{-\psi/\varepsilon}dx\right]^{1-\lambda}\right) \tag{2.19}$$
$$= \lambda\ln\left[\int_\Omega e^{-\phi/\varepsilon}dx\right] + (1-\lambda)\ln\left[\int_\Omega e^{-\psi/\varepsilon}dx\right] \ ,$$

where we have used Hölder inequality in (2.18), (2.19). Next we notice that

$$J[\phi] \ge C_1||\phi||^2_{H^1_0(\Omega^*)} + C_2 \ . \tag{2.20}$$

This follows from the estimates

$$\ln\left[\int_\Omega e^{\phi/\varepsilon}dx\right] \ge \ln\left[|\Omega|e^{\left(1/|\Omega|\int_\Omega \phi/\varepsilon dx\right)}\right] = \ln(|\Omega|) + \frac{1}{|\Omega|}\left(\int_\Omega \phi/\varepsilon dx\right) \ ,$$
$$\ln\left[\int_\Omega e^{-\phi/\varepsilon}dx\right] \ge \ln\left[|\Omega|e^{\left(-1/|\Omega|\int_\Omega \phi/\varepsilon dx\right)}\right] = \ln(|\Omega|) - \frac{1}{|\Omega|}\left(\int_\Omega \phi/\varepsilon dx\right) \ ,$$

which are direct consequence of Jensen inequality, and implying

$$J[\phi] \ge \frac{1}{2}||\nabla\phi||^2_{L^2(\Omega^*)} + \frac{M-N}{|\Omega|}\int_\Omega \phi dx + \varepsilon\left[M\ln(|\Omega|) + N\ln(|\Omega|)\right] \ .$$

Since

$$\frac{M-N}{|\Omega|}\int_\Omega \phi dx \ge -\frac{|M-N|}{|\Omega|}\int_\Omega |\phi|\,dx \ge= -\frac{|M-N|}{|\Omega|^{1/2}}||\phi||_{L^2(\Omega)} \ ,$$

and

$$-||\phi||_{L^2(\Omega)}|\Omega|^{1/2} \ge -\frac{|\Omega|}{2\delta} - \frac{\delta}{2}||\phi||^2_{L^2(\Omega^*)} \ge -\frac{|\Omega|}{2\delta} - C\frac{\delta}{2}||\nabla\phi||^2_{L^2(\Omega^*)} \ , \tag{2.21}$$

where we have used Poincaré's inequality, then by choosing δ sufficiently small and using $||\nabla\phi||_{L^2(\Omega^*)} \ge C||\phi||_{H^1_0(\Omega^*)}$ we arrive at (2.20). This implies that the functional J is coercive. Hence there exists $\alpha = \inf_{\psi\in H^1_0(\Omega^*)} J[\psi]$ and a minimizing sequence $\{\phi_j\}$ which is bounded in $H^1_0(\Omega^*)$. Therefore there exists a subsequence $\phi_{j_k} \rightharpoonup \phi$ in $H^1_0(\Omega^*)$. In order to show lower semicontinuity, that is $J[\phi] \le \liminf J[\phi_{j_k}]$, we can use Fatou's lemma on the sequences $\left\{e^{\phi_{j_k}/\varepsilon}\right\}$, $\left\{e^{-\phi_{j_k}/\varepsilon}\right\}$ (which belong to $L^1(\Omega^*)$ since $J[\phi_{j_k}]$ is bounded) to conclude

$$\int_\Omega e^{\frac{\phi}{\varepsilon}}dx = \left(\int_\Omega \liminf e^{\frac{\phi_{m_k}}{\varepsilon}}dx\right) \le \liminf\left(\int_\Omega e^{\frac{\phi_{m_k}}{\varepsilon}}dx\right) \ , \tag{2.22}$$

$$\int_\Omega e^{\frac{-\phi}{\varepsilon}}dx = \left(\int_\Omega \liminf e^{\frac{-\phi_{m_k}}{\varepsilon}}dx\right) \le \liminf\left(\int_\Omega e^{\frac{-\phi_{m_k}}{\varepsilon}}dx\right) \ . \tag{2.23}$$

Lower semicontinuity and strict convexity imply then the existence of a unique minimizer of $J[\phi]$ in $H^1_0(\Omega^*)$. □

Definition 3. *We will say that $u \in H^1_0(\Omega^*)$ is a weak solution of the problem (2.13), (2.14) if $e^{u/\varepsilon}, e^{-u/\varepsilon} \in L^1(\Omega^*)$ and for any $\psi \in C^\infty_0(\Omega^*)$ one has:*

$$\int_{\Omega^*} \nabla u\cdot\nabla\psi dx + \int_\Omega\left[\frac{M}{\int_\Omega e^{u/\varepsilon}dy}e^{u/\varepsilon} - \frac{N}{\int_\Omega e^{-u/\varepsilon}dy}e^{-u/\varepsilon}\right]\psi dx = 0 \ . \tag{2.24}$$

Notice that it is possible to extend the test space to $H_0^1(\Omega^*) \cap L^\infty(\Omega^*)$ since, for a weak solution $u \in H_0^1(\Omega^*)$, the functional $I_u : C_0^\infty(\Omega^*) \to \mathbb{R}$ defined as

$$I_u[\psi] = \int_{\Omega^*} \nabla u \cdot \nabla \psi dx + \int_\Omega \left[\frac{M}{\int_\Omega e^{u/\varepsilon} dy} e^{u/\varepsilon} - \frac{N}{\int_\Omega e^{-u/\varepsilon} dy} e^{-u/\varepsilon} \right] \psi dx \ ,$$

is continuous. It is straightforward to verify that a variational solution is indeed a weak solution.

In order to obtain higher regularity for weak solutions we must prove that weak solutions are bounded:

Lemma 4. *If $u \in H_0^1(\Omega^*)$ is a weak solution in the sense of (2.24) then $u \in L^\infty(\Omega^*)$.*

Proof. By introducing

$$a^* = 2\sqrt{\frac{MN}{\int_\Omega e^{u/\varepsilon} dy \int_\Omega e^{-u/\varepsilon} dy}}, \ u^* = \ln \sqrt{\frac{N \int_\Omega e^{u/\varepsilon} dy}{M \int_\Omega e^{-u/\varepsilon} dy}} \ ,$$

we can rewrite equation as

$$\int_{\Omega^*} \nabla u \cdot \nabla \psi dx + \int_\Omega a^* \sinh\left(\frac{u}{\varepsilon} - u^*\right) \psi dx = 0 \ . \tag{2.25}$$

Without loss of generality we can assume $u^* \leq 0$ (the analysis in the case $u^* \geq 0$ is analogous) and we will show $\varepsilon u^* \leq u \leq 0$. In order to prove $u \leq 0$ we choose $L > 0$ and $\psi = \min\{u^+, L\}$ with $u^+ = \max\{u, 0\}$. Then $0 \leq \psi \leq L$ for any $x \in \Omega^*$, and $\psi \in H_0^1(\Omega^*) \cap L^\infty(\Omega^*)$. Then, from (2.25) it follows

$$\begin{aligned} 0 &= \int_{\Omega^*} \nabla u \cdot \nabla \psi dx + \int_\Omega a^* \sinh\left(\frac{u}{\varepsilon} - u^*\right) \psi dx \\ &= \int_{\Omega^*} |\nabla \psi|^2 dx + \int_\Omega a^* \sinh\left(\frac{u}{\varepsilon} - u^*\right) \psi dx \ , \end{aligned}$$

since

$$\begin{aligned} 0 \leq u \leq L \Rightarrow \quad & \psi = u \ , \\ u < 0 \Rightarrow \quad & \psi = 0 \ , \\ u > L \Rightarrow \quad & \psi = L \ , \end{aligned}$$

implying $\int_{\Omega^*} \nabla u \cdot \nabla \psi dx = \int_{\Omega^*} |\nabla \psi|^2 dx$. Notice that $\int_\Omega a^* \sinh\left(\frac{u}{\varepsilon} - u^*\right) \psi dx \geq 0$ therefore $\int_{\Omega^*} |\nabla \psi|^2 dx = 0$ so $\psi = 0$ a.e in Ω^*, but $L > 0$ so we have $u^+ = 0$ a.e in Ω^* and $u \leq 0$ a.e in Ω^*. Let now $\psi = \max\left\{(u - \varepsilon u^*)^-, -L\right\}$

$$\begin{aligned} -L \leq u - \varepsilon u^* \leq 0 \Rightarrow \quad & \psi = u - \varepsilon u^* \ , \\ u - \varepsilon u^* > 0 \Rightarrow \quad & \psi = 0 \ , \\ u - \varepsilon u^* < -L \Rightarrow \quad & \psi = -L \ , \end{aligned}$$

and as before

$$\begin{aligned} 0 &= \int_{\Omega^*} \nabla u \cdot \nabla \psi dx + \int_\Omega a^* \sinh\left(\frac{u}{\varepsilon} - u^*\right) \psi dx \\ &= \int_{\Omega^*} |\nabla \psi|^2 dx + \int_\Omega a^* \sinh\left(\frac{u}{\varepsilon} - u^*\right) \psi dx = 0 \ , \end{aligned}$$

since also $\int_\Omega a^* \sinh\left(\frac{u}{\varepsilon} - u^*\right)\psi dx \geq 0$ then $\int_{\Omega^*} |\nabla\psi|^2 dx = 0$ and $\psi = 0$ a.e in Ω^*, but since $-L < 0$ so we have $\left(\frac{u}{\varepsilon} - u^*\right)^- = 0$ then $\frac{u}{\varepsilon} - u^* \geq 0$ a.e in Ω^*. Hence u is bounded in Ω^*. $\square$

Since u is a bounded function, the right hand side of equation (2.13) is also bounded and by classical elliptic regularity theory, $u \in W^{2,p}(\Omega^*)$ for all $p < \infty$. By Sobolev embeddings, u is then a $C^{1+\alpha}(\Omega^*)$ function for any $0 < \alpha < 1$.

In any domain D in the interior of Ω or $\Omega^*\backslash\Omega$, standard bootstrap arguments allow to improve the $W^{2,p}(D)$ regularity up to $C^\infty(D)$. We can conclude then with the following theorem:

Theorem 5. *For any $\varepsilon > 0$ there exists a unique weak solution u to (2.13), (2.14) in $H_0^1(\Omega^*)$. Moreover, $u \in W^{2,p}(\Omega^*)$ for any $p < \infty$ and $u \in C^\infty(D)$ for any $D \subset\subset \Omega$ and any $D \subset\subset \Omega^*\backslash\Omega$.*

2.3 Asymptotic behaviour near $\partial\Omega$

In this section we obtain asymptotic formulae, in the limit $\varepsilon \ll 1$, for the solutions of (2.13), (2.14) near $\partial\Omega$, as well as for the distribution of charges. As we will see the imbalance between positive and negative charges is concentrated in a very thin layer (of $O\left(\varepsilon^{1/2}\right)$ thickness) near $\partial\Omega$. If we assume $\partial\Omega$ to be sufficiently smooth, then the thickness of this boundary layer is much smaller than the radius of curvature of any point in $\partial\Omega$. Hence, one can think of the distribution of charges to be, locally near any point of $\partial\Omega$, essentially the same as for the problem in one dimension. First we will compute this one dimensional distribution and later in this section we will represent the solution to (2.13), (2.14) near $\partial\Omega$ in terms of the one dimensional solution.

2.3.1 The boundary layer

In order to analyze the distribution of net charge (i.e. of $\rho(x)$) in the neighborhood of $\partial\Omega$ for $\varepsilon \ll 1$ it is convenient first to study the one dimensional problem since the local structure of $\rho(x)$ in the direction orthogonal to $\partial\Omega$ at any (given) $x_S \in \partial\Omega$ will be given by the solution to such a problem. We expect that the negative and positive charges are balanced sufficiently far from $\partial\Omega$ and it is only in a thin layer around $\partial\Omega$ that net charge (that we assume without loss of generality to be positive) is concentrated.

We can rewrite equation (2.13) in Ω in the more convenient form

$$\Delta\overline{u} = \mu(e^{\overline{u}/\varepsilon} - e^{-\overline{u}/\varepsilon}) \ , \tag{2.26}$$

where

$$\mu = \sqrt{\frac{MN}{\int_\Omega e^{\frac{u-C}{\varepsilon}} \int_\Omega e^{-\frac{u-C}{\varepsilon}}}}, \quad u^* = \varepsilon \ln \sqrt{\frac{N\int_\Omega e^{\frac{u-C}{\varepsilon}}}{M\int_\Omega e^{-\frac{u-C}{\varepsilon}}}} = \varepsilon c^* \ , \tag{2.27}$$

and $\overline{u} = u - C - u^*$, with C given for the solution of the perfect conductor.

The expression (2.26) is particularly useful for the analysis close to $\partial\Omega$. Its one dimensional version (writing for simplicity u instead of $\overline{u}$) is

$$u_{xx} = \mu \left(e^{\frac{u}{\varepsilon}} - e^{-\frac{u}{\varepsilon}} \right) \ , \tag{2.28}$$

which integrating once leads to:

$$\frac{1}{2} u_x^2 = \mu\varepsilon \left[e^{\frac{u}{\varepsilon}} + e^{-\frac{u}{\varepsilon}} \right] + k \ ,$$

where the constant k can be computed such that $u_x \to 0$ and $u \to 0$ as $x \to -\infty$

$$k = -2\mu\varepsilon \ .$$

Then by defining $U = \frac{u}{\varepsilon}$, $X = \left(\frac{\mu}{\varepsilon}\right)^{\frac{1}{2}} x$ we arrive at:

$$\frac{1}{2} U_X^2 = \left(e^U + e^{-U} - 2 \right) \ ,$$

with explicit solutions

$$U(X) = \pm 2 \ln(\tanh(-\frac{\sqrt{2}}{2}(X + c))) \ .$$

The constant c will be chosen so that the net charge is given. Returning to the old variables (x, u), we get

$$u(x) = \pm 2\varepsilon \ln \left(\tanh(\frac{\sqrt{2}}{2} \left[\left(\frac{\mu}{\varepsilon}\right)^{\frac{1}{2}} |x| + c \right]) \right) \ , \tag{2.29}$$

which inserted in the right hand side of (2.28) yields the following formula for the charge density:

$$\rho(x) = \pm 4\mu \left(\frac{\cosh(\sqrt{2} \left[\left(\frac{\mu}{\varepsilon}\right)^{\frac{1}{2}} |x| + c \right])}{\sinh^2(\sqrt{2} \left[\left(\frac{\mu}{\varepsilon}\right)^{\frac{1}{2}} |x| + c \right])} \right) \ , \tag{2.30}$$

where c is assumed to be positive. This expression for $\rho\,(x)$ allows now the computation of the total charge, that we call σ:

$$\sigma = \int_{-\infty}^{0} \rho(x) dx = \pm \frac{2\sqrt{2}}{\sinh(\sqrt{2}c)} \left(\varepsilon\mu\right)^{\frac{1}{2}} \ ,$$

where the minus sign at the right hand side will be taken if $\sigma < 0$ and the plus sign otherwise. Therefore

$$c = \frac{1}{\sqrt{2}} \sinh^{-1} \left(\frac{2\sqrt{2} \left(\varepsilon\mu\right)^{\frac{1}{2}}}{|\sigma|} \right) \ .$$

Notice that this implies that in (2.29) the minus sign corresponds to the situation where the total charge is negative, and the plus sign corresponds to the situation where the total charge is positive. Without loss of generality, we shall always consider expression (2.29) with the plus sign at the right hand side so that $\sigma > 0$.

Since we will be working with $\varepsilon \ll 1$ it is convenient to expand the expression for c in ε and then obtain

$$c \simeq \frac{2\left(\varepsilon\mu\right)^{\frac{1}{2}}}{|\sigma|} \ . \tag{2.31}$$

Similarly, the charge density ρ can be expanded, for $|x| \ll \varepsilon^{1/2}$, as

$$\rho(x) \simeq \frac{\sigma\,|\sigma|}{2\varepsilon}\left[\frac{1}{\left[\frac{|\sigma|}{2\varepsilon}\,|x|+1\right]^2}\right] \ . \tag{2.32}$$

Notice that therefore

$$\rho(x) \simeq \frac{\sigma}{\nu} f\left(\frac{|x|}{\nu}\right) \ ,$$

where $\nu = \frac{2\varepsilon}{|\sigma|}$ and $f(\xi) = \frac{1}{(1+\xi)^2}$. Hence the charge density presents a boundary layer of $O(\nu)$ thickness, where the behaviour is selfsimilar, and formally $\rho(x) \to \sigma\delta(x=0)$.

2.3.2 Asymptotic expansion near $\partial\Omega$

In this section we will use the previous results for the one dimensional problem in order to provide a formula for the solution of the Poisson-Boltzmann equation in terms of an asymptotic expansion in the parameter ε. The main idea is to glue the one dimensional profiles for $u(x)$ in an $O(\varepsilon^{\frac{1}{2}})$ neighborhood of each point in $\partial\Omega$.

We introduce a parametrization of $\partial\Omega$ with a parameter η (or (η_1, η_2) in the case of $\partial\Omega$ being a surface). If $\partial\Omega$ is sufficiently smooth then the parametrization will also be smooth. Given a point $\mathbf{x} \in \Omega^*$ and sufficiently close to $\partial\Omega$ we can uniquely determine $\xi = dist(\mathbf{x}, \partial\Omega)$ as well as the value of η corresponding to the point $\mathbf{x}' \in \partial\Omega$ closest to $\mathbf{x}$. Indeed, Lemma 14.16 in [36] shows that for a $\partial\Omega \in C^k$, $k \geq 2$, then the distance function is also $C^k(\Gamma_\delta)$ where Γ_δ is the set of points $\mathbf{x}$ such that $dist(\mathbf{x}, \partial\Omega) < \delta$. Therefore one can label each point in an $O(\delta)$ neighborhood of $\partial\Omega$ (inside Ω and with δ sufficiently small) with a unique pair (ξ, η). Notice that the lines of constant η and constant ξ are then orthogonal. The mapping $\mathbf{x} \to (\xi, \eta)$ is invertible in that neighborhood provided $\partial\Omega \in C^2$.

We introduce next a cutoff function $\zeta(\cdot)$ defined in the following manner:

$$\begin{aligned} 0 \leq \zeta(s) \leq 1,\ \zeta(\cdot) \in C^\infty(0,\infty) \ , \\ \zeta(s) = 1,\ s \in [0, 1/2) \, , \\ \zeta(s) = 0,\ s > 1 \ , \end{aligned}$$

and rewrite the solution to (2.26) as

$$\overline{u}(\mathbf{x}) = \varepsilon \left(2\zeta \left(\frac{\xi(\mathbf{x})}{\delta} \right) \log \tanh \left(\left(\frac{\sqrt{2}(\varepsilon\mu)^{\frac{1}{2}}}{|\sigma(x_S)|} \right) \left[\frac{|\sigma(x_S)|}{2} \frac{\xi(\mathbf{x})}{\varepsilon} + 1 \right] \right) \right) + \varepsilon u_1(\mathbf{x}) \ , \tag{2.33}$$

where $\sigma(x_S)$ is a function that will be close to the surface charge density provided by the solution of the perfect conductor at $x_S = \eta(\mathbf{x})$, and where $0 < \delta \ll 1$ is a constant parameter. The function $u_1(\mathbf{x})$ will be determined so that $\overline{u}(\mathbf{x})$ satisfies (2.26).

Next we will write the differential equation satisfied by $u_1(\mathbf{x})$ that results from plugging (2.33) into (2.26). By denoting

$$u_0(\mathbf{x}) = 2\zeta \left(\frac{\xi(\mathbf{x})}{\delta} \right) \log \tanh \left(\left(\frac{\sqrt{2}(\varepsilon\mu)^{\frac{1}{2}}}{|\sigma(\eta(\mathbf{x}))|} \right) \left[\frac{|\sigma(\eta(\mathbf{x}))|}{2} \frac{\xi(\mathbf{x})}{\varepsilon} + 1 \right] \right) \ , \tag{2.34}$$

we find, from (2.26):

$$\begin{aligned} \Delta\overline{u} &= \varepsilon\Delta u_0 + \varepsilon\Delta u_1 = \mu \left(e^{\frac{\overline{u}}{\varepsilon}} - e^{-\frac{\overline{u}}{\varepsilon}} \right) \\ &= \mu(e^{u_0}e^{u_1} - e^{-u_0}e^{-u_1}) \ . \end{aligned}$$

By writing

$$\mu(e^{u_0}e^{u_1} - e^{-u_0}e^{-u_1}) = 2\mu \sinh(u_0) + 2\mu \cosh(u_0)u_1 + G\left[u_0, u_1\right] \ ,$$

where

$$G\left[u_0, u_1\right] \equiv \mu(e^{u_0}(e^{u_1} - 1 - u_1) - e^{-u_0}(e^{-u_1} - 1 + u_1)) \ , \tag{2.35}$$

we arrive at the following equation for u_1:

$$\varepsilon\Delta u_1 - 2\mu \cosh(u_0)u_1 = g(x) + G\left[u_0, u_1\right] \text{ in } \Omega \ , \tag{2.36}$$

with

$$g(x) \equiv 2\mu \sinh(u_0) - \varepsilon\Delta u_0 \ . \tag{2.37}$$

We aim to estimate u_1, solution to (2.36), and show that it is small for small values of ε. Since the right hand side of (2.36) consists of $g(x)$ plus $G\left[u_0, u_1\right]$ which is $O\left(u_1^2\right)$ for small u_1, one can expect that the size of u_1 (in terms of ε) is basically determined by the size of $g(x)$ provided it is small. In the next lemma we estimate that "size" of $g(x)$:

Lemma 6. *The function $g(x)$ defined by (2.34) and (2.37) satisfies*

$$g(x) = -\varepsilon^{\frac{1}{2}} \frac{2\sqrt{2\mu}\mathcal{H}(x)}{\sinh \left(\left(\frac{\sqrt{2}(\varepsilon\mu)^{\frac{1}{2}}}{|\sigma(\eta(x))|} \right) \left[|\sigma(\eta(x))| \frac{\xi(x)}{\varepsilon} + 2 \right] \right)} + O(\varepsilon) \ , \tag{2.38}$$

where $\mathcal{H}(x)$ is the curvature of the level line of the distance function that contains the point x and $\varepsilon > 0$ is sufficiently small.

Proof. We present first the proof in two space dimensions for the sake of simplicity. The proof in N dimensions is a trivial generalization where the parametrization of $\partial\Omega$ is $(N-1)-$dimensional. First we note that in a sufficiently small neighborhood of $\partial\Omega$ the mapping from (x,y) to (ξ,η) is an invertible diffeomorphism and the laplacian operator transforms into:

$$\Delta u_0 = \frac{\partial^2 u_0}{\partial \xi^2} + 2\frac{\partial^2 u_0}{\partial \xi \partial \eta}\left[\nabla\xi\cdot\nabla\eta\right] + \frac{\partial^2 u_0}{\partial \eta^2}|\nabla\eta|^2 + \Delta\xi\frac{\partial u_0}{\partial \xi} + \Delta\eta\frac{\partial u_0}{\partial \eta}\ . \tag{2.39}$$

By the choice of ξ and η coordinates, the isolines are mutually orthogonal and hence $\nabla\xi\cdot\nabla\eta = 0$. On the other hand, $\Delta\xi$ equals the curvature of the level lines $\xi = const$, which is bounded by the hypothesis on the regularity of $\partial\Omega$, and so are $\Delta\eta$ and $|\nabla\eta|$. We can now compute and estimate $\frac{\partial u_0}{\partial \xi}, \frac{\partial u_0}{\partial \eta}, \frac{\partial^2 u_0}{\partial \xi^2}, \frac{\partial^2 u_0}{\partial \eta^2}$: let $\alpha(\xi,\eta) = \left(\frac{\sqrt{2}(\varepsilon\mu)^{\frac{1}{2}}}{|\sigma(\eta)|}\right)\left[\frac{|\sigma(\eta)|}{2}\frac{\xi}{\varepsilon}+1\right]$, then

$$\frac{\partial u_0}{\partial \xi} = \frac{\sqrt{2\mu}}{\varepsilon^{\frac{1}{2}}}\zeta\left(\frac{\xi}{\delta}\right)\frac{2}{\sinh(2\alpha)} + \frac{2}{\delta}\zeta'\left(\frac{\xi}{\delta}\right)\log\tanh(\alpha)\ , \tag{2.40}$$

$$\frac{\partial u_0}{\partial \eta} = -4\sqrt{2}(\varepsilon\mu)^{\frac{1}{2}}\frac{\sigma'(\eta)}{\sigma(\eta)^2}\zeta\left(\frac{\xi}{\delta}\right)\frac{1}{\sinh\left(2\alpha\right)}\ , \tag{2.41}$$

$$\begin{aligned}\frac{\partial^2 u_0}{\partial \xi^2} = &-4(\frac{\mu}{\varepsilon})\zeta\left(\frac{\xi}{\delta}\right)\frac{\coth(2\alpha)}{\sinh\left(2\alpha\right)} + \frac{2\sqrt{2}(\mu)^{\frac{1}{2}}}{\varepsilon^{\frac{1}{2}}\delta}\zeta'\left(\frac{\xi}{\delta}\right)\frac{1}{\sinh\left(2\alpha\right)}\\ &+\left(\frac{2\sqrt{2}(\mu)^{\frac{1}{2}}}{\varepsilon^{\frac{1}{2}}\delta}\right)\zeta'\left(\frac{\xi}{\delta}\right)\frac{1}{\sinh\left(2\alpha\right)} + \frac{2}{\delta}\zeta''\left(\frac{\xi}{\delta}\right)\log\tanh(\alpha)\ ,\end{aligned} \tag{2.42}$$

$$\begin{aligned}\frac{\partial^2 u_0}{\partial \eta^2} = &-16(\varepsilon\mu)\left(\frac{\sigma'(\eta)}{\sigma(\eta)^2}\right)^2\zeta\left(\frac{\xi}{\delta}\right)\frac{\cosh(2\alpha)}{\sinh^2\left(2\alpha\right)}\\ &+4\sqrt{2}(\varepsilon\mu)^{\frac{1}{2}}\zeta\left(\frac{\xi}{\delta}\right)\left(\frac{\left[\sigma(\eta)\right]^2\sigma''(\eta)-2\sigma(\eta)\left[\sigma'(\eta)\right]^2}{\sigma(\eta)^4}\right)\frac{1}{\sinh\left(2\alpha\right)}\ .\end{aligned} \tag{2.43}$$

Notice that the derivatives of the cutoff function $\zeta\left(\frac{\xi}{\delta}\right)$ are nonzero only when $\xi = O\left(\delta\right)$, and are always multiplied by functions, namely $\frac{1}{\sinh(2\alpha)}$ and $\log\tanh(\alpha)$, that decay exponentially fast to zero as $\alpha\to\infty$. In fact, they are both $O\left(e^{-O(\delta)/\varepsilon^{1/2}}\right)$ and hence much smaller than any power of ε for $\varepsilon \ll 1$. On the other hand the first term at the right hand side of (2.42), equals $2\frac{\mu}{\varepsilon}\zeta\left(\frac{\xi}{\delta}\right)\sinh(u_0) + o\left(e^{-O(\delta)/\varepsilon^{1/2}}\right)$ so that

$$\begin{aligned}&-4(\frac{\mu}{\varepsilon})\zeta\left(\frac{\xi}{\delta}\right)\frac{\coth(2\alpha)}{\sinh\left(2\alpha\right)} - 2\frac{\mu}{\varepsilon}\sinh(u_0) = 2\frac{\mu}{\varepsilon}\left[\zeta\left(\frac{\xi}{\delta}\right)-1\right]\sinh(u_0) + o\left(e^{-O(\delta)/\varepsilon^{1/2}}\right)\\ &= -4\frac{\mu}{\varepsilon}\left[\zeta\left(\frac{\xi}{\delta}\right)-1\right]\frac{\coth(2\alpha)}{\sinh\left(2\alpha\right)} + o\left(e^{-O(\delta)/\varepsilon^{1/2}}\right) = o\left(e^{-O(\delta)/\varepsilon^{1/2}}\right)\ .\end{aligned}$$

The terms (2.41) and (2.43) are both $O\left(\varepsilon^0\right)$ due to the fact that the $\varepsilon^{1/2}$ or ε factors cancel out with identical factors coming from $\sinh\left(2\alpha\right)$ and $\sinh^2\left(2\alpha\right)$ when $\xi \ll 1$. Finally, the

first term at the right hand side of (2.40) is, for $\xi \lesssim O(\varepsilon)$, of order $O(\varepsilon^{-1})$ and hence

$$\frac{\partial u_0}{\partial \xi} \sim \frac{1}{\varepsilon^{\frac{1}{2}}} \frac{2\sqrt{2\mu}}{\sinh\left(\left(\frac{\sqrt{2}(\varepsilon\mu)^{\frac{1}{2}}}{|\sigma(\eta)|}\right)\left[|\sigma(\eta)|\,\frac{\xi}{\varepsilon}+2\right]\right)} \ . \tag{2.44}$$

In higher space dimensions, the laplacian operator contains the same terms as those at the right hand side of expression (2.39), but for each of the η_i (choosing them along the principal directions so that the corresponding curvature lines are mutually orthogonal) that parametrize the boundary. Each of these terms can be estimated in the same way as we did above. This concludes the proof of the lemma. □

If one formally neglects the $O(\varepsilon)$ −terms and the nonlinearities in (2.36), and also neglects the $O(\varepsilon)$ −terms in $g(x)$ given by (2.38) , then it follows

$$\begin{aligned} u_1 &\sim \varepsilon^{\frac{1}{2}} \frac{\sqrt{2/\mu}\mathcal{H}(x)}{\cosh(u_0)\sinh\left(\left(\frac{\sqrt{2}(\varepsilon\mu)^{\frac{1}{2}}}{|\sigma(\eta)|}\right)\left[|\sigma(\eta)|\,\frac{\xi(x)}{\varepsilon}+2\right]\right)} \\ &= \frac{\varepsilon^{\frac{1}{2}}}{4} \frac{\sinh\left(\left(\frac{\sqrt{2}(\varepsilon\mu)^{\frac{1}{2}}}{|\sigma(\eta)|}\right)\left[|\sigma(\eta)|\,\frac{\xi(x)}{\varepsilon}+2\right]\right)\sqrt{2/\mu}\mathcal{H}(x)}{\cosh^4\left(\left(\frac{\sqrt{2}(\varepsilon\mu)^{\frac{1}{2}}}{|\sigma(\eta)|}\right)\left[|\sigma(\eta)|\,\frac{\xi(x)}{2\varepsilon}+1\right]\right)+\sinh^4\left(\left(\frac{\sqrt{2}(\varepsilon\mu)^{\frac{1}{2}}}{|\sigma(\eta)|}\right)\left[|\sigma(\eta)|\,\frac{\xi(x)}{2\varepsilon}+1\right]\right)} \\ &\equiv u_1^0(x) \ , \end{aligned} \tag{2.45}$$

and therefore, the leading order contribution to u is given by $C + u^* + \varepsilon u_0$ and we can compute the parameter μ based on it. Since

$$\int_\Omega e^{\frac{u-C}{\varepsilon}} \int_\Omega e^{-\frac{u-C}{\varepsilon}} = \int_\Omega e^{u_0} \int_\Omega e^{-u_0} \ ,$$

and

$$\int_\Omega e^{u_0} \simeq \left(\int_\Omega (e^{u_0}-1)\right)+|\Omega| = -\int_\Omega \cosh^{-2}\left(\left(\frac{\sqrt{2}(\varepsilon\mu)^{\frac{1}{2}}}{|\sigma(\eta)|}\right)\left[|\sigma(\eta)|\,\frac{\xi(x)}{2\varepsilon}+1\right]\right)+|\Omega| \underset{\varepsilon\to 0}{\to} |\Omega| \ , \tag{2.46}$$

$$\begin{aligned} \int_\Omega e^{-u_0} &\simeq \left(\int_\Omega \left(e^{-u_0}-1\right)\right)+|\Omega| \qquad (2.47) \\ &= \int_\Omega \sinh^{-2}\left(\left(\frac{\sqrt{2}(\varepsilon\mu)^{\frac{1}{2}}}{|\sigma(\eta)|}\right)\left[|\sigma(\eta)|\,\frac{\xi(x)}{2\varepsilon}+1\right]\right)+|\Omega| \underset{\varepsilon\to 0}{\to} \frac{-M+N}{\mu}+|\Omega| \ , \end{aligned}$$

we have by (2.27)

$$\mu = \sqrt{\frac{MN}{\int_\Omega e^{\frac{u-C}{\varepsilon}} \int_\Omega e^{-\frac{u-C}{\varepsilon}}}} \underset{\varepsilon\to 0}{\to} \sqrt{\frac{MN}{\left(\frac{-M+N}{\mu}+|\Omega|\right)|\Omega|}} \ , \tag{2.48}$$

implying

$$\mu \underset{\varepsilon \to 0}{\to} \frac{M}{|\Omega|} \ . \tag{2.49}$$

Henceforth one is led to consider μ to be a uniformly bounded (in ε) parameter. We will consider it to be a constant and solve equation (2.36) based on this simplifying assumption. After that we will discuss on how the arguments need to be modified to consider a variable μ.

Note that, by the definition of c^* given by (2.27), using formulae (2.46), (2.47) and replacing $u - C$ by $u^* + \varepsilon u_0$, it follows then the trivial equation

$$c^* = \ln \sqrt{\frac{N e^{c^*} |\Omega|}{M e^{-c^* \frac{N}{M}} |\Omega|}} \ ,$$

implying that c^* is a free parameter that can only be determined from higher order corrections of u.

Remind that u is then written in Ω in the form

$$u = C + u^* + \varepsilon u_0 + \varepsilon u_1 \ . \tag{2.50}$$

Since we have also to take into consideration the problem in $\Omega^* \backslash \Omega$ we will also write there

$$u = \hat{u} + \varepsilon \hat{u}_0 + \varepsilon \hat{u}_1 \ , \tag{2.51}$$

where $\hat{u}$ is the potential for the perfect conductor case (that is $\Delta \hat{u} = 0$, $\hat{u} = 0$ in $\partial\Omega^*$ $\hat{u} = C$ in $\partial\Omega$) and $\hat{u}_0$ will be taken such that $\hat{u} + \varepsilon \hat{u}_0$ and its normal derivative in $\partial\Omega$ match continuously with $C + u^* + \varepsilon u_0 = C + \varepsilon (c^* + u_0)$ and its normal derivative respectively. Matching of the normal derivatives implies

$$\varepsilon \frac{\partial \hat{u}_0}{\partial n} = \varepsilon \frac{\partial u_0}{\partial n} - \frac{\partial \hat{u}}{\partial n} = -\sigma (x_S) + \sigma_0 (x_S) \ \text{ in } \partial\Omega \ ,$$

where $\sigma_0 (x_S)$ is the charge density of the perfect conductor. Let us denote

$$\sigma_1 (x_S) = -\frac{\partial \hat{u}_0}{\partial n} \ .$$

Hence one must find two functions $\hat{u}_0$ and $\sigma_1 (x_S)$ so that

$$\hat{u}_0 = c^* + u_0 = c^* + 2 \ln \left(\tanh(\frac{\sqrt{2} (\varepsilon \mu)^{1/2}}{|\sigma_0 (x_S) + \varepsilon \sigma_1 (x_S)|}) \right) \ \text{ in } \partial\Omega \ , \tag{2.52}$$

$$\frac{\partial \hat{u}_0}{\partial n} = -\sigma_1 (x_S) \ \text{ in } \partial\Omega \ , \tag{2.53}$$

and $\hat{u}_0$ is harmonic or its laplacian in $\Omega^* \backslash \Omega$ does not grow much with ε. Moreover, since $\int_{\partial\Omega} \sigma (x_S) = N - M$, we must impose

$$\int_{\partial\Omega} \sigma_1 (x_S) = 0 \ , \tag{2.54}$$

in order to preserve the net amount of charge. This requires an appropriate choice of c^*. This is done in the following lemma:

Lemma 7. *If $\partial\Omega \in C^{3+\alpha}$, then there exists a constant c^*, a function $\hat{u}_0 \in C^{2+\alpha}\left(\overline{\Omega^*\backslash\Omega}\right)$ and a $C^{2+\alpha}$ function $\sigma_1(x_S)$ defined in $\partial\Omega$ such that conditions (2.52), (2.53) and (2.54) are satisfied and*

$$|\Delta\hat{u}_0| \leq C_0\varepsilon \ ,$$

with C_0 independent of ε. The function $\sigma_1(x_S)$ is such that

$$\sigma_1(x_S) = -\frac{2\int_{\partial\Omega}\mathcal{N}\left[\ln|\sigma_0(x_S)|\right]}{M-N}\sigma_0(x_S) + 2\mathcal{N}\left[\ln|\sigma_0(x_S)|\right] + O(\varepsilon) \ . \tag{2.55}$$

where $\mathcal{N}[\cdot]$ is the Dirichlet to Neumann operator, restricted to $\partial\Omega$ and with zero Dirichlet data at $\partial\Omega^*$, for Laplace equation in $\Omega^*\backslash\Omega$.

Proof. We write $\hat{u}_0 = \hat{u}_0^{(1)} + \hat{u}_0^{(2)}$, where

$$\Delta\hat{u}_0^{(1)} = 0 \text{ in } \Omega^*\backslash\Omega \ , \tag{2.56}$$

$$\hat{u}_0^{(1)}\Big|_{\partial\Omega} = c^* + 2\ln\left(\tanh\frac{\sqrt{2}\,(\varepsilon\mu)^{1/2}}{|\sigma_0(x_S)|}\right) \ , \tag{2.57}$$

$$\hat{u}_0^{(1)}\Big|_{\partial\Omega^*} = 0 \ , \tag{2.58}$$

and $\hat{u}_0^{(2)}$ is such that

$$\hat{u}_0^{(2)}\Big|_{\partial\Omega} = 2\ln\frac{\tanh\frac{\sqrt{2}(\varepsilon\mu)^{1/2}}{|\sigma_0(x_S)+\varepsilon\sigma_1(x_S)|}}{\tanh\frac{\sqrt{2}(\varepsilon\mu)^{1/2}}{|\sigma_0(x_S)|}} \text{ in } \Omega^*\backslash\Omega \ , \tag{2.59}$$

$$\left.\frac{\partial\hat{u}_0^{(2)}}{\partial n}\right|_{\partial\Omega} = 0 \ , \tag{2.60}$$

$$\hat{u}_0^{(2)}\Big|_{\partial\Omega^*} = 0 \ . \tag{2.61}$$

Notice that by classical elliptic theory and the hypothesis of the smoothness of $\partial\Omega$ ($\in C^{3+\alpha}$), $\frac{\partial\hat{u}_0^{(1)}}{\partial n}$ is a $C^{2+\alpha}$ smooth function for every $\varepsilon > 0$. Since we are imposing $\left.\frac{\partial\hat{u}_0^{(2)}}{\partial n}\right|_{\partial\Omega} = 0$, then $\sigma_1(x_S)$ is also a $C^{2+\alpha}$ function. On the other hand the right hand side of (2.59) is $O(\varepsilon)$ and so is the tangential derivative of $\hat{u}_0^{(2)}$ along $\partial\Omega$. By choosing

$$\hat{u}_0^{(2)} = 2\zeta\left(\frac{\xi(\mathbf{x})}{\delta}\right)\ln\frac{\tanh\left(\frac{\sqrt{2}(\varepsilon\mu)^{1/2}}{|\sigma_0(\eta(\mathbf{x}))+\varepsilon\sigma_1(\eta(\mathbf{x}))|}\right)}{\tanh\left(\frac{\sqrt{2}(\varepsilon\mu)^{1/2}}{|\sigma_0(\eta(\mathbf{x}))|}\right)} \ ,$$

where $(\xi(\mathbf{x}), \eta(\mathbf{x}))$ is the parametrization introduced at the beginning of this section and $\mathbf{x} \in \overline{\Omega^*\backslash\Omega}$, both conditions (2.60) and (2.61) are satisfied. Notice that $\hat{u}_0^{(2)} \in C^{2+\alpha}(\overline{\Omega^*\backslash\Omega})$. When computing $\Delta\hat{u}_0^{(2)}$, both the derivatives, up to second order, in the ξ and η variables are bounded and $O(\varepsilon)$. Finally, we find the value of c^* such that condition (2.54) is satisfied.

This is done through the Dirichlet to Neumann operator $\mathcal{N}$ that maps the boundary data at $\partial\Omega$ for the problem

$$\Delta v = 0 \text{ in } \Omega^* \backslash \Omega,$$
$$v|_{\partial\Omega} = v_0, \;\; v|_{\partial\Omega^*} = 0 \; ,$$

to

$$\left.\frac{\partial v}{\partial n}\right|_{\partial\Omega} = \mathcal{N} v_0 \; .$$

Then

$$\sigma_1 (x_S) = -c^* \mathcal{N} 1 - 2\mathcal{N}\left[\ln\left(\tanh(\frac{\sqrt{2}\,(\varepsilon\mu)^{1/2}}{|\sigma_0 (x_S)|})\right)\right] \; ,$$

and condition (2.54) implies then

$$c^* = -\frac{2\int_{\partial\Omega}\mathcal{N}\left[\ln\left(\tanh(\frac{\sqrt{2}(\varepsilon\mu)^{1/2}}{|\sigma_0(x_S)|})\right)\right]}{\int_{\partial\Omega}\mathcal{N}1} = -\log(2\mu\varepsilon) + \frac{2\int_{\partial\Omega}\mathcal{N}\left[\ln|\sigma_0(x_S)|\right]}{\int_{\partial\Omega}\mathcal{N}1} + O(\varepsilon) \; .$$

Notice that, by Green's first identity, $\int_{\partial\Omega}\mathcal{N}1 = \int_{\partial\Omega} 1\mathcal{N}1 = -\int_{\Omega^*\backslash\Omega} u\Delta u - \int_{\Omega^*\backslash\Omega}|\nabla u|^2 = -\int_{\Omega^*\backslash\Omega}|\nabla u|^2 < 0$ with u harmonic and such that $u = 1$ at $\partial\Omega$, $u = 0$ at $\partial\Omega^*$. Henceforth formula (2.55) follows. This ends the proof of the lemma. □

By the previous lemma, the functions u_1 and $\hat{u}_1$ defined in (2.50) and (2.51) must be found so that they match continuously and differentiably across $\partial\Omega$. Since $\Delta\hat{u}_1 = -\Delta\hat{u}_0$ at $\Omega^*\backslash\Omega$, we can write for

$$\bar{u}_1 = \left\{ \begin{array}{cc} u_1 & x \in \Omega \\ \hat{u}_1 & x \in \Omega^*\backslash\Omega \end{array} \right\} \; ,$$

using (2.36), the following equation:

$$\mathcal{L}\overline{u}_1 \equiv \varepsilon\Delta\overline{u}_1 - \left\{ \begin{array}{c} 2\mu\cosh(u_0) \text{ in } \Omega \\ 0 \text{ in } \Omega^*\backslash\Omega \end{array} \right\} \overline{u}_1 = \left\{ \begin{array}{c} g(x) + G\left[u_0, \overline{u}_1\right] \text{ in } \Omega \\ -\varepsilon\Delta\hat{u}_0 \text{ in } \Omega^*\backslash\Omega \end{array} \right\} \; , \tag{2.62}$$

defined now in Ω^* with boundary condition $\overline{u}_1|_{\partial\Omega^*} = 0$. Our strategy will be to design a fixed point argument and we need to solve first the following auxiliary problem:

$$\mathcal{L}u \equiv \varepsilon\Delta u - \left\{ \begin{array}{c} 2\mu\cosh(u_0) \text{ in } \Omega \\ 0 \text{ in } \Omega^*\backslash\Omega \end{array} \right\} u = H(x) \text{ in } \Omega^* \; , \tag{2.63}$$

$$u = 0 \text{ on } \partial\Omega^* \; , \tag{2.64}$$

with the hypothesis that

$$|H(x)| \leq ||H||_{L^\infty(\Omega)} \leq C \quad \text{for any} \;\; x \in \Omega \; , \tag{2.65}$$

and

$$|H(x)| \leq C\varepsilon^2 \;\; \text{for any } x \in \Omega^*\backslash\Omega \; , \tag{2.66}$$

for some constant C independent of ε. Notice that the problem (2.63), (2.64) admits a weak formulation in the form: find v in $H_0^1(\Omega^*)$ such that

$$\int_{\Omega^*} (\varepsilon \nabla u \cdot \nabla v + G(x)\, uv) dx = -\int_{\Omega^*} H(x)\, v dx \ , \tag{2.67}$$

where

$$G(x) = \begin{cases} 2\mu \cosh(u_0) & \text{in } \Omega \\ 0 & \text{in } \Omega^* \backslash \Omega \end{cases} \ ,$$

for any $v \in H_0^1(\Omega^*)$.

Lemma 8. *If $H(x)$ satisfies (2.65), (2.66), then there exists a unique weak solution to problem (2.67) in $H_0^1(\Omega^*)$ and the solution is such that*

$$||u||_{Y_\varepsilon} \equiv \left(\varepsilon \int_{\Omega^*} |\nabla u|^2 dx + \varepsilon \int_{\Omega^* \backslash \Omega} |u|^2 dx + \int_\Omega u^2 dx \right)^{\frac{1}{2}} \leq C(||H||_{L^\infty(\Omega)} + \varepsilon)$$

for some constant C independent of ε.

Proof. Lax-Milgram theorem, and the fact that Ω^* is bounded so that $||\nabla u||_{L^2(\Omega^*)} \geq C\, ||u||_{L^2(\Omega^*)}$, yield existence of a unique solution to the weak problem (2.67). By taking $v = u$ in (2.67) we obtain

$$\varepsilon \int_{\Omega^*} |\nabla u|^2 dx + 2\mu \int_\Omega \cosh(u_0)\, u^2 dx = -\int_{\Omega^*} H(x) u dx \ .$$

Since $\cosh(u_0) \geq 1$, we can write

$$C \left(\varepsilon \int_{\Omega^*} |\nabla u|^2 dx + \int_\Omega u^2 dx \right) \leq -\int_{\Omega^*} H(x) u dx \ . \tag{2.68}$$

By Poincaré's inequality, $\int_{\Omega^*} u^2 dx \leq C \int_{\Omega^*} |\nabla u|^2 dx$ and therefore

$$C\, ||u||^2_{L^2(\Omega^*, w dx)} \leq -\int_{\Omega^*} H(x) u dx \ , \tag{2.69}$$

for some constant C independent of ε and where $w(x) = \begin{cases} \varepsilon & x \in \Omega^* \backslash \Omega \\ 1 & x \in \Omega \end{cases}$. By (2.68) and (2.69) then

$$||u||^2_{Y_\varepsilon} \leq C \left| \int_{\Omega^*} H(x) u dx \right| \ . \tag{2.70}$$

Using Hölder's inequality at the right hand side of (2.70) we obtain

$$\begin{aligned} \left| \int_{\Omega^*} H(x) u dx \right| &\leq \int_\Omega |H(x) u|\, dx + \int_{\Omega^* \backslash \Omega} |H(x) u|\, dx \\ &\leq ||H||_{L^\infty(\Omega)} \int_\Omega |u|\, dx + C\varepsilon^2 \int_{\Omega^* \backslash \Omega} |u|\, dx \\ &\leq ||H||_{L^\infty(\Omega)} |\Omega|^{\frac{1}{2}} ||u||_{L^2(\Omega)} + C\varepsilon^2 |\Omega^* \backslash \Omega|^{\frac{1}{2}} ||u||_{L^2(\Omega^* \backslash \Omega)} \\ &\leq C(||H||_{L^\infty(\Omega)} + \varepsilon) ||u||_{Y_\varepsilon} \ , \end{aligned}$$

to conclude

$$||u||_{Y_\varepsilon} \leq C(||H||_{L^\infty(\Omega)} + \varepsilon) \ ,$$

for some constant C independent of ε. □

Next we will obtain suitable L^∞ estimates for the weak solution defined by (2.63),(2.64). More precisely, we prove the following lemma:

Lemma 9. *The weak solution of (2.63),(2.64) satisfies the following inequality*

$$||u||_{L^\infty(\Omega^*)} \leq C\varepsilon + \left|\left|\frac{H(x)}{\mu\cosh(u_0(x))}\right|\right|_{L^\infty(\Omega)} . \tag{2.71}$$

Proof. We write $u = u_\Omega + u_{\Omega^c}$ where

$$\begin{aligned} \mathcal{L}u_\Omega &= H(x)\chi_\Omega(x) \ \text{ in } \Omega^* , \\ u_\Omega &= 0 \text{ on } \partial\Omega^* , \end{aligned} \tag{2.72}$$

and

$$\begin{aligned} \mathcal{L}u_{\Omega^c} &= H(x)\chi_{\Omega^c}(x) \ \text{ in } \Omega^* , \\ u_{\Omega^c} &= 0 \text{ on } \partial\Omega^* . \end{aligned} \tag{2.73}$$

Since the right hand side of (2.73) is bounded by $C\varepsilon^2$ (by (2.66)), elliptic theory yields

$$\varepsilon\,||u_{\Omega^c}||_{W^{2,p}(\Omega^*)} \leq C\varepsilon^2 ,$$

for any $p < \infty$ and hence, by Sobolev embeddings,

$$||u_{\Omega^c}||_{L^\infty(\Omega^*)} \leq C\varepsilon . \tag{2.74}$$

In order to estimate the L^∞ norm of u_Ω we write

$$u_\Omega = \sup_\Omega \frac{|H(x)|}{\mu\cosh(u_0(x))} + w , \tag{2.75}$$

with w satisfying then

$$\mathcal{L}w = \left(H(x) + \cosh(u_0(x)) \sup_\Omega \frac{|H(x)|}{\mu\cosh(u_0(x))}\right)\chi_\Omega(x) \geq 0 ,$$

and

$$w = -\sup_\Omega \frac{|H(x)|}{\mu\cosh(u_0(x))} \ \text{ at } \partial\Omega^*.$$

By the weak maximum principle (Theorem 8.1, [36]), $\sup w \leq \left(-\sup_\Omega \frac{|H(x)|}{\mu\cosh(u_0(x))}\right)^+ = 0$. Therefore

$$u_\Omega \leq \sup_\Omega \frac{|H(x)|}{\mu\cosh(u_0(x))} . \tag{2.76}$$

Analogously, by replacing the sup by inf in (2.75) one can show

$$u_\Omega \geq \inf_\Omega \frac{H(x)}{\mu\cosh(u_0(x))} , \tag{2.77}$$

and hence from (2.74), (2.76), (2.77) inequality (2.71) follows. □

We return next to the nonlinear problem (2.62) and use the estimate (2.71) to estimate

$$||\bar{u}_1||_{L^\infty(\Omega^*)} \leq C\varepsilon + \left|\left|\frac{g(x)}{\mu\cosh(u_0(x))}\right|\right|_{L^\infty(\Omega)} + \left|\left|\frac{G[u_0(x),\overline{u}_1(x)]}{\mu\cosh(u_0(x))}\right|\right|_{L^\infty(\Omega)} . \tag{2.78}$$

The first term of the right hand side of (2.78) can be estimated, using lemma 6 and the boundedness of the function $\frac{1}{\sinh(2\alpha)\cosh(u_0)} = \frac{\sinh(2\alpha)}{4(\cosh^4(\alpha)+\sinh^4(\alpha))}$, by $C\varepsilon^{1/2}$. Since the nonlinear term $G[u_0,\overline{u}_1]$ given by (2.35) grows quadratically with $\overline{u}_1$ for $\overline{u}_1$ sufficiently small we can deduce from (2.78) the estimate

$$||\bar{u}_1||_{L^\infty(\Omega^*)} \leq C\varepsilon + C\varepsilon^{1/2} + ||\overline{u}_1||^2_{L^\infty(\Omega)} , \tag{2.79}$$

and hence $||\bar{u}_1||_{L^\infty(\Omega^*)} \leq 2C\varepsilon^{1/2}$ for ε sufficiently small. Of course, we are relying on the existence of solution to the nonlinear problem and the boundedness of $||\bar{u}_1||_{L^\infty(\Omega^*)}$ in order to write inequality (2.79). These facts follow from the general existence and uniqueness theorem proved in Section 2.2, or can be shown by using a fixed point argument for ε sufficiently small. This is done in the following theorem:

Theorem 10. *For $\varepsilon < \overline{\varepsilon}$ with $\overline{\varepsilon}$ sufficiently small, there exists a unique bounded solution $\bar{u}_1$ to equation (2.62) and it satisfies*

$$||\bar{u}_1||_{L^\infty(\Omega^*)} \leq C\varepsilon^{1/2} ,$$

with C being a constant independent of ε.

Proof. We consider the mapping T that assigns to a function v (in a suitable space to be defined below) the solution to the problem

$$\begin{aligned} \mathcal{L}\overline{u}_1 &= \left\{ \begin{array}{c} g(x) + G[u_0, v] \text{ in } \Omega \\ -\varepsilon\Delta\hat{u}_0 \text{ in } \Omega^*\backslash\Omega \end{array} \right\} , \\ \overline{u}_1|_{\partial\Omega^*} &= 0 , \end{aligned} \tag{2.80}$$

and show that it has a unique fixed point if ε is sufficiently small. The estimates obtained in the previous lemmas suggest to look for the solution in the space

$$X_\varepsilon = \left\{ \overline{u}_1 : \Omega^* \to \mathbb{R} / \, ||\overline{u}_1||_{X_\varepsilon} \equiv ||\overline{u}_1||_{Y_\varepsilon} + ||\overline{u}_1||_{L^\infty(\Omega^*)} < \infty \right\} .$$

We therefore have to show, in order to apply Banach's fixed point theorem, that T maps a closed ball of radius ε^α (with $\frac{1}{2} < \alpha < 1$) into itself and is a contraction for ε sufficiently small. If we denote by $H(x)$ the right hand side of (2.80) then the following estimates follow: 1)

$$\begin{aligned} ||H(x)||_{L^\infty(\Omega)} &\leq ||g||_{L^\infty(\Omega)} + ||G[u_0, v]||_{L^\infty(\Omega)} \\ &\leq C + ||G[u_0, v]||_{L^\infty(\Omega)} \leq C\left(e^{||v||_{L^\infty(\Omega)}} - ||v||_{L^\infty(\Omega)}\right) , \end{aligned} \tag{2.81}$$

where we have used

$$\begin{aligned}||G\left[u_0,v\right]||_{L^\infty(\Omega)} &\leq ||\mu e^{u_0}(e^v-1-v)||_{L^\infty(\Omega)}+\left|\left|\mu e^{-u_0}(e^{-v}-1+v)\right|\right|_{L^\infty(\Omega)}\\ &\leq \frac{C}{2}(||e^v-1-v||_{L^\infty(\Omega)}+\left|\left|e^{-v}-1+v\right|\right|_{L^\infty(\Omega)})\\ &\leq C(e^{||v||_{L^\infty(\Omega)}}-1-||v||_{L^\infty(\Omega)})\ ,\end{aligned}$$

2)

$$||H\left(x\right)||_{L^\infty(\Omega^*\backslash\Omega)}=||-\varepsilon\Delta\hat{u}_0||_{L^\infty(\Omega^*\backslash\Omega)}\leq C\varepsilon^2\ , \tag{2.82}$$

and 3)

$$\begin{aligned}\left|\left|\frac{H\left(x\right)}{\mu\cosh\left(u_0\left(x\right)\right)}\right|\right|_{L^\infty(\Omega)} &\leq \left|\left|\frac{g\left(x\right)}{\mu\cosh\left(u_0\left(x\right)\right)}\right|\right|_{L^\infty(\Omega)}+\left|\left|\frac{G\left[u_0\left(x\right),v\left(x\right)\right]}{\mu\cosh\left(u_0\left(x\right)\right)}\right|\right|_{L^\infty(\Omega)}\\ &\leq C\varepsilon^{\frac{1}{2}}+C(e^{||v||_{L^\infty(\Omega)}}-1-||v||_{L^\infty(\Omega)})\ .\end{aligned} \tag{2.83}$$

Using (2.81), (2.82) and Lemma 8 we obtain

$$||u||_{Y_\varepsilon}\leq C(\varepsilon^2+e^{||v||_{L^\infty(\Omega)}}-||v||_{L^\infty(\Omega)})\ ,$$

and using (2.83) and Lemma 9 we obtain

$$||u||_{L^\infty(\Omega^*)}\leq C(\varepsilon+\varepsilon^{\frac{1}{2}}+e^{||v||_{L^\infty(\Omega)}}-1-||v||_{L^\infty(\Omega)})\ ,$$

so that

$$||u||_{X_\varepsilon}\leq C(\varepsilon+\varepsilon^{\frac{1}{2}}+e^{||v||_{L^\infty(\Omega)}}-1-||v||_{L^\infty(\Omega)})\ .$$

Hence, if $||v||_{L^\infty(\Omega)}\leq\varepsilon^{1/4}$, then

$$||u||_{X_\varepsilon}\leq 2C\varepsilon^{\frac{1}{2}}<\varepsilon^{1/4}\ , \tag{2.84}$$

for ε sufficiently small. This implies that the mapping T maps the ball of radius $\varepsilon^{1/4}$ in the X_ε topology into itself. It is also a contraction: the function

$$U\equiv Tv_1-Tv_2\ ,$$

satisfies

$$\begin{aligned}\mathcal{L}U&=\left\{\begin{array}{c}G\left[u_0,v_1\right]-G\left[u_0,v_2\right]\ \text{in}\ \Omega\\ 0\ \text{in}\ \Omega^*\backslash\Omega\end{array}\right\}\ ,\\ U|_{\partial\Omega^*}&=0\ .\end{aligned}$$

Notice that for $||v_1||_{L^\infty(\Omega)}\,,||v_2||_{L^\infty(\Omega)}\leq\varepsilon^{\frac{1}{4}}$,

$$\begin{aligned}&||G\left[u_0,v_1\right]-G\left[u_0,v_2\right]||_{L^\infty(\Omega)}\\ &\leq C\left(||e^{v_1}-e^{v_2}-(v_1-v_2)||_{L^\infty(\Omega)}+\left|\left|e^{-v_1}-e^{-v_2}+(v_1-v_2)\right|\right|_{L^\infty(\Omega)}\right)\\ &\leq 2C(e^{\max\left(||v_1||_{L^\infty(\Omega)},||v_2||_{L^\infty(\Omega)}\right)}-1)\,||v_1-v_2||_{L^\infty(\Omega)}\\ &\leq 2C(e^{\varepsilon^{\frac{1}{4}}}-1)\,||v_1-v_2||_{L^\infty(\Omega)}\ ,\end{aligned}$$

which implies, by lemmas 9, 8

$$||U||_{X_\varepsilon} \leq 2C(e^{\varepsilon^{\frac{1}{4}}} - 1)\,||v_1 - v_2||_{L^\infty(\Omega)} < \varepsilon^{1/2}\,||v_1 - v_2||_{X_\varepsilon} \ . \tag{2.85}$$

Therefore, since T applies the ball of radius $\varepsilon^{1/4}$ into itself and is a contraction by inequality (2.85) there exist a unique solution to equation (2.62) for ε sufficiently small and, by (2.84),

$$||\bar{u}_1||_{L^\infty(\Omega^*)} \leq ||\bar{u}_1||_{X_\varepsilon} \leq 2C\varepsilon^{1/2} \ ,$$

where C is a constant independent of ε. □

By inserting u into the right hand side of (2.15) we find that the charge density is then

$$\rho(x) = 4\mu \frac{\cosh\left(\left(\frac{\sqrt{2}(\varepsilon\mu)^{\frac{1}{2}}}{|\sigma(\eta(x))|}\right)\left[|\sigma(\eta(x))|\,\frac{\xi(\mathbf{x})}{\varepsilon} + 2\right]\right)}{\sinh^2\left(\left(\frac{\sqrt{2}(\varepsilon\mu)^{\frac{1}{2}}}{|\sigma(\eta(x))|}\right)\left[|\sigma(\eta(x))|\,\frac{\xi(\mathbf{x})}{\varepsilon} + 2\right]\right)} + O(1) \ , \tag{2.86}$$

for $\xi < \delta$ and $\rho = O(e^{-O(\varepsilon^{-\frac{1}{2}})})$ for $\xi \simeq \delta$. Note that, for $\xi \lesssim o(\varepsilon^{\frac{1}{2}})$ one can approximate (2.86) by

$$\rho(x) = \sigma(\eta(x))\frac{|\sigma(\eta(x))|}{2\varepsilon}\frac{1}{\left[|\sigma(\eta(x))|\,\frac{\xi(\mathbf{x})}{2\varepsilon} + 1\right]^2} + O(1) \ .$$

In the arguments above we have only assumed μ to be bounded. Since the solution obtained is L^∞, it turns out that the correction to the value of μ (as defined by the left hand side of (2.48)) given by the right hand side of (2.49) is uniformly bounded by $C\varepsilon$. One can then easily incorporate a variable μ into the fixed point arguments above and complete the proof of Theorem 1.

2.3.3 Curvature corrections to charge density and Maxwell stress

Our goal in this section is to obtain the correction that curvature produces both in the charge density and the so-called Maxwell stress tensor at $\partial\Omega$. The Maxwell stress is a second rank tensor and represents the interaction between electric forces and mechanical momentum and adds to the viscous stress tensor when imposing mechanical balance at $\partial\Omega$ as a boundary condition for the evolution of a charged fluid mass that occupies Ω. Its definition is

$$\mathcal{T}_{ij} = \varepsilon_0\varepsilon_r\left(\mathcal{E}_i\mathcal{E}_j - \frac{1}{2}\delta_{ij}\,|\mathcal{E}|^2\right) \ ,$$

where $\mathcal{E} = -\nabla V$. By nondimensionalizing by (2.7), we find

$$\mathcal{T}_{ij} = \frac{(ez)^2}{\varepsilon_0\varepsilon_r l^3}T_{ij}$$

with

$$T_{ij} = E_i E_j - \frac{1}{2}\delta_{ij} |\mathbf{E}|^2 ,$$
$$\mathbf{E} = -\nabla u \ .$$

In the local system of coordinates formed by the normal vector $\mathbf{n}$ at a point $\mathbf{x} \in \partial\Omega$ and two tangent vectors $(\mathbf{t}_1, \mathbf{t}_2)$ one would have

$$T_{nn} = E_n^2 - \frac{1}{2}\delta_{ij} |\mathbf{E}|^2 \ ,$$
$$T_{t_i n} = E_{t_i} E_n \ .$$

In the previous section we have proven that the correction to the potential $u = C + u^* + \varepsilon u_0$ provided by εu_1 is small in comparison to εu_0. Formally, by formula (2.45), such correction is at leading order given by

$$u_1^0(x) = \frac{\varepsilon^{\frac{1}{2}}}{4} \frac{\sinh(2\alpha)\sqrt{2/\mu}\mathcal{H}(x)}{\cosh^4\alpha + \sinh^4\alpha},$$

with

$$\alpha = \left(\frac{\sqrt{2}(\varepsilon\mu)^{\frac{1}{2}}}{|\sigma(\eta(x))|}\right)\left[|\sigma(\eta(x))|\,\frac{\xi(x)}{2\varepsilon} + 1\right] \ .$$

Notice that u_1^0 is $O(\varepsilon^{\frac{1}{2}})$ and includes a factor depending on the curvature of $\partial\Omega$.

Remind that the charge density is given by

$$\begin{aligned}
\rho(x) &= -\mu(e^{u_0}e^{u_1} - e^{-u_0}e^{-u_1}) \simeq -\mu(e^{u_0}e^{u_1^0} - e^{-u_0}e^{-u_1^0}) \\
&= -\mu\left(e^{u_0} - e^{-u_0}\right) - \mu\left(e^{u_0} + e^{-u_0}\right)u_1^0 - \mu\left(\frac{e^{u_0} - e^{-u_0}}{2}\right)\left(u_1^0\right)^2 + \dots \qquad (2.87) \\
&\equiv \rho_0(x) + \rho_1(x) + \rho_2(x) + \dots \ . \qquad (2.88)
\end{aligned}$$

The first term at the right hand side of (2.88), $\rho_0(x)$, is the charge density due to the boundary layer described in the previous sections and given by the first term at the right hand side of (2.86). The second term, $\rho_1(x)$ is $-2\mu\cosh(u_0)\,u_1^0$, which by formula (2.45) is

$$\rho_1(x) = -\varepsilon^{\frac{1}{2}} \frac{\sqrt{2\mu}\mathcal{H}(x)}{\sinh\left(\left(\frac{\sqrt{2}(\varepsilon\mu)^{\frac{1}{2}}}{|\sigma(\eta(x))|}\right)\left[|\sigma(\eta(x))|\,\frac{\xi(x)}{\varepsilon} + 2\right]\right)} \ ,$$

and includes a correction due to curvature. For $\varepsilon \ll 1$ and $\xi(x) \ll \varepsilon^{1/2}$, one can approximate

$$\rho(x) \simeq \rho_0(x) + \rho_1(x) \simeq \frac{2}{\varepsilon}\frac{\sigma(\eta(x))\,|\sigma(\eta(x))|}{\left(|\sigma(\eta(x))|\,\frac{\xi(x)}{\varepsilon} + 2\right)^2} - \frac{|\sigma(\eta(x))|\,\mathcal{H}(x)}{\left(|\sigma(\eta(x))|\,\frac{\xi(x)}{\varepsilon} + 2\right)} \ . \qquad (2.89)$$

We can also compute the electric field in the direction normal to $\partial\Omega$ as

$$E_n = -\frac{\partial u}{\partial n} \simeq -\varepsilon\frac{\partial u_0}{\partial \xi} - \varepsilon\frac{\partial u_1^0}{\partial \xi} + \dots \equiv E_n^0 + E_n^1 + \dots \ . \qquad (2.90)$$

The first term at the right hand side of (2.90) E_n^0, is given by formula (2.44) and the second term at the right hand side of (2.90) E_n^1 is the $\xi-$derivative of u_1^0 with a minus sign. When $\xi(x) \ll \varepsilon^{1/2}$ and $\varepsilon \ll 1$ one can then write

$$E_n \simeq -\frac{2\sigma(\eta(x))}{\left(|\sigma(\eta(x))|\frac{\xi}{\varepsilon}+2\right)} - \frac{\varepsilon}{2}\mathcal{H}(x) \ . \tag{2.91}$$

Hence, at $\partial\Omega$,

$$T_{nn} = \left(\frac{\sigma^2(\eta(x))}{2} + \frac{\varepsilon}{2}\sigma(\eta(x))\mathcal{H}(x)\right) + O(\varepsilon^2) \ .$$

In order to compute E_t, the tangential component of the electric field, we compute the tangential derivative of the potential, up to $O(\varepsilon)$, using formula (2.34):

$$E_t \simeq -\varepsilon\frac{d}{ds}\left(2\log\tanh\alpha(s)\right) = -\varepsilon\frac{d\left(2\log\tanh\alpha\right)}{d\alpha}\frac{d\alpha}{ds} \ ,$$

with $\alpha(s) = \frac{\sqrt{2}(\varepsilon\mu)^{\frac{1}{2}}}{|\sigma(s)|}$ and s the arclength parameter in the direction $\mathbf{t}$. Hence

$$E_t \simeq -\varepsilon\frac{2\left(1-\tanh^2\alpha\right)}{\tanh\alpha}\frac{d\alpha}{ds} = \varepsilon\frac{2\left|\sigma\right|_s}{|\sigma|} + O(\varepsilon^2) \ .$$

We conclude then

$$T_{t_in} = 2\varepsilon\left|\sigma\right|_{s_i} + O(\varepsilon^2) \ .$$

2.4 Numerical simulations

In this section we present numerical solutions to problem (2.13),(2.14) in various geometries and in order to verify the asymptotic expansions deduced in previous sections.

2.4.1 The boundary layer in spherical domains

We consider the problem (2.13),(2.14) with $\Omega^* = \mathbb{R}^3$ and $\Omega = \{||x|| \leq 1\}$. In this situation the potential $\hat{u}$ for the perfect conductor is

$$\hat{u} = \begin{cases} C \text{ for } |x| \leq 1 \\ \frac{C}{r} \text{ for } |x| > 1 \end{cases} \ ,$$

and the Poisson-Boltzmann equation is in spherical coordinates:

$$\frac{1}{r^2}\frac{d}{dr}\left(r^2\frac{du}{dr}\right) = \begin{cases} M\frac{e^{\frac{u}{\varepsilon}}}{\int\limits_{r\leq 1} e^{\frac{u}{\varepsilon}}} - N\frac{e^{-\frac{u}{\varepsilon}}}{\int\limits_{r\leq 1} e^{-\frac{u}{\varepsilon}}} \text{ for } r \leq 1 \\ 0 \text{ for } r > 1 \end{cases} \ , \tag{2.92}$$

$$u \to 0 \text{ as } r \to \infty \ ,$$

where the total charge $N - M$ equals the charge of the perfect conductor, i.e. $4\pi C$.

We have solved numerically, by means of a Runge-Kutta algorithm, equation (2.92) with $M = 1$, $N = \frac{1}{2}$ and with Ω being the sphere of radius 1. Based on this solutions we computed the right hand side of (2.92), i.e. minus the charge density $\rho(r)$, in Ω. According to formula (2.32) we should be able to write, locally near $r = 1$,

$$|\rho(r)| = \rho_{\max} \frac{1}{\left[\frac{(1-r)\rho_{\max}}{|\sigma|} + 1\right]^2} , \tag{2.93}$$

with $\rho_{\max} = \frac{\sigma^2}{2\varepsilon}$. Since $M - N = \frac{1}{2}$, we have $|\sigma| = \frac{1}{8\pi}$ and $\rho_{\max} = \frac{1}{128\pi^2\varepsilon}$. In figure 2.2 we represent the profiles $|\rho(r)|$ near $r = 1$ for various ε and the obtained values of $\rho_{\max}^{-1}$ as a function of ε (together with the straight line $128\pi^2\varepsilon$ to which $\rho_{\max}^{-1}$ converges asymptotically as ε tends to zero). In figure 2.3 we represent the profiles of $\frac{|\rho(r)|}{\rho_{\max}}$ as a function of $\xi = (1 - r)\rho_{\max}$ together with the curve $\left[\frac{\xi}{|\sigma|} + 1\right]^{-2}$ to which they clearly converge as $\varepsilon \to 0$. Therefore, the charge density profiles converge to the expression (2.93).

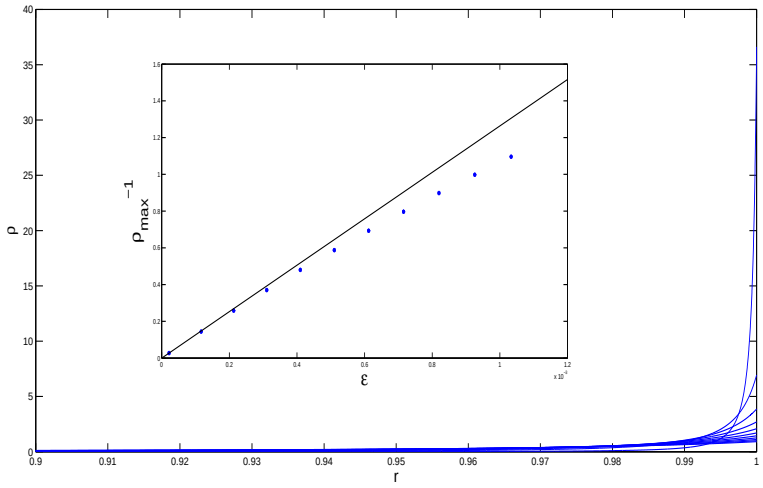

Figure 2.2: Charge density profiles near $r = 1$ for various values of ε. The maximum density is achieved for $r = 1$ and increases with decreasing ε. Inset: ρ_{max}^{-1} as a function of ε and comparison with the asymptotic value for $\varepsilon \ll 1$.

2.4.2 General domains: finite elements approximations

If one considers a domain Ω without spherical symmetry, then the structure of the charge double layer should change along the boundary of Ω. In order to test this, and compare with our analytical predictions in previous sections, we use a Finite Elements Method to compute the solutions to Poisson-Boltzmann equation written in the form

$$\Delta u = \left[\mu \sinh \frac{u - u^*}{\varepsilon}\right] \chi_\Omega \quad \text{in } \Omega^* , \tag{2.94}$$

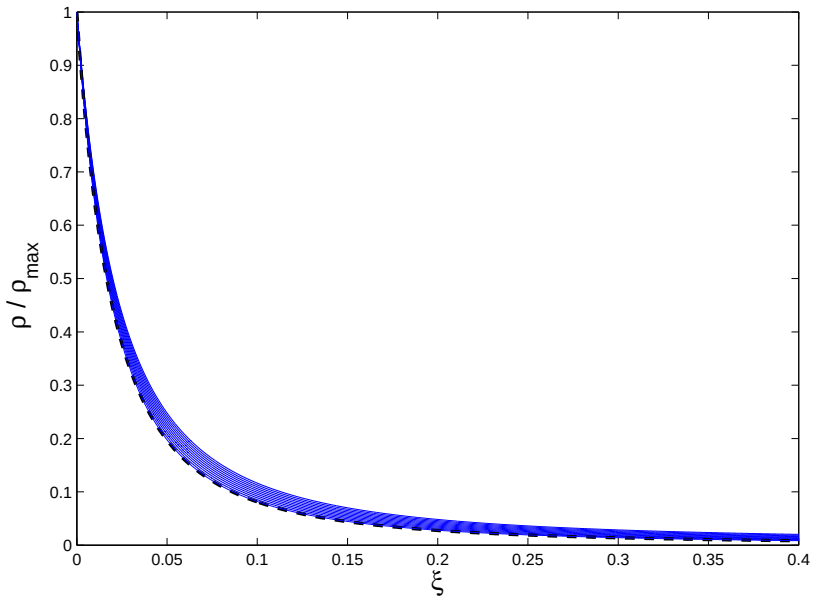

Figure 2.3: Rescaled profiles of $|\rho(r)|$ and comparison with the theoretical self-similar profile (in black dashed lines)

for different values of ε and with Ω being the ellipse

$$\frac{x^2}{4} + y^2 < \frac{1}{16} \ ,$$

and Ω^* the rectangle $[-1,1] \times [-1,1]$. χ_Ω is the characteristic function supported in Ω. Notice that, by writing $\mu \sinh \frac{u-u^*}{\varepsilon} = \frac{\mu}{2e^{\frac{u^*}{\varepsilon}}} e^{\frac{u}{\varepsilon}} - \frac{\mu}{2e^{-\frac{u^*}{\varepsilon}}} e^{-\frac{u}{\varepsilon}}$ and defining $M = \frac{\mu}{2e^{\frac{u^*}{\varepsilon}}} \int_\Omega e^{\frac{u}{\varepsilon}}$, $N = \frac{\mu}{2e^{-\frac{u^*}{\varepsilon}}} \int_\Omega e^{-\frac{u}{\varepsilon}}$ we can put equation (2.94) in the maybe more familiar form (2.13). We prefer the form (2.94) which lacks integral terms and is much easier to implement numerically.

We have used a nonlinear finite elements PDE solver with adaptive local refinement provided in the PDE toolbox of Matlab. The refinement is such that new elements are introduced at the discontinuities of the derivatives. These lie precesily at the interface $\partial\Omega$, where most of the charge is concentrated. Our meshes have a number of elements up to $2 \cdot 10^6$, so that we are able to achieve large precission. The nonlinear solver is based on an iterative process of the gradient descent type.

We have computed the solution to (2.94) with $u = 0$ at $\partial\Omega^*$. The value of u^* considered is 0.009 and the value of μ is -1. The values of ε are 0.05, 0.02, 0.01 and 0.005.

In Figure 2.4 we represent, together with $\partial\Omega$ (thick black curve), the level lines of the electric potential u for $\varepsilon = 0.05$, 0.02, 0.01, 0.005. Notice that, as ε decreases, the level lines tend to leave the interior of Ω. This implies that u tends to be constant in the interior of Ω as ε decreases and it is only close to $\partial\Omega$ that it experiences some changes. Notice also that, for $\varepsilon = 0.005$, only one level line crosses $\partial\Omega$ while for $\varepsilon = 0.05$ four level lines cross $\partial\Omega$. Hence, the potential at $\partial\Omega$ experiences the stronger changes from point to point along $\partial\Omega$

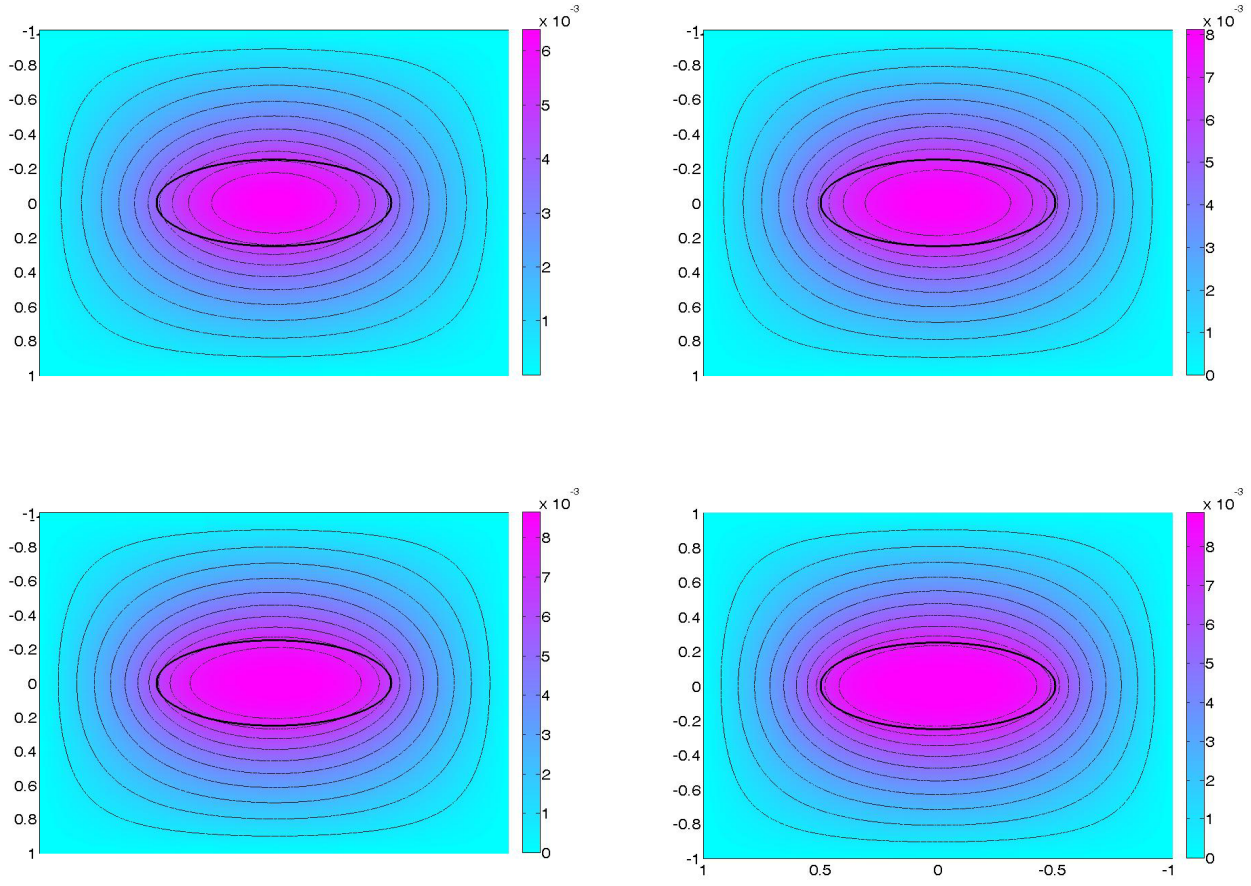

Figure 2.4: Level lines for the potential u solution to the Poisson-Boltzmann equation with $\varepsilon = 0.05, 0.02, 0.01, 0.005$ (from left to right and top to bottom)

when ε is large. It is only when ε is small that level lines for the potential tend to coincide with $\partial\Omega$ near the boundary. This means, of course, that the solutions are converging to those of a perfect conductor where the potential is constant in the whole Ω. In order to further verify this, we represent in Figure 2.5 the profiles for the potential u along the lines $\{y = 0, x > 0\}$ and $\{x = 0, y > 0\}$ for $\varepsilon = 0.05$, 0.02, 0.01, 0.005 and compare them with the profile for the perfect conductor (that we have also computed numerically by solving $\Delta u = 0$ in $\Omega^* \backslash \Omega$ subject to the boundary conditions $u = u^*$ at $\partial\Omega$ and $u = 0$ at $\partial\Omega^*$). As one can expect, the profiles approach, as $\varepsilon \to 0$, to those of the perfect conductor.

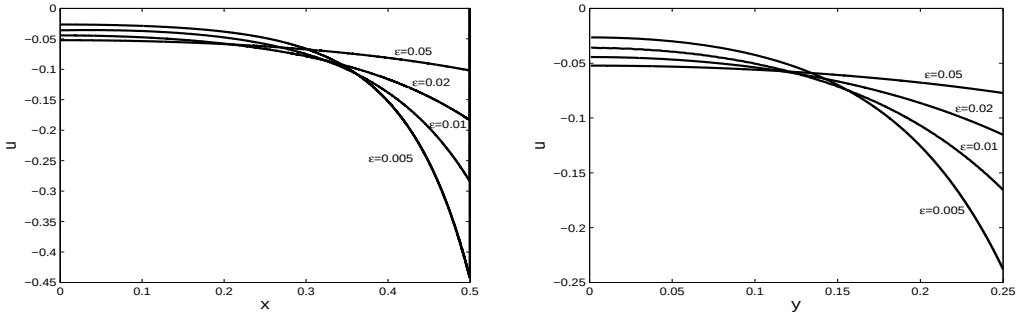

Figure 2.5: Profiles of the electrostatic potential u along the mayor axis (left) and minor axes (right) for $\varepsilon = 0.05, 0.02, 0.01, 0.005$ together with the solution for a perfect conductor that formally corresponds to $\varepsilon = 0$

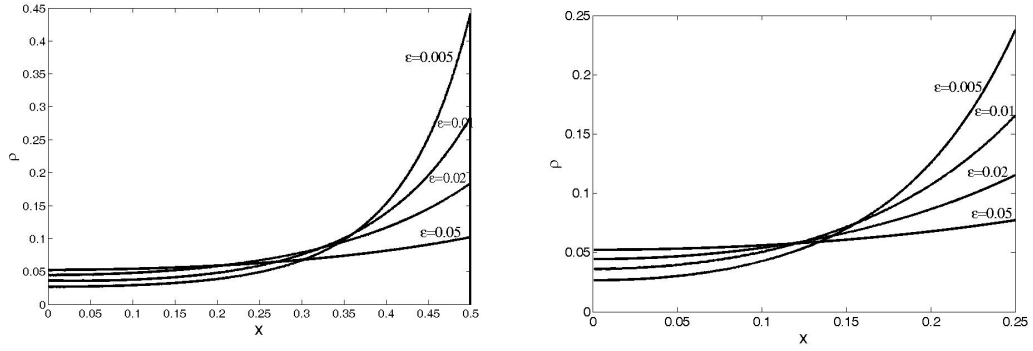

Figure 2.6: Profiles of the charge density ρ along the mayor axis (left) and minor axes (right) for $\varepsilon = 0.05, 0.02, 0.01, 0.005$

In order to check whether the charge density, defined as the right hand side of (2.94) with a minus sign, follows the asymptotic laws described in previous sections or not, we compute it along the major and the minor axis of the ellipse. In Figure 2.6 we represent the charge density along the major axis (left) and the minor axis (right) for $\varepsilon = 0.05$, 0.02, 0.01, 0.005. Notice that, as ε decreases, the charge tends to leave the center of the drop and density increases close to $\partial\Omega$. The profiles for the density do follow a selfsimilar law according to our theoretical results above: if ε is sufficiently small, then the charge density is given by equation (2.32). We consider, at leading order, σ the surface charge density in the

case of the perfect conductor and denote $\rho_{\max} = \frac{\sigma^2}{2\varepsilon}$ and $\xi = \rho_{\max}(0.5 - x)$ when considering charge along the major axis and $\xi = \rho_{\max}(0.25 - y)$ when considering charge along the minor axis. Notice that σ changes from point to point along $\partial\Omega$ and is larger in absolute value at $(x, y) = (0.5, 0)$ than at $(x, y) = (0, 0.25)$ due to the higher curvature of $\partial\Omega$ at $(0.5, 0)$. Hence, according to equation (2.32),

$$\frac{\rho}{\rho_{\max}} \simeq \frac{1}{\left[\frac{\xi}{|\sigma|} + 1\right]^2} \equiv f\left(\frac{\xi}{|\sigma|}\right) \ .$$

We have represented in Figure 2.7 the profiles of $\frac{|\rho|}{\rho_{\max}}$ vs. ξ for $\varepsilon = 0.05,\ 0.02,\ 0.01,\ 0.005$. As we can observe, both in the case of the profiles at the minor axis and the major axis, the profiles tend to converge to a selfsimilar profile. Both profiles look similar except for a scaling factor which is due to de different values of $|\sigma|$ at $(0.5, 0)$ and $(0, 0.25)$. This is in agreement with the asymptotic laws for the charge distribution, as a function of $|\sigma|$ proved in this chapter.

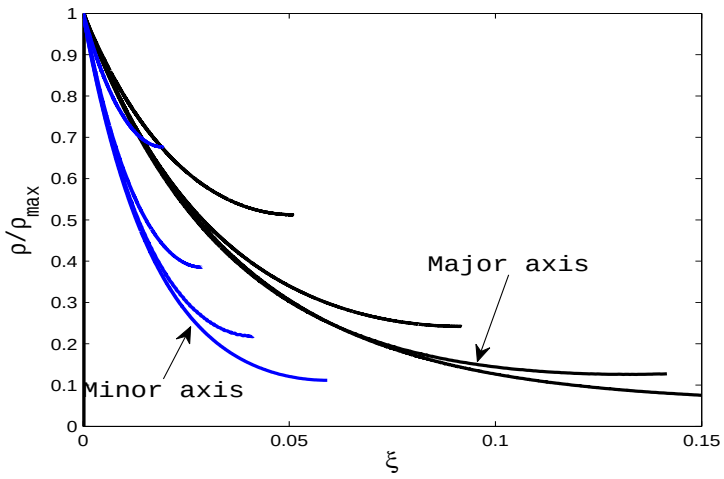

Figure 2.7: Rescaled charge density profiles along the mayor and minor axes of the ellipse

2.5 Conclusions

In this chapter we have deduced asymptotic formulae for the distribution of charge of an ionic solution near its interface with an external medium. Our main assumptions were 1) all ionic species are in dynamic equilibrium and 2) a dimensionless parameter ε which is inversely proportional to ion mobilities is very small. Our expansions contain corrections due to the geometry of the interface and hence describe possible accumulations of charge at certain regions of the interface depending on their curvature. As an application, we will focus in future works, on the case of drops of ionic solutions subject to external electric fields and on how the finite ion mobility introduces corrections on the dynamic behaviour of the

drop with respect to the studied case of infinite ion mobility (that is, the case in which the drop in the liquid is a perfect conductor).

One particular issue that we will analyze next is the formation of the so-called Rayleigh jets that appear when a drop contains a supercritical amount of electric charges (cf. [20]). We conjecture that Rayleigh jets appear due to the corrections introduced by considering a finite ion mobility or equivalently, by replacing the Maxwell stress tensor for a perfect conductor by the expressions obtained in this chapter.

Chapter 3

Coupling of Poisson-Boltzmann equation with Stokes system: The formation of Rayleigh jets

3.1 Introduction

In this chapter we will couple the electrokinetics as described by Poisson-Boltzmann approximation (see previous Chapter and [28]) with the fluid motion described by Navier-Stokes equations (see [46], [19]). One of our main motivations is to describe the so-called Rayleigh jets.

Rayleigh jets appear from charged droplets once the charge overcomes some critical value. In the case of a perfectly conducting liquid, the critical charge Q is such that the Rayleigh fissibility ratio X, defined as

$$X = \frac{Q^2}{32\gamma\pi^2\varepsilon_0 R_0^3}, \tag{3.1}$$

is larger than 1. In (3.1), γ is the surface tension coefficient, R_0 is the radius of the drop and ε_0 is the dielectric constant outside the drop.

When the drop's charge is overcritical, the drop deforms into a prolate spheroid (cf. [20], [6], [7] for experimental results and [26], [12] for numerical simulations) and conical tips tend to develop at the regions of maximum curvature. When the fluid is a perfect conductor and is modeled under Stokes approximation, it was shown in [26], [12] that conical tips develop in finite time (see figure 3.2). These conical tips, called dynamic Taylor cones (analogous to the static Taylor cones first described in [67]), present a semiangle around $20^o - 25^o$, which coincides almost exactly with the experimental measurements. Nevertheless, in the experimental observations, very fast and thin jets are produced from the conical tips (see Figures 3.1, 3.2). This is a fact that cannot be reproduced in [26], [12] under the Stokes and perfect conductor assumptions. For perfect and non-viscous fluids, jets have been reported recently in [34] where they use the level set techniques (cf. [63]) to develop an Eulerian potential flow model together an axisymmetric boundary integral calculations. Nevertheless,

for very small drops (of the order of 100 μm or smaller), Reynolds number can be very small (of the order of 10^{-4} or smaller), so that it seems necessary to investigate the formation of jets under Stokes approximation. Our hypothesis is that it is the finite electric conductivity and the presence of Debye layers in electrolyte solutions what induces the production of Rayleigh jets. The first effect, finite conductivity, implies that electric charges do not move infinitely fast inside the liquid medium. The second effect, finiteness of Debye layer, implies that positive and negative charges do not balance exactly inside the drop so that the liquid is electrically neutral at the bulk of the fluid. Instead, they form a thin layer (the so-called Debye layer) where there is a nonzero net charge.

We will show in this chapter that the hypothesis sketched above does indeed lie at the heart of the formation of Rayleigh jets and will be used to compute the jet's main characteristics such as velocity and size. Our results will also be used to discuss Rayleigh jet's features dependence on temperature and ion concentration.

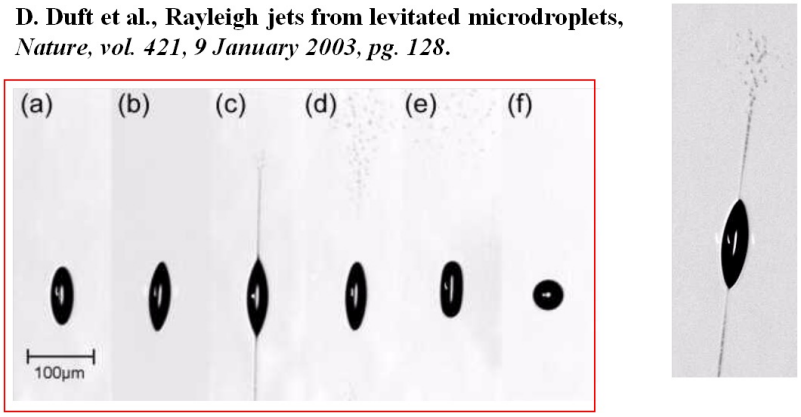

Figure 3.1: The formation of Rayleigh jets as observed in [20]. After the jet is formed in c) the drop loses an important part of its charges and relaxes to spherical shape.

3.2 Physical setting and formulation

3.2.1 Introduction

The laws of fluid motion for microfluidic systems are not any different from those that govern large scale systems such as the oceanic currents on intercontinental scales. However, the relative importance of different forces and effects change dramatically as we go from macro to micro scales. For example, surface tension forces and electrostatics play no role at all in the study of ocean currents but are enormously important in the world of microfluidics.

In microfluidics, relevant physical dimensions are sufficiently large in comparison to atomic scales that it is permissible to treat the fluid as if it were a continuum. Thus, the fluid velocity $\mathbf{v}$ and pressure p are regarded as continuous functions of position $\mathbf{x}$ and time t, and they obey the incompressible Navier-Stokes equations with external body forces

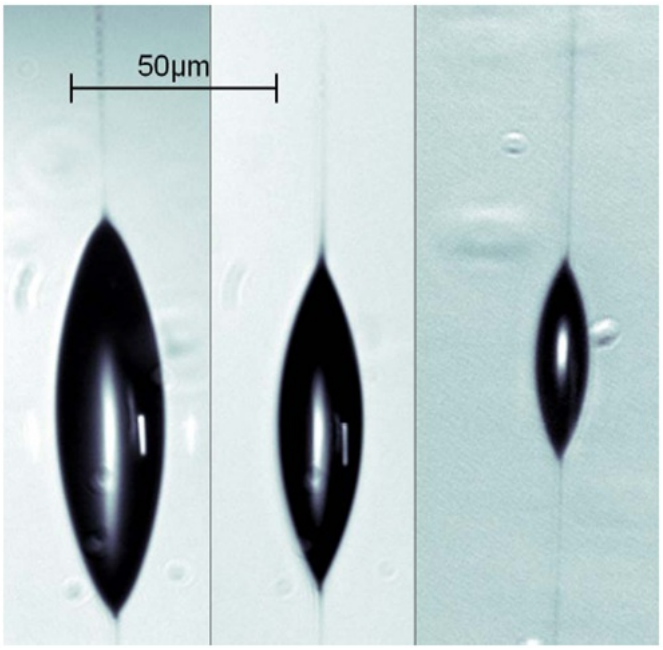

Figure 3.2: Details of the Rayleigh jets from the experiments in [7]. Note that the drop's radius is of the order of 10 μm

$\mathbf{F}_e$ acting per unit volume (e.g., gravity, electric, electromagnetic or centrifugal force).

$$\rho_0 \left(\partial_t \mathbf{v} + \mathbf{v} \cdot \nabla \mathbf{v}\right) = -\nabla p + \mu \Delta \mathbf{v} + \mathbf{F}_e. \tag{3.2}$$

This is supplemented by the continuity equation which takes into account the fact that in a liquid the density changes are slight:

$$\nabla \cdot \mathbf{v} = 0. \tag{3.3}$$

In the above, ρ_0 is the (constant) density of the fluid, μ the viscosity constant. The first equation (3.2) is the momentum equation and is an expression of Newton's second law of motion. The second equation (3.3) is the continuity equation expressing conservation of mass.

The relative size of the term on the left hand side of equation (3.2) (due to fluid inertia) to the second term on the right hand side (due to viscosity) is characterized by the Reynolds number

$$\mathrm{Re} = \frac{UL\rho_0}{\mu},$$

where U and L denote a characteristic velocity and length for the flow. In most applications of microfluidics, $\mathrm{Re} \ll 1$, in some applications, $\mathrm{Re} \sim 1$. By contrast, in large scale flows (aircraft engines, geophysical flows etc.) $\mathrm{Re} \gg 1$. We will consider masses of fluid at a very small length scale so that $\mathrm{Re} \ll 1$ and the left hand side of (3.2) which corresponds to fluid inertia can either be neglected, or treated as a small perturbation. In the former case, we arrive at the Stokes flow equations:

$$-\nabla p + \mu \Delta \mathbf{v} + \mathbf{F}_e = 0, \tag{3.4}$$

which is often referred to as slow, creeping or highly viscous flow. All of these terms mean the same thing, namely Re $\ll 1$. The unknown scalar field p in (3.4) is determined by the constraint provided by (3.3).

Electrokinetic, as we mentioned before, refers to mechanical effects that arise due to the motion of ions in liquids. The working fluid in microfluidic systems is normally water which contains ions of both signs due to dissociated water molecules or other ionic components: acids, salts, and molecules with dissociable charged groups. Normally, a volume element of such a fluid considered "infinitesimal" in the continuum view point still contains a sufficiently large number of ions of either sign for statistical fluctuations to be unimportant for the fluid element to be considered charge neutral. Therefore, the net algebraic transfer of momentum due to any ambient electric field is also zero (even though a non-zero electric current may exist in the fluid due to the ordered motion of these ions). Electrokinetic effects arise when this balance of positive and negative charges is disturbed due to external factors as we studied when we considered the Poisson-Boltzmann equation. In the macroscopic description, the drop consists of a viscous incompressible fluid containing ions, which are electrically charged and produce stresses on the fluid through the so-called Maxwell stress tensor:

$$\tau_{ij} = E_i E_j - \frac{1}{2}\delta_{ij} |\mathbf{E}|^2 ,$$

where $\mathbf{E} = -\nabla V$. Then $\mathbf{F}_e$ is the divergence of the Maxwell stress tensor τ:

$$F_i = \tau_{ij,j},$$

using Einstein notation for brevity in the formulas. We can write

$$F_i = (E_i E_j - \frac{1}{2}E_k E_k \delta_{ij})_{,j} = E_{i,j}E_j + E_{j,j}E_i - E_k E_{k,i} = V_{ij}V_i + \rho E_i - V_k V_{ki} = \rho E_i.$$

Therefore the fluid in the so called Debye Layer, experienced an electrical force with volume density $\mathbf{F}_e = \rho\mathbf{E}$ with ρ the electric charge density and $\mathbf{E} = -\nabla V$ the local electric field with V the electric potential.

3.2.2 The model

Let us consider now a droplet $\Omega(t)$ of a viscous incompressible fluid containing ions electrically charged, the droplet is suspended in a dielectric and also incompressible viscous fluid $\Omega^*(t) \setminus \overline{\Omega(t)}$, which is in contact with electrodes to zero potential, and which we would like to take infinite. In this case, the boundary $\partial\Omega(t)$ will move with the flow, so we have to take into account also the exterior fluid dynamics.

Let us remind that the mathematical formulation corresponding to the model of the electric potential V in $\Omega^*(t)$ that consists of an electrolitic droplet $\Omega(t)$ surrounded by a dielectric fluid $\Omega^*(t) \setminus \overline{\Omega(t)}$, is the Poisson-Boltzmann equation

$$\begin{aligned} \Delta V(\mathbf{x},t) &= \frac{M(\mathbf{x},t)}{\int_\Omega e^{V/\varepsilon} d\mathbf{x}} e^{V/\varepsilon} - \frac{N(\mathbf{x},t)}{\int_\Omega e^{-V/\varepsilon} d\mathbf{x}} e^{-V/\varepsilon} \text{ in } \Omega^*(t), \\ V(\mathbf{x},t) &\longrightarrow O\left(|\mathbf{x}|^{-1}\right) \text{ on } \partial\Omega^*(t), \end{aligned} \tag{3.5}$$

with

$$M(\mathbf{x},t) = \begin{cases} M & \mathbf{x} \in \Omega(t) \\ 0 & \mathbf{x} \in \Omega^*(t) \setminus \Omega(t) \end{cases} \quad \text{and } N(\mathbf{x}) = \begin{cases} N & \mathbf{x} \in \Omega(t) \\ 0 & \mathbf{x} \in \Omega^*(t) \setminus \Omega(t) \end{cases},$$

that, as we have seen, comes from an adimensionalization of the physical problem.

We had assumed that the droplet contains a net amount of electric charge Q, so if we denote σ the surface charge density in the droplet $\Omega(t)$, we know that $\sigma(\mathbf{x},t) = -\frac{\partial V}{\partial \mathbf{n}}\big|_{\partial\Omega(t)}$ and satisfies

$$\int_{\partial\Omega(t)} \sigma(\mathbf{x},t)\, dS(\mathbf{x}) = Q. \tag{3.6}$$

Q constant in time because of the charge conservation law.

Then the model governing the liquid flow in the droplet $\Omega(t)$ and in the exterior fluid is the Stokes system including the electric body force per unit volume $\rho\mathbf{E} = -\rho\nabla V$ in the momentum equation for the droplet:

$$-\nabla p^{(1)}(\mathbf{x},t) + \mu_1 \Delta \mathbf{v}^{(1)}(\mathbf{x},t) + \rho(\mathbf{x},t)\,\mathbf{E}(\mathbf{x},t) = 0 \ \mathbf{x} \in \Omega(t), \tag{3.7}$$

$$-\nabla p^{(2)}(\mathbf{x},t) + \mu_2 \Delta \mathbf{v}^{(2)}(\mathbf{x},t) = 0 \ \mathbf{x} \in \Omega^*(t) \setminus \overline{\Omega(t)}, \tag{3.8}$$

$$\nabla \cdot \mathbf{v}^{(k)}(\mathbf{x},t) = 0 \ \mathbf{x} \notin \partial\Omega(t), \ k = 1,2, \tag{3.9}$$

where $\mathbf{v}^{(k)}$ is the velocity field, $p^{(k)}$ is the pressure, μ_k the viscosity for $k = 1, 2$, the respective inner and outer viscosities.

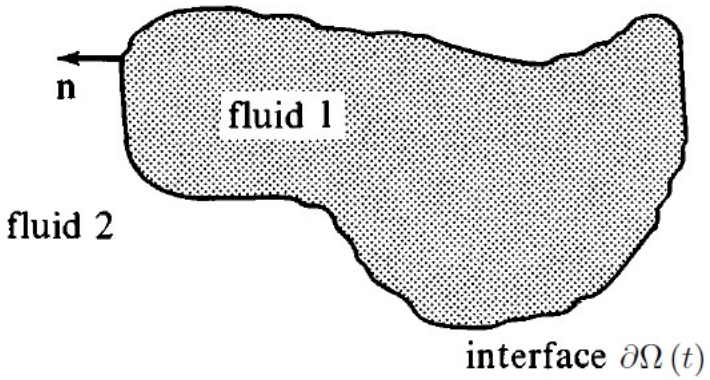

Figure 3.3: Two fluids interacting.

The normal component of the velocity has to be continuous across the boundary and we need

$$\mathbf{v}^{(1)} \cdot \mathbf{n} = \mathbf{v}^{(2)} \cdot \mathbf{n} \ \equiv \mathbf{v} \cdot \mathbf{n} \text{ on } \partial\Omega(t),$$

The dependence on t comes from the motion of the boundary $\partial\Omega(t)$ given by the equation

$$\frac{d\mathbf{x}}{dt} \cdot \mathbf{n} = \mathbf{v}(\mathbf{x},t) \cdot \mathbf{n}, \tag{3.10}$$

with $\mathbf{n}$ exterior to $\Omega(t)$, expressing the fact that the surface of the drop moves in the direction of its normal, following the normal component of the velocity field. Note that the tangential velocity does not change the geometry of $\partial\Omega(t)$ but only redistributes its points.

3.2.3 Boundary conditions

As we have seen, to describe a flow in the presence of an interface we must consider the flow on each side of the interface separately, and then require proper matching conditions for the velocity. Now we will study which are the conditions for the surface forces, in fact we will find a constitutive relation for the discontinuity in the interfacial surface forces.

Two types of forces are exerted on any piece of material: homogeneous forces acting on its volume, and surface forces acting on its boundary. We have already talked about the body forces acting in our two fluids, now we will determine the surface forces exerted on $\partial\Omega(t)$ and the suitable conditions on $\partial\Omega^*(t)$ to establish completely the mathematical problem that will allow us to study the evolution of the boundary of the electrolitic droplet.

Consider an infinitesimal surface drawn in the interior of a fluid or at the boundaries, lying in a plane that is perpendicular to the unit vector $\mathbf{n}$, that is pointing outside $\Omega(t)$. The force per unit area acting on this surface is denoted by $\mathbf{f}$ and called the traction. By definition, the traction depends on position in the fluid $\mathbf{x}$, and on the orientation of the infinitesimal surface determined by the unit vector $\mathbf{n}$. To signify this dependence, we write $\mathbf{f}(\mathbf{x}, \mathbf{n})$.

Analysis reveals [55] that the traction vector depends linearly on the normal vector

$$f_j(\mathbf{x}, \mathbf{n}) = T_{ij}(\mathbf{x})\, n_i, \tag{3.11}$$

where T_{ij} is the Cauchy stress tensor; summation over the repeated index i in the spatial coordinates x, y and z is implied on the right-hand side of (3.11).

We had assumed that our viscous fluids are Newtonian and incompressible, so the stress tensor T_{ij} is related to the pressure p and to the rate-of-deformation tensor by the linear constitutive equation

$$T_{ij}^{(k)} = -\delta_{ij} p^{(k)} + \mu_k \left(\frac{\partial v_i^{(k)}}{\partial x_j} + \frac{\partial v_j^{(k)}}{\partial x_i} \right) \qquad k = 1, 2,$$

expressing the effects of the forces acting in a fluid: pressure, that always acts in the direction of $\mathbf{n}$ corresponding to the diagonal part of $T_{ij}^{(k)}$, and viscous friction or viscosity, that for being a force needs to be shear, i.e. a gradient of the velocity. The general expression characterizing the amount of shearing is the symmetric part of the rate-of-deformation tensor

$$\mathbf{e}^{(k)} = \frac{\partial v_i^{(k)}}{\partial x_j} + \frac{\partial v_j^{(k)}}{\partial x_i}.$$

For an isotropic fluid, as in our case, the viscous contribution to $T_{ij}^{(k)}$ is simply proportional to $\mathbf{e}^{(k)}$, the constant of proportionality being the viscosity μ_k.

Traction jump across a fluid interface

Let us consider a thin fluid layer straddling a three dimensional surface, as illustrated in Figure 3.4. We define a vector $\mathbf{a}$, be the unit vector tangential to the layer edge. The surface

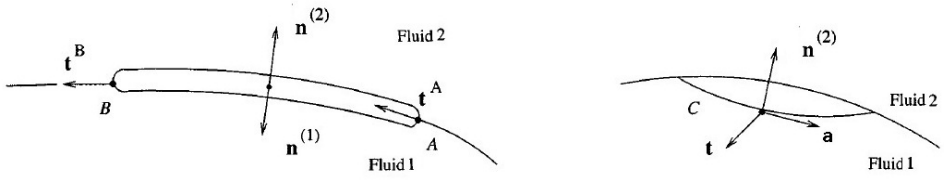

Figure 3.4: Schematic representation of the domains and geometrical components.

tension pulls the layer in the direction of the unit vector $\mathbf{t}$ that is tangential to the interface and normal to both $\mathbf{n}$ and $\mathbf{a}$. We have then

$$\mathbf{t} = \mathbf{a} \times \mathbf{n}.$$

Next we balance the surface force due to the fluid stress and the edge force due to the surface tension, and find

$$\mathbf{T^{(2)}}\mathbf{n}\Delta S + \mathbf{T}^{(1)}(-\mathbf{n})\Delta S + \oint_C \gamma \mathbf{t} dl = 0,$$

where ΔS is the surface area of the layer, and l is the arc length around the layer edge C. Then the hydrodynamic traction undergoes a discontinuity defined as

$$\Delta\mathbf{f} = \mathbf{f}^{(2)} - \mathbf{f}^{(1)} = \left(\mathbf{T^{(2)}} - \mathbf{T^{(1)}}\right)\mathbf{n} = -\frac{1}{\Delta S}\oint_C \gamma \mathbf{t} dl,$$

where $\mathbf{f}^{(2)} = \mathbf{T}^{(2)} \cdot \mathbf{n}$ is the traction exerted on the surface of the drop due to the exterior fluid and $\mathbf{f}^{(1)} = \mathbf{T}^{(1)} \cdot \mathbf{n}$ is the traction exerted on the surface due to the drop. It can be shown that, in the limit as $\Delta S \longrightarrow 0$, if the loop C shrinks to a point and the surface tension γ is constant, last equation reduces to

$$\Delta\mathbf{f} = \left(\mathbf{T^{(2)}} - \mathbf{T^{(1)}}\right)\mathbf{n} = 2\gamma\mathcal{H}\mathbf{n}, \tag{3.12}$$

where $\mathcal{H} = \frac{\mathcal{H}_1+\mathcal{H}_2}{2}$ is the mean curvature of the interface. It is possible to redefine variables in such a way that $\gamma = 1$.

Tangential effects only redistribute the points in the boundary, that is why are unimportant in this case. We will also assume that the flow vanishes at infinity.

In the next section we will transform the problem (3.7)-(3.10) containing the bulk force $\rho\mathbf{E}$, with boundary condition (3.12) into a problem without external bulk forces but where condition (3.12) is modified to include electrokinetic stresses.

3.2.4 Coupling Poisson-Boltzmann and Stokes

Let us take t fixed, the charge density inside the droplet $\Omega(t)$ is

$$\rho(\mathbf{x},t) = -\Delta V(\mathbf{x},t) = \frac{N}{\int_{\Omega(t)} e^{-V/\varepsilon} d\mathbf{x}} e^{-V/\varepsilon} - \frac{M}{\int_{\Omega(t)} e^{V/\varepsilon} d\mathbf{x}} e^{V/\varepsilon}.$$

Denote

$$f\left(V\left(\mathbf{x},t\right)\right)=\frac{N}{\int_{\Omega(t)}e^{-V/\varepsilon}d\mathbf{x}}e^{-V/\varepsilon}-\frac{M}{\int_{\Omega(t)}e^{V/\varepsilon}d\mathbf{x}}e^{V/\varepsilon},$$

then

$$\rho\mathbf{E}=-f\left(V\right)\nabla V.$$

If we take the real function with real values F defined as:

$$F\left(x\right)=-\varepsilon\frac{N}{\int_{\Omega(t)}e^{-V/\varepsilon}d\mathbf{x}}e^{-x/\varepsilon}-\varepsilon\frac{M}{\int_{\Omega(t)}e^{V/\varepsilon}d\mathbf{x}}e^{x/\varepsilon},$$

we have

$$\frac{dF}{dx}\left(V\left(\mathbf{x},t\right)\right)=\frac{N}{\int_{\Omega(t)}e^{-V/\varepsilon}d\mathbf{x}}e^{-V/\varepsilon}-\frac{M}{\int_{\Omega(t)}e^{V/\varepsilon}d\mathbf{x}}e^{V/\varepsilon}=\rho\left(\mathbf{x},t\right).$$

By the chain rule applied to the composition $F\circ V:\Omega\left(t\right)\longrightarrow\mathbb{R}$,

$$\begin{aligned}\nabla\left(F\circ V\left(\mathbf{x},t\right)\right)&=\frac{dF}{dx}\left(V(\mathbf{x},t)\right)\nabla V\left(\mathbf{x},t\right),\\&=\rho\nabla V=-\rho\mathbf{E},\end{aligned}$$

then the equation (3.7) can be rewritten as

$$-\nabla\left(p^{(1)}+F\circ V\right)+\mu_1\Delta\mathbf{v}^{(1)}=0\qquad\mathbf{x}\in\Omega\left(t\right).\tag{3.13}$$

Let us denote

$$P^{(1)}=p^{(1)}+F\circ V,\tag{3.14}$$

and

$$P^{(2)}=p^{(2)},\tag{3.15}$$

we have

$$-\nabla P^{(2)}+\mu_2\Delta\mathbf{v}^{(2)}=0\qquad\mathbf{x}\in\Omega^{*}\left(t\right)\setminus\overline{\Omega\left(t\right)}.\tag{3.16}$$

The boundary conditions on the free boundary $\partial\Omega\left(t\right)$ in terms of the new pressure (3.14) becomes

$$\left[-\left(P^{(2)}-P^{(1)}\right)\delta_{ij}+\mu_2\left(\frac{\partial v_i^{(2)}}{\partial x_j}+\frac{\partial v_i^{(2)}}{\partial x_i}\right)-\mu_1\left(\frac{\partial v_i^{(1)}}{\partial x_j}+\frac{\partial v_i^{(1)}}{\partial x_i}\right)\right]n_j=2\mathcal{H}n_i+\left(F\circ V\right)n_i.$$

The equations (3.13) and (3.16) states that the pressure, viscous, and body forces, balance at any instant in time even though the flow may be unsteady. The instantaneous structure of the flow depends solely on the present boundary configuration and boundary conditions, and is independent of the history of motion. The history of motion enters the problem only by determining the current location of the boundaries. Therefore we will work with the steady state problem and, as we will see, we can use recursivity and the evolution formula

(3.10) to obtain an approximate solution in an evolved domain. We will consider then the steady state problem and drop off the dependence on time:

$$\Omega_1 = \Omega(t).$$

We want to work with an infinite ambient fluid, therefore we will assume

$$\Omega_2 = \mathbb{R}^3 \backslash \overline{\Omega(t)}.$$

Finally, the system that models our problem is:

$$-\nabla P^{(k)}(\mathbf{x}) + \mu_k \Delta \mathbf{v}^{(k)}(\mathbf{x}) = 0 \ , \ \mathbf{x} \in \Omega_k, \tag{3.17}$$

$$\nabla \cdot \mathbf{v}^{(k)} = 0 \ , \ \mathbf{x} \in \Omega_k, \tag{3.18}$$

$$\left(\mathbf{T}^{(2)} - \mathbf{T}^{(1)}\right)\mathbf{n} = (2\mathcal{H} + (F \circ V))\,\mathbf{n} \text{ on } \partial\Omega_1, \tag{3.19}$$

$$\mathbf{v} \longrightarrow \mathbf{0} \text{ as } |\mathbf{x}| \longrightarrow \infty. \tag{3.20}$$

3.2.5 The asymptotic boundary conditions for $\varepsilon \ll 1$

From the analysis in a previous chapter (see also [28]) we found an asymptotic expansion for the potential V in a domain Ω in a small layer close to the boundary $\partial\Omega$. We will use that expansion to obtain the boundary conditions for the system (3.17)-(3.20).

We know that the potential in the boundary layer inside Ω_1 can be written in the form

$$V = C + u^* + \overline{u},$$

with $\overline{u}$ solution of

$$\Delta \overline{u} = \mu\left(e^{\overline{u}/\varepsilon} - e^{-\overline{u}/\varepsilon}\right) \text{ in } \Omega_1,$$

C a constant associated to the perfect conductor problem and to (3.6), $\mu = \sqrt{\frac{MN}{\int_{\Omega_1} e^{(V-C)/\varepsilon} \int_{\Omega_1} e^{-(V-C)/\varepsilon}}}$ and $u^* = \varepsilon \ln \sqrt{\frac{N \int_{\Omega_1} e^{(V-C)/\varepsilon}}{M \int_{\Omega_1} e^{-(V-C)/\varepsilon}}} = \varepsilon c^*$.

We have then in a fixed $\mathbf{x}$

$$\begin{aligned} F(V(\mathbf{x})) &= -\varepsilon \left[\frac{M}{\int_{\Omega_1} e^{V/\varepsilon} dV} e^{V/\varepsilon} + \frac{N}{\int_{\Omega_1} e^{-V/\varepsilon} dV} e^{-V/\varepsilon} \right] \\ &= -\varepsilon \left[\frac{M}{\int_{\Omega_1} e^{(C+u^*+\overline{u})/\varepsilon} dV} e^{(C+u^*+\overline{u})/\varepsilon} + \frac{N}{\int_{\Omega_1} e^{-(C+u^*+\overline{u})/\varepsilon} dV} e^{-(C+u^*+\overline{u})/\varepsilon} \right]. \end{aligned}$$

Canceling the constants $e^{C/\varepsilon}$ and $e^{-C/\varepsilon}$ in both terms:

$$\begin{aligned} F(V(\mathbf{x})) &= -\varepsilon \left[\frac{M}{\int_{\Omega_1} e^{(V-C)/\varepsilon} dV} e^{c^*+\overline{u}/\varepsilon} + \frac{N}{\int_{\Omega_1} e^{-(V-C)/\varepsilon} dV} e^{-c^*-\overline{u}/\varepsilon} \right] \\ &= -\varepsilon \left[\frac{M}{\int_{\Omega_1} e^{(V-C)/\varepsilon} dV} \sqrt{\frac{N \int_{\Omega_1} e^{(V-C)/\varepsilon}}{M \int_{\Omega_1} e^{-(V-C)/\varepsilon}}} e^{\overline{u}/\varepsilon} + \frac{N}{\int_{\Omega_1} e^{-(V-C)/\varepsilon} dV} \sqrt{\frac{M \int_{\Omega_1} e^{-(V-C)/\varepsilon}}{N \int_{\Omega_1} e^{(V-C)/\varepsilon}}} e^{-\overline{u}/\varepsilon} \right], \end{aligned}$$

therefore

$$F\left(V(\mathbf{x})\right) = -\varepsilon\mu\left[e^{\overline{u}/\varepsilon} + e^{-\overline{u}/\varepsilon}\right] = -2\varepsilon\mu\cosh\left(\frac{\overline{u}}{\varepsilon}\right) \tag{3.21}$$

We already obtained in Chapter 2 that

$$\begin{aligned}\overline{u}\left(\mathbf{x}\right) &= \varepsilon\left(2\zeta\left(\frac{\xi\left(\mathbf{x}\right)}{\delta}\right)\log\tanh\left(\frac{\sqrt{2}\left(\varepsilon\mu\right)^{1/2}}{\left|\sigma\left(x_S\right)\right|}\right)\left[\frac{\sigma\left(x_S\right)}{2}\frac{\xi\left(\mathbf{x}\right)}{\varepsilon}+1\right]\right)+\varepsilon u_1\left(\mathbf{x}\right)\\ &= \varepsilon u_0\left(\mathbf{x}\right)+\varepsilon u_1\left(\mathbf{x}\right),\end{aligned}$$

with

$$u_0\left(\mathbf{x}\right) = 2\zeta\left(\frac{\xi\left(\mathbf{x}\right)}{\delta}\right)\log\tanh\left(\frac{\sqrt{2}\left(\varepsilon\mu\right)^{1/2}}{\left|\sigma\left(x_S\right)\right|}\right)\left[\frac{\sigma\left(x_S\right)}{2}\frac{\xi\left(\mathbf{x}\right)}{\varepsilon}+1\right],$$

$\sigma\left(x_S\right) \simeq -\frac{\partial V}{\partial \mathbf{n}}$ in $\partial\Omega_1$, σ is approximately the surface charge density of the potential for the perfect conductor, in fact is the surface charge density for the perfect conductor in $x_S = \eta\left(\mathbf{x}\right)$ plus corrections. Let us remind that $u_1\left(\mathbf{x}\right)$ is an order ε correction to the potential and satisfies the equation

$$\varepsilon\Delta u_1 - 2\mu\cosh\left(u_0\right)u_1 = g\left(x\right) + G\left[u_0, u_1\right] \text{ in } \Omega_1,$$

with $g\left(x\right) = 2\mu\sinh\left(u_0\right) - \varepsilon\Delta u_0$, G a nonlinear function of u_1 and u_0. We have

$$u_1\left(\mathbf{x}\right) = u_1^0\left(\mathbf{x}\right) + u_1^1\left(\mathbf{x}\right).$$

Therefore

$$\left|\left|u_1\left(\mathbf{x}\right)\right|\right|_{L^\infty(\Omega)} \leq C\varepsilon^{1/2}.$$

We also found an expression

$$\begin{aligned}u_1^0\left(\mathbf{x}\right) &\equiv \frac{\varepsilon^{1/2}}{2}\frac{\sqrt{2/\mu}\kappa\left(\mathbf{x}\right)\sinh\left(\frac{\sqrt{2}(\varepsilon\mu)^{1/2}}{|\sigma(x_S)|}\right)\left[\left|\sigma\left(x_S\right)\right|\frac{\xi(\mathbf{x})}{\varepsilon}+2\right]}{\cosh^4\left[\left(\frac{\sqrt{2}(\varepsilon\mu)^{1/2}}{|\sigma(x_S)|}\right)\left[\left|\sigma\left(x_S\right)\right|\frac{\xi(\mathbf{x})}{2\varepsilon}+1\right]\right]+\sinh^4\left[\left(\frac{\sqrt{2}(\varepsilon\mu)^{1/2}}{|\sigma(x_S)|}\right)\left[\left|\sigma\left(x_S\right)\right|\frac{\xi(\mathbf{x})}{2\varepsilon}+1\right]\right]}\\ &= O\left(\varepsilon^{1/2}\right),\end{aligned}$$

and hence

$$\left|\left|u_1^1\left(\mathbf{x}\right)\right|\right|_{L^\infty(\Omega_1)} \leq C\varepsilon^{1/2}.$$

In $\partial\Omega_1$,

$$\begin{aligned}u_0\left(x_S\right) &= 2\zeta\left(\frac{\xi\left(x_S\right)}{\delta}\right)\log\tanh\left(\frac{\sqrt{2}\left(\varepsilon\mu\right)^{1/2}}{\left|\sigma\left(x_S\right)\right|}\right)\left[\frac{\sigma\left(x_S\right)}{2}\frac{\xi\left(x_S\right)}{\varepsilon}+1\right]\\ &= 2\log\tanh\left(\frac{\sqrt{2}\left(\varepsilon\mu\right)^{1/2}}{\left|\sigma\left(x_S\right)\right|}\right),\end{aligned} \tag{3.22}$$

$$u_1\left(x_S\right) = \frac{\varepsilon^{1/2}}{2}\frac{\sqrt{2/\mu}\mathcal{H}\left(x_S\right)\sinh\left(\frac{2\sqrt{2}(\varepsilon\mu)^{1/2}}{|\sigma(x_S)|}\right)}{\cosh^4\left[\left(\frac{\sqrt{2}(\varepsilon\mu)^{1/2}}{|\sigma(x_S)|}\right)\right]+\sinh^4\left[\left(\frac{\sqrt{2}(\varepsilon\mu)^{1/2}}{|\sigma(x_S)|}\right)\right]}. \tag{3.23}$$

We remind that $\mathcal{H}(\mathbf{x})$ is the curvature of the level surface of the distance function that contains the point $\mathbf{x}$. In the limit when $\mathbf{x} \longrightarrow \partial\Omega$, that curvature tends to the mean curvature of the interface at x_S.

Then at $x_S \in \partial\Omega_1$

$$\begin{aligned} F(V(x_S)) &= -2\varepsilon\mu\cosh\left(\frac{\overline{u}}{\varepsilon}\right) = -2\varepsilon\mu\cosh\left(u_0 + u_1^0 + \varepsilon^{1/2}O(\varepsilon^a)\right) \\ &= -2\varepsilon\mu\cosh\left(2\log\tanh\frac{\sqrt{2}(\varepsilon\mu)^{1/2}}{|\sigma(x_S)|}\right) \\ &- \varepsilon^{3/2}\frac{\sqrt{2\mu}\mathcal{H}(x_S)\sinh\left(2\log\tanh\frac{\sqrt{2}(\varepsilon\mu)^{1/2}}{|\sigma(x_S)|}\right)\sinh\left(\frac{2\sqrt{2}(\varepsilon\mu)^{1/2}}{|\sigma(x_S)|}\right)}{\cosh^4\left(\frac{\sqrt{2}(\varepsilon\mu)^{1/2}}{|\sigma(x_S)|}\right) + \sinh^4\left(\frac{\sqrt{2}(\varepsilon\mu)^{1/2}}{|\sigma(x_S)|}\right)} \\ &+ \varepsilon^{1/2}O\left(\varepsilon^2\right). \end{aligned}$$

We have

$$-2\varepsilon\mu\cosh\left(2\log\tanh\frac{\sqrt{2}(\varepsilon\mu)^{1/2}}{|\sigma(x_S)|}\right) = -\frac{\sigma(x_S)^2}{2} - \frac{2}{3}\mu\varepsilon + O\left(\varepsilon^2\right)$$

$$-\varepsilon^{3/2}\sqrt{2\mu}\mathcal{H}(x_S)\frac{\sinh\left(2\log\tanh\frac{\sqrt{2}(\varepsilon\mu)^{1/2}}{|\sigma(x_S)|}\right)\sinh\left(\frac{2\sqrt{2}(\varepsilon\mu)^{1/2}}{|\sigma(x_S)|}\right)}{\cosh^4\left(\frac{\sqrt{2}(\varepsilon\mu)^{1/2}}{|\sigma(x_S)|}\right) + \sinh^4\left(\frac{\sqrt{2}(\varepsilon\mu)^{1/2}}{|\sigma(x_S)|}\right)} = \mathcal{H}(x_S)|\sigma(x_S)|\varepsilon + O\left(\varepsilon^2\right).$$

Therefore in $\partial\Omega_1$

$$F(V(x_S)) = -\frac{\sigma(x_S)^2}{2} - \frac{2}{3}\mu\varepsilon + \mathcal{H}(x_S)|\sigma(x_S)|\varepsilon + O\left(\varepsilon^2\right). \tag{3.24}$$

Assuming $\mu \ll 1$ we can redefine the pressure to drop off $-\frac{2}{3}\mu\varepsilon$ and we have:

$$F(V(x_S)) = -\frac{\sigma(x_S)^2}{2} + \mathcal{H}(x_S)|\sigma(x_S)|\varepsilon + O\left(\varepsilon^2\right). \tag{3.25}$$

We know also that the surface charge density for the electrolyte, i.e $-\frac{\partial V}{\partial \mathbf{n}}(x_S)$, $x_S \in \partial\Omega_1$ is approximately the function $\sigma(x_S)$:

$$\sigma(x_S) = \sigma_0(x_S) + \varepsilon\sigma_1(x_S) + O(\varepsilon^2),$$

σ_0 the charge density for the perfect conductor and σ_1 is the correction given by the lemma 3.2 in [28] (see also the previous chapter) and it has the expression

$$\sigma_1(x_S) = -\frac{2\int_{\partial\Omega}\mathcal{N}(\ln(\sigma_0))}{Q}\sigma_0(x_S) + 2\mathcal{N}(\ln(\sigma_0)) + O(\varepsilon),$$

$\mathcal{N}$ the Dirichlet to Neumann operator restricted to $\partial\Omega_1$.

Therefore

$$F(V(x_S)) = -\frac{\sigma_0(x_S)^2}{2} - \varepsilon\sigma_0(x_S)\sigma_1(x_S) + \mathcal{H}(x_S)\sigma_0(x_S)\varepsilon + O\left(\varepsilon^2\right). \tag{3.26}$$

Let us note that when $\varepsilon \longrightarrow 0$ (i.e physically the mobility of the ions tend to infinity)

$$F\left(V\left(x_S\right)\right) = -\frac{\sigma_0\left(x_S\right)^2}{2},$$

that corresponds (as it should be) to the perfect conductor case.

The expansion leading to (3.26) in terms of powers of ε assumed $\varepsilon, \mu \ll 1$. As we will see in the next section, ε is in general a small parameter. Nevertheless the combination $\frac{(\varepsilon\mu)^{1/2}}{|\sigma|}$ might not be small for very concentrated ionic solutions (implying large values of μ). In this case the expression for $F(V)$ might need to be changed accordingly. For very concentrated ionic solutions, using (3.21), (3.22), (3.23) we straightforwardly arrive at

$$\begin{aligned} F(V) &= -2\varepsilon\mu\cosh(u_0+u_1) \\ &\simeq -\varepsilon\mu e^{-u_0-u_1} = -\frac{\sigma^2}{2} g_1\left(s\right) e^{-\varepsilon g_2(s)\frac{\mathcal{H}(x)}{|\sigma|}}, \end{aligned}$$

where $s = \frac{\sqrt{2}(\varepsilon\mu)^{\frac{1}{2}}}{\sigma}$ and

$$\begin{aligned} g_1\left(s\right) &= s^2\coth^2 s, \\ g_2\left(s\right) &= \frac{1}{s}\frac{\sinh(2s)}{\cosh^4 s + \sinh^4 s}. \end{aligned}$$

If $s \to 0$, and $\varepsilon \ll 1$, then $g_1\left(s\right) \to 1, g_2\left(s\right) \to 2$ and we recover the result for dilute solutions. In Figures 3.5, 3.6 we represent $g_1(s)$ and $g_2(s)$ respectively.

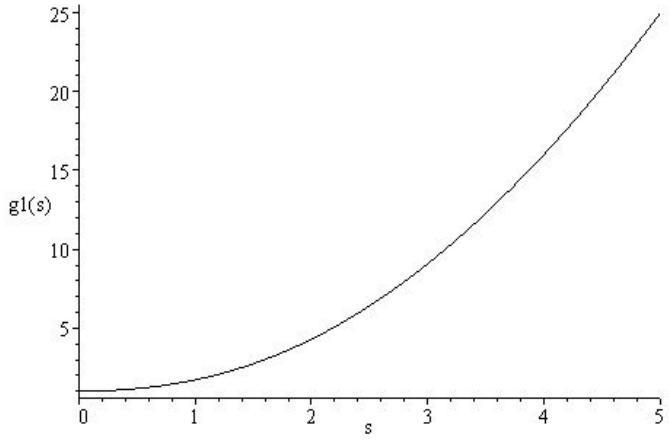

Figure 3.5: The function $g_1(s)$

Let us note that among other quantities, we will need σ_0 and $\mathcal{N}\left(\ln\left(\sigma_0\right)\right)$ to completely obtain the boundary conditions for our model so we will set up integral equations to obtaining them. Before doing so, let us analyze the orders of magnitude for the quantities that will be involved in our model.

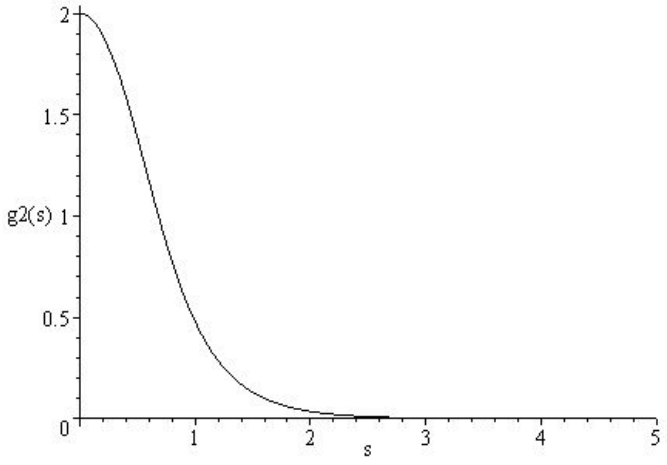

Figure 3.6: The function $g_2(s)$

3.3 Orders of magnitude

In order to get an idea of the orders of magnitude involved in the arguments developed above, we compute here the numerical values of various quantities in realistic physical situations.

The dielectric permitivity in vacuum ε_0, charge of the electron e, Boltzmann constant k_B, molecular mass of salt, molecular mass of sodium Iodide, surface tension of water-air interface at 25^o, Avogadro number N_A, seawater salt concentration and saturation (that is, maximum possible) salt concentration are

$$\begin{aligned}
\varepsilon_0 &= 8.8541878 \times 10^{-12}\ C^2 N^{-1} m^{-2},\\
e &= 1.60217657 \times 10^{-19}\ C,\\
k_B &= 1.3806488 \times 10^{-23}\ JK^{-1},\\
\text{Molecular mass } NaCl &: 58.4430 \pm 0.0001 g/mol,\\
\text{Molecular mass } NaI &: 149.894242 \pm 0.000001 g/mol,\\
\gamma \text{ (water/air, } 25^o C) &: 71.99 \pm 0.05\ mN{\cdot}m^{-1},\\
N_A &= 6.023\ \times 10^{23}\ mol^{-1},\\
\text{Seawater salt concentration} &: 35\ g/l,\\
\text{Saturation salt concentration} &: 359\ g/l,
\end{aligned}$$

respectively. We are assuming binary ionic solutions, where $NaCl$ (or NaI) molecules produce Na^+ and Cl^- (or Na^+ and I^-) ions. With all these numbers, assuming a temperature of $25^o C$ (298 K) we can compute (approximating the relative permittivity $\varepsilon_r \simeq 1$, valid for almost all liquids.)

$$\varepsilon = \frac{\varepsilon_0 k_B T R_0}{e^2 z^2} \sim \frac{(8.8541878 \times 10^{-12})\,(1.3806488 \times 10^{-23}) \times 298}{(1.60217657 \times 10^{-19})^2} R_0 = 1419 R_0,$$

where R_0 is the radius of the drop. We take, for instance, $R_0 = 10\ \mu m$, that is

$$R_0 = 10^{-5} m,$$

and hence the dimensionless parameter ε has a value

$$\varepsilon = 1419 R_0 = 0.01419,$$

which is an $O(10^{-2})$ quantity. This justifies the assumption $\varepsilon \ll 1$ in previous sections.

We compute next the Debye length λ_D. Let's take ion concentration as the concentration of salt in seawater:

$$n_\infty = \frac{35\ g/l}{58.4430\ g/mol} = 0.599 \frac{mol}{l},$$

and then

$$\lambda_D = \sqrt{\frac{(8.8541878 \times 10^{-12})\,(1.3806488 \times 10^{-23}) \times 298}{2\,(1.60217657 \times 10^{-19})^2\,(599 \times 6.022\ \times 10^{23})}}\ m = 4.435\,2 \times 10^{-11}\ m.$$

If we compare the Debye length with the radius of the drop we find

$$\frac{\lambda_D}{R_0} = 4.435\,2 \times 10^{-5},$$

which justifies the assumption that Debye layers, whose thickness is of the order of Debye length, consist of a thin layer near the boundary of drops. In the situation described, the number of positive ions is

$$M = 0.599 \frac{N_A}{(10^4)^3} = 0.599 \frac{6.022\ \times 10^{23}}{(10^4)^3} = 3.607\,2 \times 10^{11}\ \text{ions}$$

and hence the Rayleigh fissibility ratio will be

$$X = \frac{Q^2}{32\gamma\pi^2\varepsilon_0 R_0^3} = \frac{N_e^2 e^2}{32\gamma\pi^2\varepsilon_0 R_0^3} = \frac{(1.60217657 \times 10^{-19})^2}{32\,(0.07199)\,\pi^2\,(8.8541878 \times 10^{-12})\,10^{-15}} N_e^2 = 1.2751 \times 10^{-13} N_e^2,$$

where N_e is the number of free electrons. In order to make the drop unstable, we must have a number of free electrons

$$N_e \sim 2.8 \times 10^6,$$

which is roughly one free electron for each 10^5 positive (or negative) ions.

We remind now the relation between the physical potential V and the unknown in Poisson-Boltzmann equation u:

$$V = \frac{ez}{\varepsilon_0 R_0} u.$$

Therefore, the rescaled surface charge density σ rescaled with the physical surface charge density Σ in the form

$$\sigma = -\frac{\partial u}{\partial \mathbf{n}'} = -\frac{\varepsilon_0 R_0^2}{ez} \frac{\partial V}{\partial \mathbf{n}} = \frac{R_0^2}{ez} \Sigma,$$

where $\frac{\partial}{\partial \mathbf{n}'}$ denotes the normal derivative in rescaled variables and $\frac{\partial}{\partial \mathbf{n}}$ the normal derivative in physical space. If we take a spherical drop, then the total charge is $4\pi R_0^2 \Sigma$ so that

$$\sigma = \frac{N_e}{4\pi}.$$

In our asymptotic analysis of Poisson-Boltzmann equation, the following quantity appears:

$$\chi \equiv \frac{\sqrt{2}\left(\varepsilon\mu\right)^{\frac{1}{2}}}{\sigma},$$

and then, for a spherical drop of salt seawater at $25^{o}C$ and charged at critical charge value,

$$\chi = \frac{4\pi\sqrt{2}\left(\varepsilon\mu\right)^{\frac{1}{2}}}{N_e} = \frac{4\pi\sqrt{2}(0.01419 \times 3.607\,2 \times 10^{11})^{\frac{1}{2}}}{2.8 \times 10^{6}} = 0.45409,$$

a quantity that decreases with lower ion concentration (lower μ) and larger number of free electrons N_e. On the other hand, at saturation, salt concentration μ is roughly ten times the value for seawater salt concentration and hence

$$\chi \simeq (10)^{\frac{1}{2}} 0.45409 = 1.4360.$$

3.4 The Boundary Integral Equation for a harmonic function

3.4.1 Introduction

We are interested now in calculating the boundary condition:

$$F\left(V\right) = -\frac{\sigma_0\left(x_S\right)^2}{2} - \varepsilon\sigma_0\left(x_S\right)\sigma_1\left(x_S\right) + \mathcal{H}\left(x_S\right)\sigma_0\left(x_S\right)\varepsilon + O\left(\varepsilon^2\right),$$

where $\sigma_0\left(x_S\right)$ is the surface charge density for the perfect conductor and

$$\sigma_1\left(x_S\right) = -2\frac{\int_{\partial\Omega}\mathcal{N}\left(\ln\left(\sigma_0\right)\right)}{Q}\sigma_0\left(x_S\right) + 2\mathcal{N}\left(\ln\left(\sigma_0\right)\right) + O\left(\varepsilon\right),$$

with Q the net amount of electric charge, $\mathcal{N}$ the Dirichlet to Neumann operator restricted to $\partial\Omega_1$. The functions $\sigma_0\left(x_S\right)$ and $\mathcal{N}\left(\ln\left(\sigma_0\right)\right)$ are related to the Laplace equation in Ω_2.

Strictly speaking, the domain depends on time because it is evolved by the velocity field and pressure, so we have a free boundary problem, but as we said before, we can fix a time t and deal with the steady state problem because we can use recursivity and an evolution formula depending on velocity to obtain the solution in the new domain $\Omega\left(t+\Delta t\right)$. Let us consider

$$\begin{aligned} \Delta u\left(\mathbf{x}\right) &= 0 \text{ in } \Omega_2, \\ u\left(\mathbf{x}\right)|_{\partial\Omega_1} &= u_0\left(\mathbf{x}\right), \\ u\left(\mathbf{x}\right) &\longrightarrow O\left(\left|\mathbf{x}\right|^{-1}\right) \text{ for } \left|\mathbf{x}\right| \longrightarrow \infty. \end{aligned} \tag{3.27}$$

The last problem is related with $F\left(V\right)$ in the following sense: if we take $u_0\left(\mathbf{x}\right) = C$ for an appropriate constant C we have $\sigma_0\left(\mathbf{x}\right) = -\frac{\partial u}{\partial \mathbf{n}}\big|_{\partial\Omega_1}$ and if $u_0\left(\mathbf{x}\right) = \ln\left(\sigma_0\left(\mathbf{x}\right)\right)$ then $\mathcal{N}\left(\ln\left(\sigma_0\right)\right) = \frac{\partial u}{\partial \mathbf{n}}\big|_{\partial\Omega_1}$, so let us obtain first an integral formula for the harmonic function in (3.27).

3.4.2 Integral equation

Let us consider a ball $B(\mathbf{0}, R)$ of radius R and center at the origin and contains Ω_1 (see Fig. 3.7) and denote $\Omega_R^* = B(\mathbf{0}, R)$, we will consider the auxiliar problem

$$\begin{aligned} \Delta u(\mathbf{x}) &= 0 \text{ in } \Omega_R^* \backslash \overline{\Omega_1}, \\ u(\mathbf{x})|_{\partial\Omega} &= u_0(\mathbf{x}), \\ u(\mathbf{x}) &= O\left(R^{-1}\right) \text{ on } \partial\Omega_R^*. \end{aligned} \tag{3.28}$$

By classical theory for elliptic problems we know that the solution to this problem exists and is unique for each R.

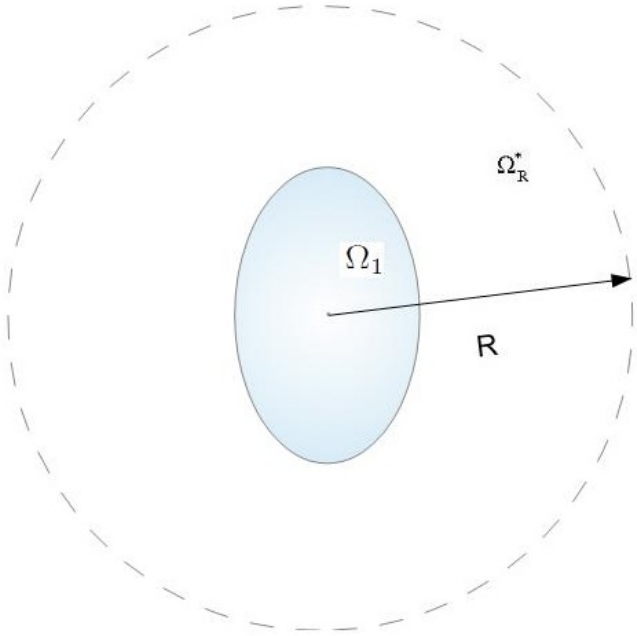

Figure 3.7: The domains Ω_R^* and Ω_1. Let us note that $\Omega_R^* \setminus \Omega_1 \to \Omega_2$ when $R \to \infty$

Let us consider a scalar partial differential equation

$$(\mathcal{L}u)(x) = f(x) \quad x \in U \subset \mathbb{R}^n.$$

Definition 11. *A fundamental solution of the PDE is the solution of*

$$(\mathcal{L}_y G(x, y))(x, y) = \delta(y - x) \quad x, y \in \mathbb{R}^n$$

in the distributional sense.

Green's functions are distributions. A Green function $G(\mathbf{x}, \mathbf{x}_0)$ of Laplace equation in $\mathbb{R}^3$ satisfies the Laplace equation singularly forced in distributional sense

$$\Delta_{\mathbf{x}} G(\mathbf{x}, \mathbf{x}_0) = -\delta(\mathbf{x} - \mathbf{x}_0), \tag{3.29}$$

where δ is the Dirac Delta function in $\mathbb{R}^3$. The point $\mathbf{x}$ is the variable field point and $\mathbf{x}_0$ is the fixed location of the singular point or pole. A property of Green functions is symmetry, so $G(\mathbf{x},\mathbf{x}_0) = G(\mathbf{x}_0,\mathbf{x})$.

Using Fourier transform or by simple inspection we can find that $G(\mathbf{x},\mathbf{x}_0) = \frac{1}{4\pi|\mathbf{x}-\mathbf{x}_0|}$ is a fundamental solution to (3.29).

For G the fundamental solution and u satisfying (3.28), we multiply the first equation in (3.28) by G, and using the Green theorem for distributions [15] we have

$$\begin{aligned}\int_{\Omega_R^*\backslash\overline{\Omega_1}} u(\mathbf{x})\,\Delta G(\mathbf{x},\mathbf{x}_0)\,dV(\mathbf{x}) &= -\int_{\Omega_R^*\backslash\overline{\Omega_1}} u(\mathbf{x})\,\delta(\mathbf{x}-\mathbf{x}_0)\,dV(\mathbf{x}) \qquad (3.30)\\ &= \int_{\partial\left(\Omega_R^*\backslash\overline{\Omega_1}\right)} u(\mathbf{x})\,\frac{\partial G(\mathbf{x},\mathbf{x}_0)}{\partial\widetilde{\mathbf{n}}}dS(\mathbf{x}) - \int_{\Omega_R^*\backslash\overline{\Omega_1}} \nabla u(\mathbf{x})\cdot\nabla G(\mathbf{x},\mathbf{x}_0)\,dV(\mathbf{x}),\end{aligned}$$

with $\widetilde{\mathbf{n}}$ normal exterior to $\Omega_R^*\backslash\overline{\Omega_1}$. Also

$$0 = \int_{\Omega_R^*\backslash\overline{\Omega_1}} \Delta u(\mathbf{x})\,G(\mathbf{x},\mathbf{x}_0)\,dV(\mathbf{x}) = \int_{\partial\left(\Omega_R^*\backslash\overline{\Omega_1}\right)} \frac{\partial u(\mathbf{x})}{\partial\widetilde{\mathbf{n}}}G(\mathbf{x},\mathbf{x}_0)\,dS(\mathbf{x}) - \int_{\Omega_R^*\backslash\overline{\Omega_1}} \nabla u(\mathbf{x})\cdot\nabla G(\mathbf{x},\mathbf{x}_0)\,dV(\mathbf{x}) \qquad (3.31)$$

Substracting (3.30) of (3.31) we obtain

$$\int_{\Omega_R^*\backslash\overline{\Omega_1}} u(\mathbf{x})\,\delta(\mathbf{x}-\mathbf{x}_0)\,dV(\mathbf{x}) = \int_{\partial\left(\Omega_R^*\backslash\overline{\Omega_1}\right)} G(\mathbf{x},\mathbf{x}_0)\,\frac{\partial u(\mathbf{x})}{\partial\widetilde{\mathbf{n}}}dS(\mathbf{x}) - \int_{\partial\left(\Omega_R^*\backslash\overline{\Omega_1}\right)} u(\mathbf{x})\,\frac{\partial G(\mathbf{x},\mathbf{x}_0)}{\partial\widetilde{\mathbf{n}}}dS(\mathbf{x}). \qquad (3.32)$$

We can perform the last procedure for each R so we can take $R \longrightarrow \infty$ and due to the nature of u, G, $\frac{\partial u}{\partial\widetilde{\mathbf{n}}}$, $\frac{\partial G}{\partial\widetilde{\mathbf{n}}}$ using the normal $\mathbf{n}$ exterior to Ω_1 we have:

For $\mathbf{x}_0 \in \Omega_1$

$$0 = -\int_{\partial\Omega_1} G(\mathbf{x},\mathbf{x}_0)\,\frac{\partial u(\mathbf{x})}{\partial\mathbf{n}}dS(\mathbf{x}) + \int_{\partial\Omega_1} u(\mathbf{x})\,\frac{\partial G(\mathbf{x},\mathbf{x}_0)}{\partial\mathbf{n}}dS(\mathbf{x}). \qquad (3.33)$$

For $\mathbf{x}_0 \notin \overline{\Omega_1}$

$$u(\mathbf{x}_0) = -\int_{\partial\Omega_1} G(\mathbf{x},\mathbf{x}_0)\,\frac{\partial u(\mathbf{x})}{\partial\mathbf{n}}dS(\mathbf{x}) + \int_{\partial\Omega_1} u(\mathbf{x})\,\frac{\partial G(\mathbf{x},\mathbf{x}_0)}{\partial\mathbf{n}}dS(\mathbf{x}). \qquad (3.34)$$

Equation (3.34) provides us with a boundary integral representation for a harmonic function in terms of the boundary values and the boundary distribution of the normal derivative, but we are interested in obtaining a formula for points $\mathbf{x}_0 \in \partial\Omega_1$ that allows us to use the known values for $u(\mathbf{x}_0)$ and then inverting numerically the integral form of the harmonic equation like was done in [26] to obtain $\left.\frac{\partial u(\mathbf{x})}{\partial\mathbf{n}}\right|_{\partial\Omega_1}$. We can approach to $\partial\Omega_1$ from points of Ω_1 and use the formula (3.33), and from points of $\mathbb{R}^3\backslash\bar{\Omega}_1$ and use (3.34) and we should be capable to obtain the same formula from both approximations to deal with a well posed problem.

Let us adopt the electrostatic terminology for the integrals in (3.33) and in (3.34). We will call to $-\int_{\partial\Omega_1} G(\mathbf{x},\mathbf{x}_0)\frac{\partial u(\mathbf{x})}{\partial \mathbf{n}}dS(\mathbf{x})$ the single layer integral, and double layer integral to $\int_{\partial\Omega_1} u(\mathbf{x})\frac{\partial G(\mathbf{x},\mathbf{x}_0)}{\partial \mathbf{n}}dS(\mathbf{x})$.

If $\mathbf{x}_0 \longrightarrow \partial\Omega_1$ from Ω_1 or from $\overline{\Omega_1}^c = \Omega_2$ the single layer potential varies continuously when the point approximates and then crosses $\partial\Omega_1$, so we will study the double layer potential that is discontinuous in $\partial\Omega_1$. For the moment we will suppose that all the boundaries are smooth, i.e they do not exhibit conical, edge-like, or cusp-like corners.

Let us consider (3.29) in $\mathbb{R}^3$.

If $\mathbf{x}_0 \in \Omega_1$, then using the divergence theorem

$$-1 = -\int_{\Omega_1} \delta(\mathbf{x}-\mathbf{x}_0)\,dV(\mathbf{x}) = \int_{\Omega_1} \Delta G(\mathbf{x},\mathbf{x}_0)\,dV(\mathbf{x}) = \int_{\partial\Omega_1} \frac{\partial G}{\partial \mathbf{n}}(\mathbf{x},\mathbf{x}_0)\,dS(\mathbf{x}).$$

If $\mathbf{x}_0 \notin \overline{\Omega_1}$

$$0 = -\int_{\Omega_1} \delta(\mathbf{x}-\mathbf{x}_0)\,dV(\mathbf{x}) = \int_{\Omega_1} \Delta G(\mathbf{x},\mathbf{x}_0)\,dV(\mathbf{x}) = \int_{\partial\Omega_1} \frac{\partial G}{\partial \mathbf{n}}(\mathbf{x},\mathbf{x}_0)\,dS(\mathbf{x}).$$

If $\mathbf{x}_0 \in \partial\Omega_1$ the integral $\int_{\partial\Omega_1} \frac{\partial G}{\partial \mathbf{n}}(\mathbf{x},\mathbf{x}_0)\,dS(\mathbf{x})$ is a principal value integral. Let us consider a ball centered in $\mathbf{x}_0$ and radius ε. We start considering the part of the ball $B(\mathbf{x}_0,\varepsilon)$ that lies outside Ω_1, let us denote S_ε its boundary. Let us denote $\partial\Omega_\varepsilon^0$ the subset of $\partial\Omega_1$ without a plane "disk" on $\partial\Omega_1$ centered in $\mathbf{x}_0$ and radius ε and $\partial\Omega_\varepsilon = \partial\Omega_\varepsilon^0 \cup S_\varepsilon$. V_ε will denote the volume bounded for $\partial\Omega_\varepsilon$, so in this case $\mathbf{x}_0 \in V_\varepsilon$. We have

$$\int_{\partial\Omega_\varepsilon} \frac{\partial G}{\partial \mathbf{n}}(\mathbf{x},\mathbf{x}_0)\,dS(\mathbf{x}) = \int_{\partial\Omega_\varepsilon^0} \frac{\partial G}{\partial \mathbf{n}}(\mathbf{x},\mathbf{x}_0)\,dS(\mathbf{x}) + \int_{S_\varepsilon} \frac{\partial G}{\partial \mathbf{n}}(\mathbf{x},\mathbf{x}_0)\,dS(\mathbf{x}),$$

with $\mathbf{n}$ exterior to V_ε. The divergence theorem implies

$$-1 = -\int_{V_\varepsilon} \delta(\mathbf{x}-\mathbf{x}_0)\,dV(\mathbf{x}) = \int_{\partial\Omega_\varepsilon} \frac{\partial G}{\partial \mathbf{n}}(\mathbf{x},\mathbf{x}_0)\,dS(\mathbf{x}),$$

so that

$$-1 = \int_{\partial\Omega_\varepsilon^0} \frac{\partial G}{\partial \mathbf{n}}(\mathbf{x},\mathbf{x}_0)\,dS(\mathbf{x}) + \int_{S_\varepsilon} \frac{\partial G}{\partial \mathbf{n}}(\mathbf{x},\mathbf{x}_0)\,dS(\mathbf{x}).$$

Let us calculate

$$\lim_{\varepsilon\longrightarrow 0}\int_{\partial\Omega_\varepsilon^0} \frac{\partial G}{\partial \mathbf{n}}(\mathbf{x},\mathbf{x}_0)\,dS(\mathbf{x}).$$

We note (assuming that both limits exist)

$$\lim_{\varepsilon\longrightarrow 0}\int_{\partial\Omega_\varepsilon^0} \frac{\partial G}{\partial \mathbf{n}}(\mathbf{x},\mathbf{x}_0)\,dS(\mathbf{x}) = -1 - \lim_{\varepsilon\longrightarrow 0}\int_{S_\varepsilon} \frac{\partial G}{\partial \mathbf{n}}(\mathbf{x},\mathbf{x}_0)\,dS(\mathbf{x}),$$

with $\mathbf{n}$ exterior to V_ε.

The normal exterior to S_ε is $\mathbf{e}_r$ and $\frac{\partial G(\mathbf{x},\mathbf{x}_0)}{\partial \mathbf{n}} = \frac{\partial G(\mathbf{x},\mathbf{x}_0)}{\partial r} = -\frac{1}{4\pi r^2}$

$$\int_{S_\varepsilon} \frac{\partial G(\mathbf{x},\mathbf{x}_0)}{\partial \mathbf{n}} dS(\mathbf{x}) = -\frac{1}{4\pi}\int_0^{2\pi}\int_{\pi/2}^{\pi} \frac{1}{|\mathbf{x}-\mathbf{x}_0|^2}\varepsilon^2 \sin\theta d\theta d\phi = -\frac{1}{2}.$$

So in this case

$$\lim_{\varepsilon\longrightarrow 0}\int_{\partial\Omega_\varepsilon^0} \frac{\partial G}{\partial \mathbf{n}}(\mathbf{x},\mathbf{x}_0)\, dS(\mathbf{x}) = -\frac{1}{2}.$$

Let us consider now the part of the ball $B(\mathbf{x}_0,\varepsilon)$ that lies inside Ω_1 and denote its boundary in Ω_1 by S_ε, and $\partial\Omega_\varepsilon = \partial\Omega_\varepsilon^0 \cup S_\varepsilon$ and V_ε the corresponding volume (see Figure 3.8).

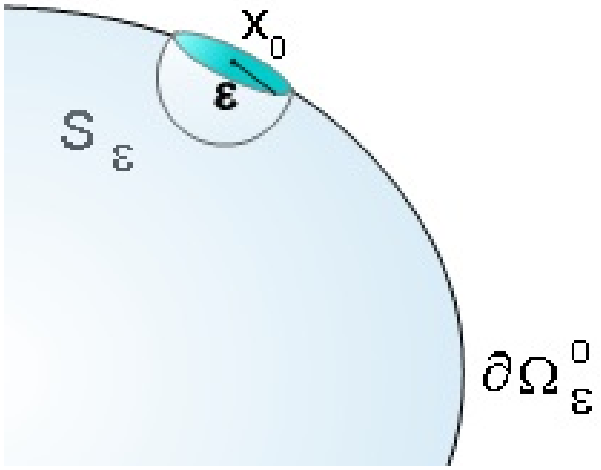

Figure 3.8: We remove from the boundary $\partial\Omega$ a disc of radius ε and we denote the resulting surface by $\partial\Omega_\varepsilon^0$. We have $\partial\Omega_\varepsilon^0 \to \partial\Omega$

In this case $\mathbf{x}_0 \notin V_\varepsilon$

$$0 = -\int_{V_\varepsilon} \delta(\mathbf{x}-\mathbf{x}_0)\, dV(\mathbf{x}) = \int_{\partial\Omega_\varepsilon} \frac{\partial G}{\partial \mathbf{n}}(\mathbf{x},\mathbf{x}_0)\, dS(\mathbf{x}),$$

as before $\mathbf{n}$ exterior to V_ε.

In this case the normal exterior to S_ε is $-\mathbf{e}_r$ and $\frac{\partial G(\mathbf{x},\mathbf{x}_0)}{\partial \mathbf{n}} = -\frac{\partial G(\mathbf{x},\mathbf{x}_0)}{\partial r} = \frac{1}{4\pi r^2}$

$$\int_{S_\varepsilon} \frac{\partial G(\mathbf{x},\mathbf{x}_0)}{\partial \mathbf{n}} dS(\mathbf{x}) = \frac{1}{4\pi}\int_0^{\pi}\int_0^{\pi} \frac{1}{|\mathbf{x}-\mathbf{x}_0|^2}\varepsilon^2 \sin\theta d\theta d\phi = \frac{1}{2},$$

and we have again

$$\begin{aligned}\lim_{\varepsilon\longrightarrow 0}\int_{\partial\Omega_\varepsilon^0} \frac{\partial G}{\partial \mathbf{n}}(\mathbf{x},\mathbf{x}_0)\, dS(\mathbf{x}) &= -\lim_{\varepsilon\longrightarrow 0}\int_{S_\varepsilon} \frac{\partial G}{\partial \mathbf{n}}(\mathbf{x},\mathbf{x}_0)\, dS(\mathbf{x}),\\ &= -\frac{1}{2}.\end{aligned}$$

Then we can say

$$\int_{\partial\Omega}^{PV} \frac{\partial G}{\partial \mathbf{n}}(\mathbf{x}, \mathbf{x}_0)\, dS(\mathbf{x}) = -\frac{1}{2},$$

where the symbol PV denotes the fact that the integral is understood in the principal value sense.

We have then:

$$\int_{\partial\Omega_1} \frac{\partial G}{\partial \mathbf{n}}(\mathbf{x}, \mathbf{x}_0)\, dS(\mathbf{x}) = \begin{cases} 0 \text{ if } x_0 \notin \overline{\Omega_1} \\ -\frac{1}{2} \text{ if } x_0 \in \partial\Omega_1 \text{ (PV integral)} \\ -1 \text{ if } x_0 \in \Omega_1 \end{cases}, \tag{3.35}$$

with $\mathbf{n}$ the normal exterior to Ω_1.

Now let us return to the deduction of the formula.

If $\mathbf{x}_0 \longrightarrow \partial\Omega_1$ from points of Ω_1

$$\lim_{\mathbf{x}_0 \longrightarrow \partial\Omega_1} \int_{\partial\Omega_1} u(\mathbf{x}) \frac{\partial G(\mathbf{x}, \mathbf{x}_0)}{\partial \mathbf{n}} dS(\mathbf{x}) = \lim_{\varepsilon \longrightarrow 0} \left[\int_{\partial\Omega_\varepsilon^0} u(\mathbf{x}) \frac{\partial G(\mathbf{x}, \mathbf{x}_0)}{\partial \mathbf{n}} dS(\mathbf{x}) + \int_{S_\varepsilon} u(\mathbf{x}) \frac{\partial G(\mathbf{x}, \mathbf{x}_0)}{\partial \mathbf{n}} dS(\mathbf{x}) \right],$$

with $\partial\Omega_\varepsilon^0$ as before and S_ε the (out Ω_1) semisphere of radius ε (Figure 3.9).

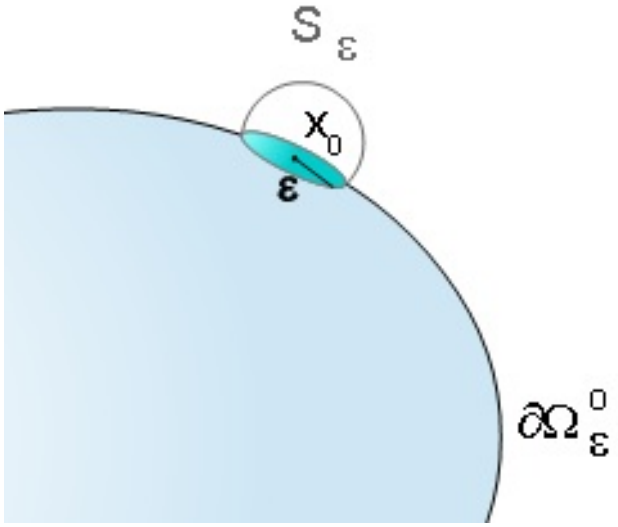

Figure 3.9: As before, we remove from the boundary $\partial\Omega$ a disc of radius ε and we denote again the resulting surface by $\partial\Omega_\varepsilon^0$.

$$\lim_{\varepsilon \longrightarrow 0} \int_{S_\varepsilon} u(\mathbf{x}) \frac{\partial G(\mathbf{x}, \mathbf{x}_0)}{\partial \mathbf{n}} dS(\mathbf{x}) = -\frac{u(\mathbf{x}_0)}{2},$$

because u is continuous and

$$\int_{S_\varepsilon} \frac{\partial G(\mathbf{x}, \mathbf{x}_0)}{\partial \mathbf{n}} dS(\mathbf{x}) = -\frac{1}{2}.$$

Then

$$\lim_{\mathbf{x}_0 \longrightarrow \partial\Omega_1} \int_{\partial\Omega_1} u(\mathbf{x}) \frac{\partial G(\mathbf{x}, \mathbf{x}_0)}{\partial \mathbf{n}} dS(\mathbf{x}) = \int_{\partial\Omega_1}^{PV} u(\mathbf{x}) \frac{\partial G(\mathbf{x}, \mathbf{x}_0)}{\partial \mathbf{n}} dS(\mathbf{x}) - \frac{u(\mathbf{x}_0)}{2}.$$

And (3.33) implies

$$u(\mathbf{x}_0) = -2 \int_{\partial\Omega_1} G(\mathbf{x}, \mathbf{x}_0) \frac{\partial u}{\partial \mathbf{n}}(\mathbf{x}) dS(\mathbf{x}) + 2 \int_{\partial\Omega_1}^{PV} u(\mathbf{x}) \frac{\partial G(\mathbf{x}, \mathbf{x}_0)}{\partial \mathbf{n}} dS(\mathbf{x}).$$

If now $\mathbf{x}_0 \longrightarrow \partial\Omega_1$ from points of Ω_2, we have

$$\lim_{\mathbf{x}_0 \longrightarrow \partial\Omega_1} \int_{\partial\Omega_1} u(\mathbf{x}) \frac{\partial G(\mathbf{x}, \mathbf{x}_0)}{\partial \mathbf{n}} dS(\mathbf{x}) = \lim_{\varepsilon \longrightarrow 0} \left[\int_{\partial\Omega_\varepsilon^0} u(\mathbf{x}) \frac{\partial G(\mathbf{x}, \mathbf{x}_0)}{\partial \mathbf{n}} dS(\mathbf{x}) + \int_{S_\varepsilon} u(\mathbf{x}) \frac{\partial G(\mathbf{x}, \mathbf{x}_0)}{\partial \mathbf{n}} dS(\mathbf{x}) \right],$$

with S_ε the corresponding (inside Ω_1) semisphere S_ε of radius ε. In this case, similarly as before we obtain

$$\lim_{\varepsilon \longrightarrow 0} \int_{S_\varepsilon} u(\mathbf{x}) \frac{\partial G(\mathbf{x}, \mathbf{x}_0)}{\partial \mathbf{n}} dS(\mathbf{x}) = \frac{u(\mathbf{x}_0)}{2}.$$

Then

$$\lim_{\mathbf{x}_0 \longrightarrow \partial\Omega_1} \int_{\partial\Omega_1} u(\mathbf{x}) \frac{\partial G(\mathbf{x}, \mathbf{x}_0)}{\partial \mathbf{n}} dS(\mathbf{x}) = \int_{\partial\Omega_1}^{PV} u(\mathbf{x}) \frac{\partial G(\mathbf{x}, \mathbf{x}_0)}{\partial \mathbf{n}} dS(\mathbf{x}) + \frac{u(\mathbf{x}_0)}{2}.$$

So the equation (3.34) implies.

$$u(\mathbf{x}_0) = -2 \int_{\partial\Omega_1} G(\mathbf{x}, \mathbf{x}_0) \frac{\partial u}{\partial \mathbf{n}}(\mathbf{x}) dS(\mathbf{x}) + 2 \int_{\partial\Omega_1}^{PV} u(\mathbf{x}) \frac{\partial G(\mathbf{x}, \mathbf{x}_0)}{\partial \mathbf{n}} dS(\mathbf{x}), \tag{3.36}$$

the same equation as before.

3.4.3 Axisymmetric Formulas and Regularity

The single layer integral.

The free space Green's function exhibits a $\frac{1}{r}$ singularity, where r is the distance of the evaluation point from the singular point. Since the order of this singularity is lower than the area of a small disc of radius r (that is πr^2), the integral is weakly singular. Consequently, the Fredholm- Riesz theory of compact operators may be used to study the properties of the solution [4] and the improper integral may be computed accurately by numerical methods. The single layer potential is a Fredholm integral that is continuous as $\mathbf{x}_0$ crosses $\partial\Omega_1$.

We calculate the axisymmetric expression corresponding to the single layer potential:

Assuming axisymmetry in the domain and symmetry in the boundary condition, using

$$\begin{aligned}\mathbf{x} &= (r(z)\cos\theta, r(z)\sin\theta, z),\\ \mathbf{x}_0 &= (r(z_0)\cos\theta_0, r(z_0)\sin\theta_0, z_0).\end{aligned}$$

If we make correspond the z axis with the axis of rotation of the generating curve and the x axis with r, we obtain the differential of the cylindrical surface is $dS = r(z)\,dld\theta = r(z)\sqrt{1+r'(z)^2}d\theta dz$ with $dl = \sqrt{1+r'(z)^2}dz$ the differential of arc length. The axisymmetry in the solution and the boundary conditions, implies independence of θ in the normal vector so we have

$$\mathbf{n} = n_r(r,z)\,\mathbf{e}_r + n_z(r,z)\,\mathbf{e}_z = \frac{1}{\sqrt{1+r'(z)^2}}\mathbf{e}_r - \frac{r'(z)}{\sqrt{1+r'(z)^2}}\mathbf{e}_z,$$

for

$$\begin{aligned}\mathbf{e}_r &= (\cos\theta, \sin\theta, 0),\\ \mathbf{e}_z &= (0,0,1),\end{aligned}$$

then

$$\begin{aligned}\int_{\partial\Omega_1} G(\mathbf{x},\mathbf{x}_0)\frac{\partial u}{\partial \mathbf{n}}(\mathbf{x})\,dS(\mathbf{x}) &= \int_a^b\int_0^{2\pi} G(\mathbf{x},\mathbf{x}_0)\frac{\partial u}{\partial \mathbf{n}}(r,z)\,r(z)\sqrt{1+r'(z)^2}d\theta dz,\\ &= \int_a^b\left(\int_0^{2\pi} G(\mathbf{x},\mathbf{x}_0)\,d\theta\right)\frac{\partial u}{\partial \mathbf{n}}(r,z)\,r(z)\sqrt{1+r'(z)^2}dz,\end{aligned}$$

where

$$\begin{aligned}G(\mathbf{x},\mathbf{x}_0) &= \frac{1}{4\pi|\mathbf{x}-\mathbf{x}_0|} = \frac{1}{4\pi\left[(r(z)\cos\theta - r(z_0)\cos\theta_0)^2 + (r(z)\sin\theta - r(z_0)\sin\theta_0)^2 + (z-z_0)^2\right]^{1/2}},\\ &= \frac{1}{4\pi\left[r(z)^2 + r(z_0)^2 - 2r(z)\,r(z_0)\cos(\theta-\theta_0) + (z-z_0)^2\right]^{1/2}}.\end{aligned}$$

Changing variables, using a trigonometric identity and the periodicity of the integrand we obtain

$$\begin{aligned}\int_0^{2\pi} G(\mathbf{x},\mathbf{x}_0)\,d\theta &= \frac{1}{4\pi}\int_{-\theta_0}^{2\pi-\theta_0}\frac{du}{\left[r(z)^2 + r(z_0)^2 - 2r(z)\,r(z_0)\cos u + (z-z_0)^2\right]^{1/2}}, \qquad (3.37)\\ &= \frac{1}{4\pi}\int_0^{2\pi}\frac{du}{\sqrt{(r+r_0)^2 + (z-z_0)^2 - 4r_0 r\cos^2\frac{u}{2}}}.\end{aligned}$$

But

$$(r+r_0)^2 + (z-z_0)^2 - 4r_0 r\cos^2\frac{u}{2} = \left[(r+r_0)^2 + (z-z_0)^2\right]\left[1 - \frac{4r_0 r}{(r+r_0)^2+(z-z_0)^2}\cos^2\frac{u}{2}\right].$$

If we denote

$$k^2 = \frac{4r_0 r}{(r+r_0)^2 + (z-z_0)^2},$$

and the integral (3.37) as $G^{AX}(r, z, r_0, z_0)$, we arrive to

$$G^{AX}(r, z, r_0, z_0) = \frac{1}{4\pi\sqrt{(r+r_0)^2 + (z-z_0)^2}} \int_0^{2\pi} \frac{du}{\sqrt{1 - k^2 \cos^2 \frac{u}{2}}}.$$

Notice that

$$\int_0^{2\pi} \frac{du}{\sqrt{1 - k^2 \cos^2 \frac{u}{2}}} = 4 \int_0^{\pi/2} \frac{d\eta}{\sqrt{1 - k^2 \cos^2 \eta}},$$

and remind the definition of the complete elliptic integral of the first kind (see [1]):

$$F(k) = \int_0^{\pi/2} \frac{d\eta}{\sqrt{1 - k^2 \cos^2 \eta}}.$$

Then

$$\begin{aligned} \int_{\partial\Omega_1} G(\mathbf{x}, \mathbf{x}_0) \frac{\partial u}{\partial \mathbf{n}}(\mathbf{x}) \, dS(\mathbf{x}) &= \int_a^b G^{AX}(r, z, r_0, z_0) \frac{\partial u}{\partial \mathbf{n}}(r, z) \, r(z) \sqrt{1 + r'(z)^2} dz, \qquad (3.38) \\ &= \frac{1}{\pi} \int_a^b \frac{F(k)}{\sqrt{(z-z_0)^2 + (r+r_0)^2}} \frac{\partial u}{\partial \mathbf{n}}(r, z) \, r(z) \sqrt{1 + r'(z)^2} dz. \end{aligned}$$

The elliptic integral $F(k)$ has an integrable singularity when $k(r, z, r_0, z_0) = \sqrt{\frac{4r_0 r}{(z-z_0)^2 + (r+r_0)^2}} = 1$, and it occurs when the evaluation point $(r(z), z)$ coincides with the pole $(r(z_0), z_0)$. Notice also that for k to be well defined, we have to avoid that evaluation point to be very close to the extremes of the interval of definition of z, or otherwise we would have to deal with an indeterminacy.

The singularities of the single layer potential are integrable, and if we take the poles different from the evaluation points for the approximation of the integral (like the middle points for example) we will have a well defined single layer for the numerics, and we will have also reflected functions taking reflected poles. Let us note that:

$$\begin{aligned} k(r(-z), -z, r(z_0), z_0) &= \sqrt{\frac{4r(z_0) r(z)}{(z - (-z_0))^2 + (r(z) + r(-z_0))^2}} \\ &= k(r(z), z, r(-z_0), -z_0). \end{aligned}$$

If

$$F(k) = \int_0^{\pi/2} \frac{d\eta}{\sqrt{1 - k^2 \cos^2 \eta}},$$

we then also have

$$F(k(r(-z), -z, r(z_0), z_0)) = F(k(r(z), z, r(-z_0), -z_0)).$$

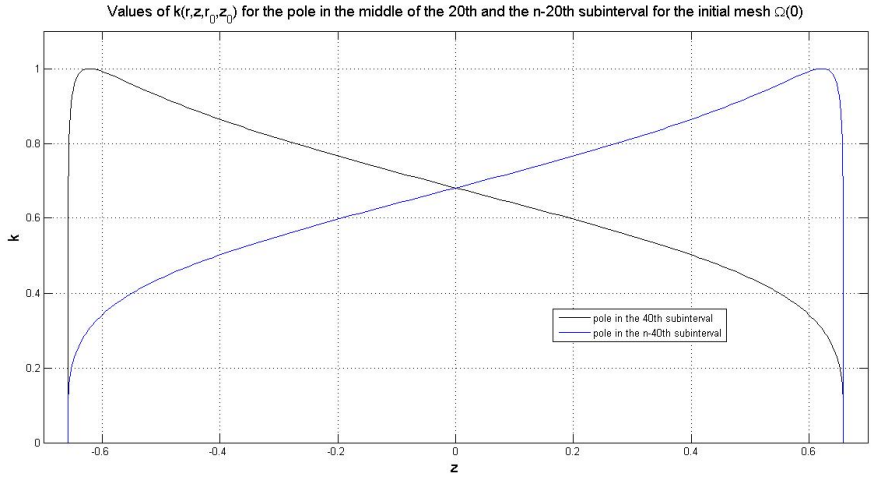

Figure 3.10: The argument of the elliptic integrals

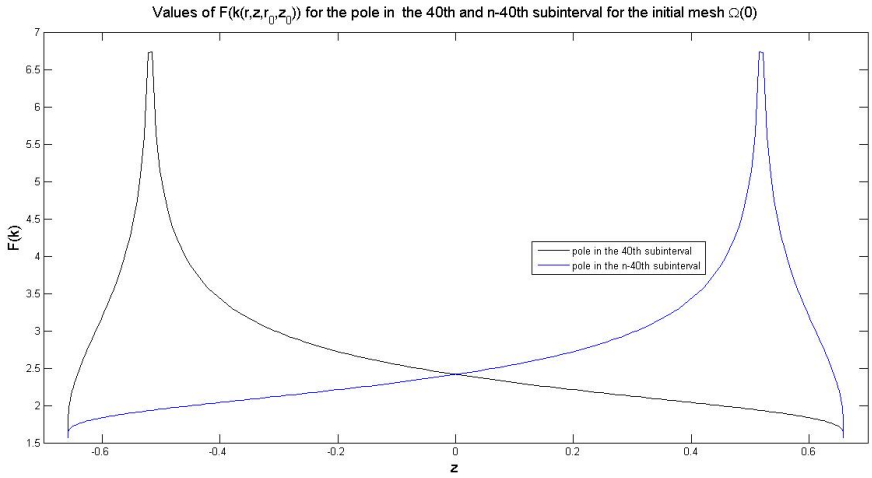

Figure 3.11: The complete elliptic integral of the first kind

If we define $D\left(r\left(z\right),z,r_0,z_0\right)=\frac{1}{\sqrt{\left(z-z_0\right)^2+\left(r(z)+r(z_0)\right)^2}}$, then we also have

$$D\left(r\left(-z\right),-z,r_0,z_0\right)=D\left(r\left(z\right),z,r\left(-z_0\right),-z_0\right).$$

Because of the symmetry of $r\left(z\right)$ we have that $r'\left(z\right)$ is odd, and the product $\sqrt{1+r'\left(z\right)^2}r\left(z\right)$ is an even function.

Therefore we have reflected functions: if we take an initial symmetric $\Omega\left(0\right)$ we will have in the integrand of the single layer, the same function but taking the reflected pole and z values.

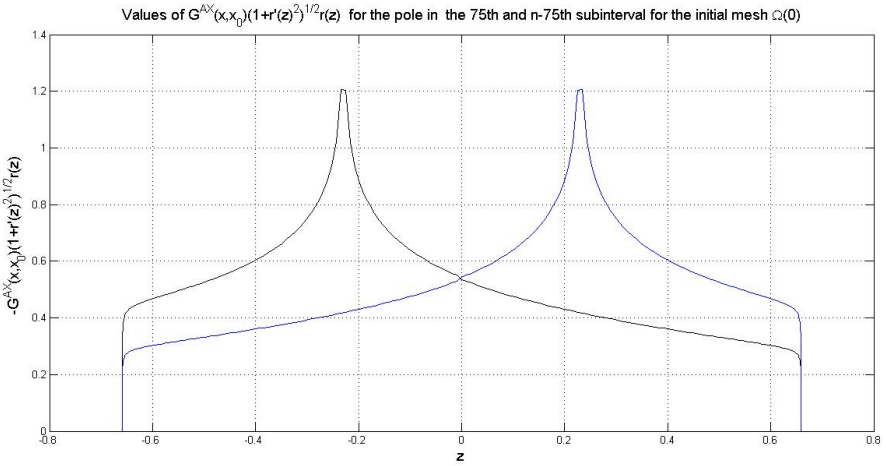

Figure 3.12: The function $\frac{1}{\pi}\frac{F(k)}{\sqrt{(z-z_0)^2+(r+r_0)^2}}r(z)\sqrt{1+r'(z)^2}$

The double layer integral

When $\partial\Omega_1$ is a smooth surface with a continuously varying normal vector, as the integration point $\mathbf{x}$ approaches the evaluation point $\mathbf{x}_0$, the normal vector $\mathbf{n}$ tends to become orthogonal to the nearly tangential vector $(\mathbf{x}-\mathbf{x}_0)$. Consequently the numerator of the integrand of the double layer potential behaves quadratically with respect to the scalar distance $r=|\mathbf{x}-\mathbf{x}_0|$ and the order of the singularity is reduced from $\frac{1}{r^2}$ to $\frac{1}{r}$. Let us see the computation of the principal value of the double layer potential.

If we want to work with regular integrals (instead of PV integrals) let us consider the identity

$$\int_{\partial\Omega_1}^{PV}\frac{\partial G}{\partial \mathbf{n}}(\mathbf{x},\mathbf{x}_0)\,dS(\mathbf{x})=-\frac{1}{2},$$

with $\mathbf{n}$ the normal exterior to Ω_1 and $x_0\in\partial\Omega$. Therefore

$$u(\mathbf{x}_0)\int_{\partial\Omega_1}^{PV}\frac{\partial G}{\partial \mathbf{n}}(\mathbf{x},\mathbf{x}_0)\,dS(\mathbf{x})=-\frac{u(\mathbf{x}_0)}{2},$$

so that

$$-u(\mathbf{x}_0)\int_{\partial\Omega_1}^{PV}\frac{\partial G}{\partial \mathbf{n}}(\mathbf{x},\mathbf{x}_0)\,dS(\mathbf{x})-\frac{u(\mathbf{x}_0)}{2}=0, \tag{3.39}$$

and adding zero as defined by (3.39)

$$\int_{\partial\Omega_1}^{PV} u(\mathbf{x}) \frac{\partial G(\mathbf{x},\mathbf{x}_0)}{\partial \mathbf{n}} dS(\mathbf{x}) = \int_{\partial\Omega_1}^{PV} u(\mathbf{x}) \frac{\partial G(\mathbf{x},\mathbf{x}_0)}{\partial \mathbf{n}} dS(\mathbf{x})$$
$$= \int_{\partial\Omega_1}^{PV} u(\mathbf{x}) \frac{\partial G(\mathbf{x},\mathbf{x}_0)}{\partial \mathbf{n}} dS(\mathbf{x}) - u(\mathbf{x}_0) \int_{\partial\Omega_1}^{PV} \frac{\partial G}{\partial \mathbf{n}}(\mathbf{x},\mathbf{x}_0)\, dS(\mathbf{x}) - \frac{u(\mathbf{x}_0)}{2}$$
$$= \int_{\partial\Omega_1}^{PV} [u(\mathbf{x}) - u(\mathbf{x}_0)] \frac{\partial G(\mathbf{x},\mathbf{x}_0)}{\partial \mathbf{n}} dS(\mathbf{x}) - \frac{u(\mathbf{x}_0)}{2}.$$

If u is Lipschitz

$$|u(\mathbf{x}) - u(\mathbf{x}_0)| \leq C |\mathbf{x} - \mathbf{x}_0|,$$
$$|u(\mathbf{x}) - u(\mathbf{x}_0)| \left| \frac{\partial G(\mathbf{x},\mathbf{x}_0)}{\partial \mathbf{n}} \right| \leq \overline{C} |\mathbf{x} - \mathbf{x}_0| \frac{1}{|\mathbf{x} - \mathbf{x}_0|^2} = \frac{\overline{C}}{|\mathbf{x} - \mathbf{x}_0|} \text{ with } \mathbf{x} \neq \mathbf{x}_0.$$

Using a Taylor series for the integrand we see that although the integrand is not regular, the integral in principal values is not a PV integral. Then the regularized equation for the harmonic function u (3.36) that results when the point of integration $x_0 \in \partial\Omega_1$, is:

$$u(\mathbf{x}_0) = -2 \int_{\partial\Omega_1} G(\mathbf{x},\mathbf{x}_0) \frac{\partial u}{\partial \mathbf{n}}(\mathbf{x})\, dS(\mathbf{x}) + 2 \int_{\partial\Omega_1}^{PV} u(\mathbf{x}) \frac{\partial G(\mathbf{x},\mathbf{x}_0)}{\partial \mathbf{n}} dS(\mathbf{x})$$

$$u(\mathbf{x}_0) = -2 \int_{\partial\Omega_1} G(\mathbf{x},\mathbf{x}_0) \frac{\partial u}{\partial \mathbf{n}}(\mathbf{x})\, dS(\mathbf{x}) + 2 \int_{\partial\Omega_1} [u(\mathbf{x}) - u(\mathbf{x}_0)] \frac{\partial G(\mathbf{x},\mathbf{x}_0)}{\partial \mathbf{n}} dS(\mathbf{x}) - u(\mathbf{x}_0),$$

and we arrive to the equation:

$$u(\mathbf{x}_0) = -\int_{\partial\Omega_1} G(\mathbf{x},\mathbf{x}_0) \frac{\partial u}{\partial \mathbf{n}}(\mathbf{x})\, dS(\mathbf{x}) + \int_{\partial\Omega_1} [u(\mathbf{x}) - u(\mathbf{x}_0)] \frac{\partial G(\mathbf{x},\mathbf{x}_0)}{\partial \mathbf{n}} dS(\mathbf{x}), \quad (3.40)$$

valid for points $\mathbf{x}_0 \in \partial\Omega_1$.

We will show that the regularized axisymmetric expression for the double layer integral is:

$$\int_{\partial\Omega_1} [u(\mathbf{x}) - u(\mathbf{x}_0)] \frac{\partial G(\mathbf{x},\mathbf{x}_0)}{\partial \mathbf{n}} dS(\mathbf{x})$$

$$= \frac{1}{2\pi} \int_a^b [u(\mathbf{x}) - u(\mathbf{x}_0)] \left(-\frac{F(k)}{\sqrt{(z-z_0)^2 + (r+r_0)^2}} + \right.$$

$$\left. \frac{E(k)\left[(z-z_0)^2 + 2(z-z_0) r(z) r'(z) + (r_0 - r)(r_0 + r)\right]}{\sqrt{(z-z_0)^2 + (r+r_0)^2}\left((z-z_0)^2 + (r-r_0)^2\right)} \right) dz.$$

We have

$$\int_{\partial\Omega_1} [u(\mathbf{x}) - u(\mathbf{x}_0)] \frac{\partial G(\mathbf{x},\mathbf{x}_0)}{\partial \mathbf{n}} dS(\mathbf{x}) =$$

$$\int_{\partial\Omega_1}\left[u\left(\mathbf{x}\right)-u\left(\mathbf{x}_0\right)\right]\frac{\partial G}{\partial\mathbf{n}}\left(\mathbf{x},\mathbf{x}_0\right)dS\left(\mathbf{x}\right)$$
$$=\int_a^b\int_0^{2\pi}\left[u\left(\mathbf{x}\right)-u\left(\mathbf{x}_0\right)\right]\left(\nabla_{\mathbf{x}}G\left(\mathbf{x},\mathbf{x}_0\right)\cdot\mathbf{n}\left(\mathbf{x}\right)\right)r\left(z\right)\sqrt{r'\left(z\right)^2+1}d\theta dz$$
$$=\int_a^b\left[u\left(\mathbf{x}\right)-u\left(\mathbf{x}_0\right)\right]\left(\int_0^{2\pi}\left(\nabla_{\mathbf{x}}G\left(\mathbf{x},\mathbf{x}_0\right)\cdot\mathbf{n}\left(\mathbf{x}\right)\right)d\theta\right)r\left(z\right)\sqrt{r'\left(z\right)^2+1}dz.$$

Since u has no dependence on θ:

$$\int_0^{2\pi}\frac{\partial G}{\partial\mathbf{n}}\left(\mathbf{x},\mathbf{x}_0\right)d\theta=\int_0^{2\pi}\nabla G\left(\mathbf{x},\mathbf{x}_0\right)\cdot\mathbf{n}\left(\mathbf{x}\right)d\theta$$

$$=\int_0^{2\pi}\left[\frac{\partial G}{\partial r}\left(\mathbf{x},\mathbf{x}_0\right)\mathbf{e}_r+\frac{1}{r}\frac{\partial G}{\partial\theta}\left(\mathbf{x},\mathbf{x}_0\right)\mathbf{e}_\theta+\frac{\partial G}{\partial z}\left(\mathbf{x},\mathbf{x}_0\right)\mathbf{e}_z\right]\left[\frac{1}{\sqrt{1+r'\left(z\right)^2}}\mathbf{e}_r-\frac{r'\left(z\right)}{\sqrt{1+r'\left(z\right)^2}}\mathbf{e}_z\right]d\theta.$$

$$=n_r\left(r,z\right)\int_0^{2\pi}\frac{\partial G}{\partial r}\left(\mathbf{x},\mathbf{x}_0\right)d\theta+n_z\left(r,z\right)\int_0^{2\pi}\frac{\partial G}{\partial z}\left(\mathbf{x},\mathbf{x}_0\right)d\theta.$$

We can set

$$\int_0^{2\pi}\frac{\partial G}{\partial r}\left(\mathbf{x},\mathbf{x}_0\right)d\theta=\frac{\partial}{\partial r}\left(\int_0^{2\pi}G\left(\mathbf{x},\mathbf{x}_0\right)d\theta\right)=\frac{\partial G^{AX}\left(r,z,r_0,z_0\right)}{\partial r},$$

and

$$\int_0^{2\pi}\frac{\partial G}{\partial z}\left(\mathbf{x},\mathbf{x}_0\right)d\theta=\frac{\partial}{\partial z}\left(\int_0^{2\pi}G\left(\mathbf{x},\mathbf{x}_0\right)d\theta\right)=\frac{\partial G^{AX}\left(r,z,r_0,z_0\right)}{\partial z},$$

so that

$$\int_0^{2\pi}\frac{\partial G}{\partial\mathbf{n}}\left(\mathbf{x},\mathbf{x}_0\right)d\theta=n_r\left(r,z\right)\frac{\partial G^{AX}\left(r,z,r_0,z_0\right)}{\partial r}+n_z\left(r,z\right)\frac{\partial G^{AX}\left(r,z,r_0,z_0\right)}{\partial z},$$
$$=\left[\frac{\partial G^{AX}\left(r,z,r_0,z_0\right)}{\partial r}\mathbf{e}_r+\frac{\partial G^{AX}\left(r,z,r_0,z_0\right)}{\partial z}\mathbf{e}_z\right]\left[n_r\left(r,z\right)\mathbf{e}_r+n_z\left(r,z\right)\mathbf{e}_z\right],$$
$$=\nabla_{(r,z)}G^{AX}\left(r,z,r_0,z_0\right)\cdot\mathbf{n}\left(\mathbf{x}\right)=\frac{\partial G^{AX}\left(r,z,r_0,z_0\right)}{\partial\mathbf{n}},$$

and

$$\int_{\partial\Omega_1}\left[u\left(\mathbf{x}\right)-u\left(\mathbf{x}_0\right)\right]\frac{\partial G\left(\mathbf{x},\mathbf{x}_0\right)}{\partial\mathbf{n}}dS\left(\mathbf{x}\right)=\int_a^b\left[u\left(\mathbf{x}\right)-u\left(\mathbf{x}_0\right)\right]\frac{\partial G^{AX}\left(r,z,r_0,z_0\right)}{\partial\mathbf{n}}r\left(z\right)\sqrt{r'\left(z\right)^2+1}dz.$$

Using the complete elliptic integral of the second kind (see [1])

$$E\left(k\right)=\int_0^{\pi/2}\sqrt{1-k^2\sin^2\theta}d\theta,$$

we arrive at

$$\frac{\partial G^{AX}\left(r,z,r_0,z_0\right)}{\partial r}=\frac{1}{2r\pi\left(\left(z-z_0\right)^2+\left(r+r_0\right)^2\right)^{1/2}}\left(\frac{E\left(k\right)\left(\left(z-z_0\right)^2+\left(r_0-r\right)\left(r_0+r\right)\right)}{\left(z-z_0\right)^2+\left(r-r_0\right)^2}-F\left(k\right)\right),$$

and

$$\frac{\partial G^{AX}\left(r,z,r_0,z_0\right)}{\partial z}=-\frac{\left(z-z_0\right)E\left(k\right)}{\pi\sqrt{\left(z-z_0\right)^2+\left(r+r_0\right)^2}\left(\left(z-z_0\right)^2+\left(r-r_0\right)^2\right)},$$

so that

$$\frac{\partial G^{AX}\left(r,z,r_0,z_0\right)}{\partial\mathbf{n}}=\nabla_{(r,z)}G^{AX}\left(r,z,r_0,z_0\right)\cdot\mathbf{n}\left(\mathbf{x}\right),$$

$$=\left[\frac{E\left(k\right)\left[\left(z-z_0\right)^2+\left(r_0-r\right)\left(r_0+r\right)\right]}{2r\pi\sqrt{\left(z-z_0\right)^2+\left(r+r_0\right)^2}\left(\left(z-z_0\right)^2+\left(r-r_0\right)^2\right)}-\frac{F\left(k\right)}{2\pi r\sqrt{\left(z-z_0\right)^2+\left(r+r_0\right)^2}}\right]\left(\frac{1}{\sqrt{1+r'\left(z\right)^2}}\right)$$

$$+\left[-\frac{\left(z-z_0\right)E\left(k\right)}{\pi\sqrt{\left(z-z_0\right)^2+\left(r+r_0\right)^2}\left(\left(z-z_0\right)^2+\left(r-r_0\right)^2\right)}\right]\left(-\frac{r'\left(z\right)}{\sqrt{1+r'\left(z\right)^2}}\right),$$

$$=\frac{E\left(k\right)\left[\left(z-z_0\right)^2+2\left(z-z_0\right)r\left(z\right)r'\left(z\right)+\left(r_0-r\right)\left(r_0+r\right)\right]}{2\pi r\sqrt{\left(z-z_0\right)^2+\left(r+r_0\right)^2}\left(\left(z-z_0\right)^2+\left(r-r_0\right)^2\right)\sqrt{1+r'\left(z\right)^2}}$$

$$-\frac{F\left(k\right)}{2\pi r\sqrt{\left(z-z_0\right)^2+\left(r+r_0\right)^2}\sqrt{1+r'\left(z\right)^2}}.$$

Then the double layer potential for the axisymmetric case is

$$\int_a^b\left[u\left(\mathbf{x}\right)-u\left(\mathbf{x}_0\right)\right]\left(\frac{E\left(k\right)\left[\left(z-z_0\right)^2+\left(r_0-r\right)\left(r_0+r\right)+2\left(z-z_0\right)r\left(z\right)r'\left(z\right)\right]}{2\pi rA^{1/2}C\sqrt{1+r'\left(z\right)^2}}\right.$$

$$\left.-\frac{F\left(k\right)}{2\pi rA^{1/2}\sqrt{1+r'\left(z\right)^2}}\right)r\left(z\right)\sqrt{r'\left(z\right)^2+1}dz$$

Simplifying we obtain

$$\frac{1}{2\pi}\int_a^b\left[u\left(\mathbf{x}\right)-u\left(\mathbf{x}_0\right)\right]\left(\frac{-F\left(k\right)}{\sqrt{\left(z-z_0\right)^2+\left(r+r_0\right)^2}}\right.$$

$$\left.+\frac{E\left(k\right)\left[\left(z-z_0\right)^2+2\left(z-z_0\right)r\left(z\right)r'\left(z\right)+\left(r_0-r\right)\left(r_0+r\right)\right]}{\sqrt{\left(z-z_0\right)^2+\left(r+r_0\right)^2}\left(\left(z-z_0\right)^2+\left(r-r_0\right)^2\right)}\right)dz. \tag{3.41}$$

The function $(r_0 - r)(r_0 + r)$ is a regular and even function and $E(k)$ is also regular for every admissible value of k and it has the same kind of symmetry with respect to the poles as F and the other functions involved in (3.41)

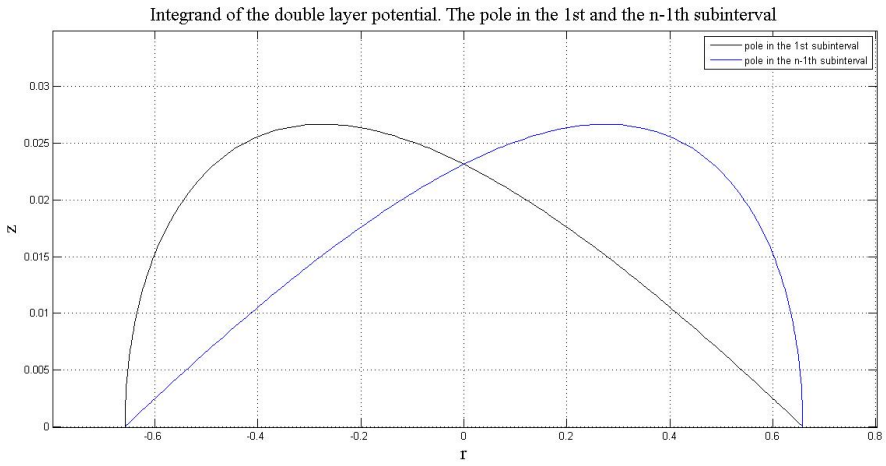

Figure 3.13: The regularized integrand of the double layer potential.

3.4.4 The axisymmetric boundary integral equation

When $\mathbf{x}_0 \in \partial\Omega_1$ the equation (3.40)

$$u(\mathbf{x}_0) = -\int_{\partial\Omega_1} G(\mathbf{x}, \mathbf{x}_0) \frac{\partial u}{\partial \mathbf{n}}(\mathbf{x})\, dS(\mathbf{x}) + \int_{\partial\Omega_1} [u(\mathbf{x}) - u(\mathbf{x}_0)] \frac{\partial G(\mathbf{x}, \mathbf{x}_0)}{\partial \mathbf{n}} dS(\mathbf{x}),$$

for an axisymmetric surface becomes

$$\begin{aligned}
u(\mathbf{x}_0) &= -\int_a^b G^{A\mathbf{x}}(r, z, r_0, z_0) \frac{\partial u}{\partial n}(r, z)\, r(z) \sqrt{1 + r'(z)^2} dz \\
&+ \int_a^b [u(\mathbf{x}) - u(\mathbf{x}_0)] \frac{\partial G^{A\mathbf{x}}}{\partial n}(r, z, r_0, z_0)\, r(z) \sqrt{1 + r'(z)^2} dz \\
&= -\frac{1}{\pi} \int_a^b \frac{F(k)}{\sqrt{(z - z_0)^2 + (r + r_0)^2}} \frac{\partial u}{\partial n}(r, z)\, r(z) \sqrt{1 + r'(z)^2} dz \\
&+ \frac{1}{2\pi} \int_a^b [u(\mathbf{x}) - u(\mathbf{x}_0)] \left(-\frac{F(k)}{\sqrt{(z - z_0)^2 + (r + r_0)^2}} + \right. \\
&\left. \frac{E(k) \left[(z - z_0)^2 + 2(z - z_0) r(z) r'(z) + (r_0 - r)(r_0 + r) \right]}{\sqrt{(z - z_0)^2 + (r + r_0)^2} \left((z - z_0)^2 + (r - r_0)^2 \right)} \right) dz.
\end{aligned}$$

This is an expression to the potential in terms of elliptic integrals. We will use these expressions latter in the Boundary Elements Method (BEM) for obtaining local approximations to $F(V)$.

We already have an integral equation for the boundary condition, next we will obtain a similar representation for the velocity field in the Stokes flow.

3.5 The Boundary Integral Formulation for Stokes System

3.5.1 Introduction

In the construction of our model, we wrote two equations for the velocity and pressure on either side of the interface, and one expression for the interfacial boundary condition in terms of the surface charge density σ_0, the curvature $\mathcal{H}$, and a correction σ_1, we already have a boundary integral equation for calculating the boundary conditions, now we will obtain a boundary integral representation for obtaining the velocity, that finally will allow us to study the evolution of our droplet in terms of ε and the amount of charge when we combine the integral representations with a numerical method.

3.5.2 Integral equation

We will obtain a boundary integral representation of the flow in a similar way as we did for Laplace equation but using an appropriate Green's function to this case. This is a well known problem whose solution and deduction can be found, for instance, in [54], [14] and [33]. We will give just the principal steps because the central ideas are very similar to the integral representation for Laplace equation given before. In this case we will use Einstein notation for brevity in the formulas.

We are interested in finding the velocity field at the interface between the droplet and the surrounding fluid, because the evolution of the droplet is determined by the normal proyection of this velocity field. Therefore let us start determining the velocity at the interior of the droplet, then at the exterior fluid and finally we will find an expression valid at the interface.

At the interior fluid we have

$$\begin{aligned} -\nabla P^{(1)}(\mathbf{x}) + \mu_1 \Delta \mathbf{v}^{(1)}(\mathbf{x}) = 0,\ \mathbf{x} \in \Omega_1, \\ \nabla \cdot \mathbf{v}^{(1)} = 0,\ \mathbf{x} \in \Omega_1. \end{aligned}$$

Or equivalently

$$\nabla \cdot \mathbf{T}^{(1)} = 0,\ \mathbf{x} \in \Omega_1, \tag{3.42}$$

$$\nabla \cdot \mathbf{v}^{(1)} = 0,\ \mathbf{x} \in \Omega_1. \tag{3.43}$$

for

$$T_{ij}^{(1)} = -P^{(1)}\delta_{ij} + \mu_1 \left(\frac{\partial v_i^{(1)}}{\partial x_j} + \frac{\partial v_i^{(1)}}{\partial x_i} \right).$$

Let us consider now an auxiliar equation

$$-\nabla P(\mathbf{x}) + \mu_1 \Delta \mathbf{u}(\mathbf{x}) = -\delta(\mathbf{x} - \mathbf{x}_0), \tag{3.44}$$

$$\nabla \cdot \mathbf{u}(\mathbf{x}) = 0, \tag{3.45}$$

defined in $\mathbb{R}^3$, where $\mathbf{x}_0$ is an arbitrary point and δ is the three dimensional delta function. Like in the fundamental solution for the Laplace equation, we call $\mathbf{x}_0$ the pole or source point, and $\mathbf{x}$ the observation or field point.

Introducing the Green's function $\mathbb{G}$, the solution to (3.44)-(3.45) is

$$\mathbf{u}(\mathbf{x}) = \frac{1}{8\pi\mu_1}\mathbb{G}_{ij}(\mathbf{x}, \mathbf{x}_0) = \frac{1}{8\pi\mu_1}\left(\frac{\delta_{ij}}{r} + \frac{\hat{x}_i \hat{x}_j}{r^3}\right),$$

with δ_{ij} the Kronecker Delta and $\hat{\mathbf{x}} = \mathbf{x} - \mathbf{x}_0$, $r = |\mathbf{x} - \mathbf{x}_0|$, $\hat{x}_i = x_i - x_{0i}$.

The equation (3.44) can be writen in terms of the stress tensor $\mathbb{T}$ defined as follows

$$\mathbb{T}_{ijk} = -\delta_{ik} P_j(\mathbf{x}, \mathbf{x}_0) + \frac{\partial \mathbb{G}_{ij}(\mathbf{x}, \mathbf{x}_0)}{\partial x_k} + \frac{\partial \mathbb{G}_{kj}(\mathbf{x}, \mathbf{x}_0)}{\partial x_i},$$

as

$$\nabla \cdot \mathbf{T} = -\delta(\mathbf{x} - \mathbf{x}_0), \tag{3.46}$$

where

$$\mathbf{T}_{ik}(\mathbf{x}) = \frac{1}{8\pi}\mathbb{T}_{ijk}(\mathbf{x}, \mathbf{x}_0) = -6\frac{\hat{x}_i \hat{x}_j \hat{x}_k}{r^5}.$$

Multiplying (3.42) by $\mathbf{u}$ and (3.46) by $\mathbf{v}^{(1)}$ we can obtain

$$\begin{aligned}\mathbf{v}^{(1)}\delta(\mathbf{x} - \mathbf{x}_0) &= \mathbf{u}\left(\nabla \cdot \mathbf{T}^{(1)}\right) - \mathbf{v}^{(1)}(\nabla \cdot \mathbf{T}) \\ &= \nabla \cdot \left(\mathbf{u} \cdot \mathbf{T}^{(1)} - \mathbf{v}^{(1)} \cdot \mathbf{T}\right),\end{aligned}$$

using (3.42), (3.43), (3.46), (3.45), and the Divergence Theorem to transform the volume integral to a surface integral, we have

$$\begin{aligned}\int_{\Omega_1} v_j^{(1)}(\mathbf{x})\,\delta(\mathbf{x} - \mathbf{x}_0)\,dV(\mathbf{x}) = &\frac{1}{8\pi\mu_1}\int_{\partial\Omega_1} \mathbb{G}_{ij}(\mathbf{x}, \mathbf{x}_0)\,T_{ik}^{(1)}(\mathbf{x})\,n_k(\mathbf{x})\,dS(\mathbf{x}) \\ &- \frac{1}{8\pi}\int_{\partial\Omega_1} v_i^{(1)}(\mathbf{x})\,\mathbb{T}_{ijk}(\mathbf{x}, \mathbf{x}_0)\,n_k(\mathbf{x})\,dS(\mathbf{x}),\end{aligned} \tag{3.47}$$

for $\mathbf{n}$ exterior to Ω_1. Similarly to the Laplace equation, the first integral in the right hand side is called single layer potential and the second one, double layer potential. A detailed discussion about the physical meaning and properties of this potentials can be found in [54].

If we denote $\mathbf{f}^{(1)} = \mathbf{T}^{(1)} \cdot \mathbf{n}$ and take $\mathbf{x}_0 \in \Omega_1$

$$\begin{aligned}v_j^{(1)}(\mathbf{x}_0) = &\frac{1}{8\pi\mu_1}\int_{\partial\Omega_1} \mathbb{G}_{ij}(\mathbf{x}, \mathbf{x}_0)\,f_i^{(1)}(\mathbf{x})\,dS(\mathbf{x}) \\ &- \frac{1}{8\pi}\int_{\partial\Omega_1} v_i^{(1)}(\mathbf{x})\,\mathbb{T}_{ijk}(\mathbf{x}, \mathbf{x}_0)\,n_k(\mathbf{x})\,dS(\mathbf{x}).\end{aligned} \tag{3.48}$$

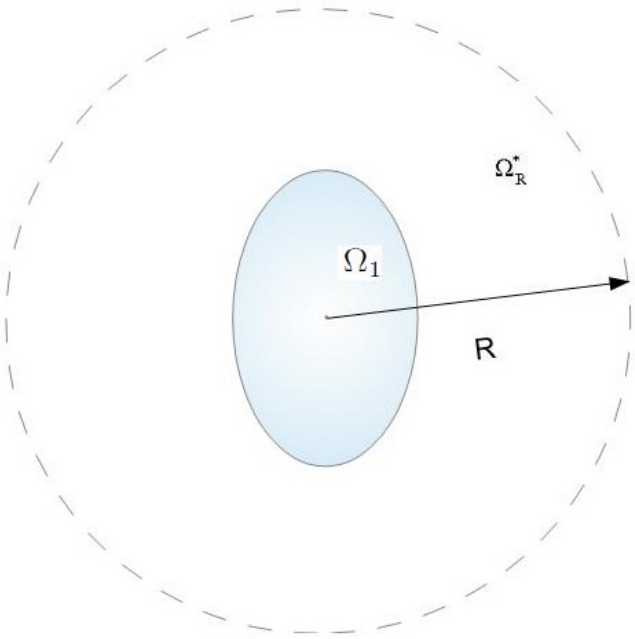

Figure 3.14: Let us note that $\Omega_R^* \setminus \Omega_1 \to \Omega_2$ when $R \to \infty$

For the unbounded exterior fluid Ω_2 we have

$$\nabla \cdot \mathbf{T}^{(2)} = 0,\ \mathbf{x} \in \Omega_2 \tag{3.49}$$

$$\nabla \cdot \mathbf{v}^{(2)} = 0,\ \mathbf{x} \in \Omega_2, \tag{3.50}$$

we can construct again a ball $B(\mathbf{x},R)$ that contains Ω_1 (see Fig. 3.14). Taking $R \longrightarrow \infty$ and using that the flux vanishes at infinity, for the Divergence Theorem and the auxiliar system in $\mathbb{R}^3$, we have that

$$\begin{aligned} \mathbf{v}^{(2)}(\mathbf{x})\,\delta(\mathbf{x}-\mathbf{x}_0) &= \mathbf{u}\left(\nabla \cdot \mathbf{T}^{(2)}\right) - \mathbf{v}^{(2)}\left(\nabla \cdot \mathbf{T}\right) \\ &= \nabla \cdot \left(\mathbf{u} \cdot \mathbf{T}^{(2)} - \mathbf{v}^{(2)} \cdot \mathbf{T}\right), \end{aligned}$$

implies

$$\begin{aligned} \int_{\Omega_2} v_j^{(2)}(\mathbf{x})\,\delta(\mathbf{x}-\mathbf{x}_0)\,dV(\mathbf{x}) = &-\frac{1}{8\pi\mu_1}\int_{\partial\Omega_1} \mathbb{G}_{ij}(\mathbf{x},\mathbf{x}_0)\,T_{ik}^{(2)}(\mathbf{x})\,n_k(\mathbf{x})\,dS(\mathbf{x}) \\ &+\frac{1}{8\pi}\int_{\partial\Omega_1} v_i^{(2)}(\mathbf{x})\,\mathbb{T}_{ijk}(\mathbf{x},\mathbf{x}_0)\,n_k(\mathbf{x})\,dS(\mathbf{x}), \end{aligned} \tag{3.51}$$

with $\mathbf{n}$ the normal exterior to Ω_1. If we denote $\mathbf{f}^{(2)} = \mathbf{T}^{(2)} \cdot \mathbf{n}$, multiplying (3.51) by $\frac{1}{\mu_2}$ we have

$$-\frac{1}{8\pi\mu_1\mu_2}\int_{\partial\Omega_1} \mathbb{G}_{ij}(\mathbf{x},\mathbf{x}_0)\,f_i^{(2)}(\mathbf{x})\,dS(\mathbf{x}) + \frac{1}{8\pi\mu_2}\int_{\partial\Omega_1} v_i^{(2)}(\mathbf{x})\,\mathbb{T}_{ijk}(\mathbf{x},\mathbf{x}_0)\,n_k(\mathbf{x})\,dS(\mathbf{x}) = 0, \tag{3.52}$$

for $\mathbf{x}_0 \in \Omega_1$.

If we add (3.52) to an appropriate multiple to (3.48) and denote $\Delta f_i(\mathbf{x}) = f_i^{(2)}(\mathbf{x}) - f_i^{(1)}(\mathbf{x})$ we have

$$v_j^{(1)}(\mathbf{x}_0) = -\frac{1}{8\pi\mu_1}\int_{\partial\Omega_1}\mathbb{G}_{ij}(\mathbf{x},\mathbf{x}_0)\,\Delta f_i(\mathbf{x})\,dS(\mathbf{x}) + \frac{\mu_2-\mu_1}{8\pi\mu_1}\int_{\partial\Omega_1} v_i(\mathbf{x})\,\mathbb{T}_{ijk}(\mathbf{x},\mathbf{x}_0)\,n_k(\mathbf{x})\,dS(\mathbf{x}), \tag{3.53}$$

for $\mathbf{x}_0 \in \Omega_1$ and using $v_i^{(1)}(\mathbf{x}) = v_i^{(2)}(\mathbf{x})$ at the boundary.

If $\mathbf{x}_0 \in \Omega_2$ in (3.47) we have

$$0 = \int_{\Omega_1} v_j^{(1)}(\mathbf{x})\,\delta(\mathbf{x}-\mathbf{x}_0)\,dV(\mathbf{x}) = \frac{1}{8\pi\mu_1}\int_{\partial\Omega_1}\mathbb{G}_{ij}(\mathbf{x},\mathbf{x}_0)\,T_{ik}^{(1)}(\mathbf{x})\,n_k(\mathbf{x})\,dS(\mathbf{x}) - \frac{1}{8\pi}\int_{\partial\Omega_1} v_i(\mathbf{x})\,\mathbb{T}_{ijk}(\mathbf{x},\mathbf{x}_0$$

and multiplying by $\frac{1}{\mu_2}$

$$\frac{1}{8\pi\mu_1\mu_2}\int_{\partial\Omega_1}\mathbb{G}_{ij}(\mathbf{x},\mathbf{x}_0)\,T_{ik}^{(1)}(\mathbf{x})\,n_k(\mathbf{x})\,dS(\mathbf{x}) - \frac{1}{8\pi\mu_2}\int_{\partial\Omega_1} v_i(\mathbf{x})\,\mathbb{T}_{ijk}(\mathbf{x},\mathbf{x}_0)\,n_k(\mathbf{x})\,dS(\mathbf{x}) = 0. \tag{3.54}$$

The equation (3.51) becomes

$$v_j^{(2)}(\mathbf{x}) = -\frac{1}{8\pi\mu_1}\int_{\partial\Omega_1}\mathbb{G}_{ij}(\mathbf{x},\mathbf{x}_0)\,T_{ik}^{(2)}(\mathbf{x})\,n_k(\mathbf{x})\,dS(\mathbf{x}) + \frac{1}{8\pi}\int_{\partial\Omega_1} v_i(\mathbf{x})\,\mathbb{T}_{ijk}(\mathbf{x},\mathbf{x}_0)\,n_k(\mathbf{x})\,dS(\mathbf{x}). \tag{3.55}$$

Adding an appropriate multiple of (3.55) to (3.54)

$$v_j^{(2)}(\mathbf{x}) = -\frac{1}{8\pi\mu_2}\int_{\partial\Omega_1}\mathbb{G}_{ij}(\mathbf{x},\mathbf{x}_0)\,\Delta f_i(\mathbf{x})\,dS(\mathbf{x}) + \frac{\mu_2-\mu_1}{8\pi\mu_2}\int_{\partial\Omega_1} v_i(\mathbf{x})\,\mathbb{T}_{ijk}(\mathbf{x},\mathbf{x}_0)\,n_k(\mathbf{x})\,dS(\mathbf{x}), \tag{3.56}$$

$\mathbf{x}_0 \in \Omega_2$, $\mathbf{n}$ exterior to Ω_1.

If $\mathbf{x}_0 \longrightarrow \partial\Omega_1$, we have that the single layer potential is continuous when crosses $\partial\Omega$, but the double layer potential satisfies

Proposition 1.

$$\lim_{\mathbf{x}\longrightarrow\partial\Omega_1}\int_{\partial\Omega_1} v_i(\mathbf{x})\,\mathbb{T}_{ijk}(\mathbf{x},\mathbf{x}_0)\,n_k(\mathbf{x})\,dS(\mathbf{x}) = \mp 4\pi v_j(\mathbf{x}_0) + \int_{\partial\Omega_1}^{PV} v_i(\mathbf{x})\,\mathbb{T}_{ijk}(\mathbf{x},\mathbf{x}_0)\,n_k(\mathbf{x})\,dS(\mathbf{x}),$$

for $\mathbf{n}$ *exterior to* $\partial\Omega_1$. *The minus sign when* $\mathbf{x}_0$ *approaches to* $\partial\Omega_1$ *from* Ω_1 *and plus when it is from* Ω_2.

Therefore

$$v_j(\mathbf{x}_0) = \frac{-1}{4\pi(\mu_1+\mu_2)} \int_{\partial\Omega_1} \mathbb{G}_{ij}(\mathbf{x},\mathbf{x}_0)\,\Delta f_i(\mathbf{x})\,dS \tag{3.57}$$
$$+ \frac{\mu_2-\mu_1}{4\pi(\mu_1+\mu_2)} \int_{\partial\Omega_1}^{PV} v_i(\mathbf{x})\,\mathbb{T}_{ijk}(\mathbf{x},\mathbf{x}_0)\,n_k(\mathbf{x})\,dS(\mathbf{x}),$$

with $\mathbf{n}$ exterior to Ω_1 and

$$\mathbb{G}_{ij}(\mathbf{x},\mathbf{x}_0) = \frac{\delta_{ij}}{|\mathbf{x}-\mathbf{x}_0|} + \frac{(x_i-x_{0,i})(x_j-x_{0,j})}{|\mathbf{x}-\mathbf{x}_0|^3},$$

$$\mathbb{T}_{ijk}(\mathbf{x},\mathbf{x}_0) = -6\frac{(x_i-x_{0,i})(x_j-x_{0,j})(x_k-x_{0,k})}{|\mathbf{x}-\mathbf{x}_0|^5},$$

for $i,j,k \in \{1,2,3\}$, where

$$\Delta f_i(\mathbf{x}) = (2\mathcal{H}(\mathbf{x}) + F(V))n_i \tag{3.58}$$
$$= \left(2\mathcal{H}(\mathbf{x}) - \frac{\sigma_0(\mathbf{x})^2}{2} - \varepsilon\sigma_0(\mathbf{x})\sigma_1(\mathbf{x}) + \mathcal{H}(\mathbf{x})\sigma_0(\mathbf{x})\varepsilon\right)n_i,$$

corresponding to the boundary condition (3.19). The equation (3.57) is the integral equation for the velocity at the interface $\partial\Omega_1$ that will be used to determine the evolution of the droplet together with the boundary conditions (3.58).

3.5.3 The axisymmetric boundary integral equation for the velocity

We obtained an integral equation for the interface between two fluids (3.57) without assuming a particular symmetry in the velocity or the forces terms. Like in the Laplace case, it is possible to symplify the equation (3.57) using that we are expecting an axisymmetric flow. Let us choose again the symmetry axis, the z axis. It is possible to obtain expressions for the single and double layer in terms of elliptic integrals (cf. [54]) using cylindrical coordinates and that for an axysimmetric flow we have that velocity, force and normal vectors can be expressed in terms of $\{\mathbf{e}_r, \mathbf{e}_z\}$ only:

$$\mathbf{v} = v_r\mathbf{e}_r + v_z\mathbf{e}_z$$
$$\mathbf{f} = f_r\mathbf{e}_r + f_z\mathbf{e}_z$$
$$\mathbf{n} = n_r\mathbf{e}_r + n_z\mathbf{e}_z,$$

using also that the components of the velocity are decoupled. Performing the boundary integrations in the azimuthal direction it is possible obtain

$$v_\alpha(\mathbf{x}_0) = \frac{-1}{4\pi(\mu_1+\mu_2)} \int_C \Delta f_\alpha(\mathbf{x})\,M_{\alpha\beta}(\mathbf{x},\mathbf{x}_0)\,dl \tag{3.59}$$
$$+ \frac{\mu_2-\mu_1}{4\pi(\mu_1+\mu_2)} \int_C q_{\alpha\beta\gamma}(\mathbf{x},\mathbf{x}_0)\,v_\beta(\mathbf{x})\,n_\gamma(\mathbf{x})\,dl,$$

where α, β, γ are either r or z indicating the radial and axial components respectively, C the generating curve on the rz (xz) axis. If we use the basis $\{\mathbf{e}_r, \mathbf{e}_z\}$ and the variables $\mathbf{x}, \mathbf{x}_0$ in cylindrical coordinates $\mathbf{x} = (r\cos\theta, r\sin\theta, z), \mathbf{x}_0 = (r_0, 0, z_0) \in C$, the matrices $\mathbf{M}$ and $\mathbf{q}$ on the right hand side of (3.59) in terms of the elliptic integrals $E(k)$ and $F(k)$, become

$$
\begin{aligned}
M_{rr} &= \frac{k}{r_0 r}\sqrt{\frac{r}{r_0}}\left(\left(r^2 + r_0^2 + 2(z-z_0)^2\right)F(k)\right. \\
&\quad \left. - \frac{2(z-z_0)^4 + 3(z-z_0)^2(r_0^2+r^2) + (r_0^2-r^2)^2}{(z-z_0)^2 + (r-r_0)^2}E(k)\right) \\
M_{rz} &= -\frac{k(z-z_0)}{r_0}\sqrt{\frac{r}{r_0}}\left(F(k) + \frac{r_0^2 - r^2 - (z-z_0)^2}{(z-z_0)^2 + (r-r_0)^2}E(k)\right) \\
M_{zr} &= \frac{k(z-z_0)}{\sqrt{r_0 r}}\left(F(k) - \frac{r_0^2 - r^2 + (z-z_0)^2}{(z-z_0)^2 + (r-r_0)^2}E(k)\right) \\
M_{zz} &= 2k\sqrt{\frac{r}{r_0}}\left(F(k) + \frac{(z-z_0)^2}{(z-z_0)^2 + (r-r_0)^2}E(k)\right),
\end{aligned}
$$

and respective formulas for $\mathbf{q}$ (see [54]). Let us note that it will be necessary to remove the singularities caused by the tendency of k to 1 caused by the the approximation of $\mathbf{x}$ to $\mathbf{x}_0$, therefore, we add cero in a convenient way using

$$
\int_{\partial\Omega_1} \mathbb{G}_{ij}(\mathbf{x}, \mathbf{x}_0)\, n_i(\mathbf{x})\, dS(\mathbf{x}) = 0
$$

and we will have improper but well defined integrals if we choose as poles the middle points in the numerical method.

3.6 Numerical Implementation and numerical results

Because of the nature of the domains (not necessarily as simple as a ball) we have to use a numerical method, the Boundary Element Method (BEM) to approximate the functions involved in the boundary condition and also to approximate the velocity field $\mathbf{v}$. We will start with Laplace problem for obtaining $F(V)$, then we will approximate the solutions for the Stokes system, and finally we will use the evolution formula to study the behaviour of $\partial\Omega(t)$, the evolving boundary of the drop, in terms of t, ε, and the total charge Q.

3.6.1 Boundary Element Method (BEM) for Laplace equation in 3-D

Roughly speaking, the boundary element method involves discretizing a surface $\partial\Omega$ in a collection of N boundary elements that we will denote E_j, $j = 1, \ldots, N$, in such a way that $\partial\Omega \simeq \cup_{j=1}^{N} E_j$ and then to obtain an approximation of the function (or its normal derivative, or both) in the elements E_j.

Let us consider again the regularized equation satisfied by the harmonic function u for $\mathbf{x}_0 \in \partial\Omega_1$

$$u(\mathbf{x}_0) = -\int_{\partial\Omega_1} G(\mathbf{x},\mathbf{x}_0)\frac{\partial u}{\partial \mathbf{n}}(\mathbf{x})\,dS(\mathbf{x}) + \int_{\partial\Omega_1}(u(\mathbf{x})-u(\mathbf{x}_0))\frac{\partial G}{\partial \mathbf{n}}(\mathbf{x},\mathbf{x}_0)\,dS(\mathbf{x}),$$

$\mathbf{n}$ exterior to Ω_1.

If we replace the integrals on $\partial\Omega_1$ with sums of integrals on the boundary elements we obtain the discrete representation:

$$u(\mathbf{x}_0) \simeq -\sum_{j=1}^{N}\int_{E_i} G(x,x_0)\frac{\partial u}{\partial \mathbf{n}}(\mathbf{x})\,dS(x) + \sum_{j=1}^{N}\int_{E_j}(u(\mathbf{x})-u(\mathbf{x}_0))\frac{\partial G}{\partial \mathbf{n}}(\mathbf{x},\mathbf{x}_0)\,dS(x).$$

We introduce local approximations to the distribution of the harmonic function u and its normal derivative $\frac{\partial u}{\partial \mathbf{n}}$. In the simplest approximation, we approximate both distributions with constant functions on each element, denoted respectively u_j and $\left(\frac{\partial u}{\partial \mathbf{n}}\right)_j$, $j = 1,\ldots,N$ and we obtain a discrete boundary element representation (from now on we will use an equal symbol):

$$u(\mathbf{x}_0) = -\sum_{j=1}^{N}\left(\frac{\partial u}{\partial \mathbf{n}}\right)_j\int_{E_i} G(\mathbf{x},\mathbf{x}_0)\,dS(\mathbf{x}) + \sum_{j=1}^{N}(u(\mathbf{x})-u(\mathbf{x}_0))\int_{E_j}\frac{\partial G}{\partial \mathbf{n}}(\mathbf{x},\mathbf{x}_0)\,dS(\mathbf{x}).$$

Denoting $b_0 = u(\mathbf{x}_0) - \sum_{j=1}^{N}(u_j - u(\mathbf{x}_0))\int_{E_j}\frac{\partial G}{\partial \mathbf{n}}(\mathbf{x},\mathbf{x}_0)\,dS(\mathbf{x})$ and $A_{j0} = \int_{E_j} G(\mathbf{x},\mathbf{x}_0)\,dS(\mathbf{x})$ we obtain

$$b_0 = \sum_{j=1}^{N} A_{j0}\left(-\frac{\partial u}{\partial \mathbf{n}}\right)_j. \tag{3.60}$$

Let us remember that, if we take particular values of the boundary condition in $\partial\Omega$ for the Dirichlet problem to the Laplace equation

$$\begin{aligned}\Delta u(\mathbf{x}) &= 0 \text{ in } \Omega_2,\\ u(\mathbf{x})|_{\partial\Omega} &= u_0(\mathbf{x}),\\ u(\mathbf{x}) &\longrightarrow O\left(|\mathbf{x}|^{-1}\right) \text{ for } |\mathbf{x}| \longrightarrow \infty,\end{aligned}$$

with $u_0 = C$ or $u_0 = \ln(\sigma_0)$ respectively, the normal derivative of the potential u restricted to $\partial\Omega_1$ allows us to obtain σ_0 and $\mathcal{N}(\ln(\sigma_0))$. Therefore, using (3.60) and poles properly chosen we can obtain the discrete version of the normal derivative in each case above mentioned by inverting a matrix.

3.6.2 The BEM for the axisymmetric Laplace equation.

For the axisymmetric case we will also assume that $\Omega(0)$, the initial geometry of the droplet, is a small perturbation of the sphere given by a generating curve $(r(z), z)$ that is also symmetric with respect to the equatorial plane i.e $r(-z) = r(z)$.

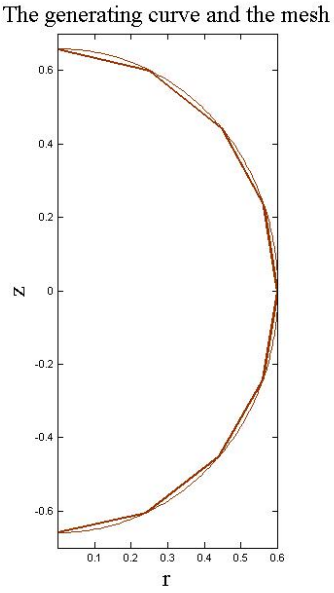

Figure 3.15: The generating curve for the axisymmetric surface and a mesh approximating it.

A surface element corresponds to a linear element on the generating curve.

Let us remember the regularized axisymmetric expression for the potential

$$u(\mathbf{x}_0) = -\frac{1}{\pi}\int_a^b \frac{F(k)}{\sqrt{(z-z_0)^2+(r+r_0)^2}}\frac{\partial u}{\partial n}(r,z)\, r(z)\sqrt{1+r'(z)^2}dz$$
$$+\frac{1}{2\pi}\int_a^b (u(r,z)-u(r_0,z_0))\left(-\frac{F(k)}{\sqrt{(z-z_0)^2+(r+r_0)^2}}+\right.$$
$$\left.+\frac{E(k)\left[(z-z_0)^2+2(z-z_0)\, r(z)\, r'(z)+(r_0-r)(r_0+r)\right]}{\sqrt{(z-z_0)^2+(r+r_0)^2}\left((z-z_0)^2+(r-r_0)^2\right)}\right)dz,$$

for $\mathbf{x}_0 \in \partial\Omega_1$. We will find discretized expressions for the simple and double layers.

Discretized axisymmetric expressions.

We are assuming that the forces acting in the drop are axially symmetric, and will result also symmetric with respect to the axis perpendicular to the rotation axis, because the electric field that originates the charge, comes from the unbalance of the ions and the respective charge with the free electrons, and we don't have an exterior field that could affect the symmetric distribution of the charge in the boundary. We will observe that fact in the equations.

Let us consider a mesh on the axisymmetric surface generated by the generating curve $(r(z), z)$, the mesh is determined by n points $(r_1, z_1), \ldots, (r_n, z_n)$ on $(r(z), z)$, where $r_j = r(z_j)$; they determine $n-1$ elements E_j on the surface. Let us take a pole in the ith subinterval (different from the endpoints of the subinterval) and let us denote it by $\mathbf{x}_0 = (r_0^i, z_0^i)$ where $r_0^i = r(z_0^i)$. We will find axisymmetric expressions that can be used to approximate the boundary condition for the system we want to solve.

Single and double layer discretization. The integral of the Green's function in the initial axisymmetric surface $\Omega(0)$ becomes:

$$\begin{aligned}\int_{E_j} G(\mathbf{x}, \mathbf{x}_0)\, dS(\mathbf{x}) &= \int_{z_j}^{z_{j+1}} \int_0^{2\pi} G(\mathbf{x}, \mathbf{x}_0) \sqrt{1 + r'(z)^2}\, r(z)\, d\theta dz \\ &= \frac{1}{\pi} \int_{z_j}^{z_{j+1}} G^{AX}(\mathbf{x}, \mathbf{x}_0) \sqrt{1 + r'(z)^2}\, r(z)\, dz \\ &= \frac{1}{\pi} \int_{z_j}^{z_{j+1}} \frac{F(k)}{\sqrt{(z - z_0^i)^2 + (r + r_0^i)^2}} \sqrt{1 + r'(z)^2}\, r(z)\, dz,\end{aligned}$$

with

$$k = \sqrt{\frac{4 r_0^i r}{(z - z_0^i)^2 + (r + r_0^i)^2}},$$

and F the elliptic integral. We have two types of local integrals, those defined on the subinterval that contains the pole and those that doesn't. As we mentioned before, the complete integral is regular but an improper integral, and this is considered in the numerics using aditional refinement in the subinterval with the pole.

Let us denote

$$I_1(z_j, z_{j+1}, z_0^i, r_0^i) = \int_{z_j}^{z_{j+1}} \frac{F(k(r(z), z, z_0^i, r_0^i))}{\sqrt{(z - z_0^i)^2 + (r + r_0^i)^2}} \sqrt{1 + r'(z)^2}\, r(z)\, dz,$$

if we take $z = -\omega$, by a change of variables and due to the symmetry with respect to the poles or parity of the functions involved, we have

$$\begin{aligned}I_1(z_j, z_{j+1}, z_0^i, r_0^i) &= \int_{z_{n-j}}^{z_{n-j+1}} \frac{F\left(k\left(r(\omega), \omega, z_0^{n-i}, r_0^{n-i}\right)\right)}{\sqrt{\left(\omega - z_0^{n-i}\right)^2 + \left(r(\omega) + r_0^{n-i}\right)^2}} \sqrt{1 + r'(\omega)^2}\, r(\omega)\, d\omega \qquad (3.61) \\ &= I_1(z_{n-j}, z_{n-j+1}, z_0^{n-i}, r_0^{n-i}).\end{aligned}$$

Now for the discretized double layer potential we have a similar result. If

$$\int_{E_j} \frac{\partial G}{\partial \mathbf{n}}(\mathbf{x},\mathbf{x}_0)\,dS(\mathbf{x}) = \int_{z_j}^{z_{j+1}} \int_0^{2\pi} \frac{\partial G}{\partial \mathbf{n}}(\mathbf{x},\mathbf{x}_0)\,dS(\mathbf{x})$$
$$= \frac{1}{2\pi}\int_{z_j}^{z_{j+1}} \frac{\partial G^{AX}}{\partial \mathbf{n}}(\mathbf{x},\mathbf{x}_0)\sqrt{1+r'(z)^2}r(z)\,dz$$
$$= \frac{1}{2\pi}\int_{z_j}^{z_{j+1}} \left(\frac{-F\left(k\left(r(z),z,z_0^i,r_0^i\right)\right)}{\sqrt{\left(z-z_0^i\right)^2+\left(r+r_i^M\right)^2}} + \right.$$
$$\left. \frac{E\left(k\left(r(z),z,z_0^i,r_0^i\right)\right)\left[\left(z-z_0^i\right)^2+2\left(z-z_0^i\right)r(z)r'(z)+\left(r_0^i-r\right)\left(r_0^i+r\right)\right]}{\sqrt{\left(z-z_0^i\right)^2+\left(r+r_0^i\right)^2}\left(\left(z-z_0^i\right)^2+\left(r-r_0^i\right)^2\right)} \right) dz$$

with E and F as before, the elliptic integrals, and we define

$$I_2(z_j,z_{j+1},z_0^i,r_0^i) = \int_{z_j}^{z_{j+1}} \left(\frac{-F\left(k\left(r(z),z,z_0^i,r_0^i\right)\right)}{\sqrt{\left(z-z_0^i\right)^2+\left(r+r_0^i\right)^2}} + \right.$$
$$\left. \frac{E\left(k\left(r(z),z,z_0^i,r_0^i\right)\right)\left[\left(z-z_0^i\right)^2+2\left(z-z_0^i\right)r(z)r'(z)+\left(r_0^i-r\right)\left(r_0^i+r\right)\right]}{\sqrt{\left(z-z_0^i\right)^2+\left(r+r_0^i\right)^2}\left(\left(z-z_0^i\right)^2+\left(r-r_0^i\right)^2\right)} \right) dz,$$

we have

$$I_2(z_j,z_{j+1},z_0^i,r_0^i) = I_2(z_{n-j},z_{n-j+1},z_0^{n-i},r_0^{n-i}). \tag{3.62}$$

We want to avoid numerical problems due to the nature of the singularities of the Green function and its normal derivative, therefore we will vary the poles $\mathbf{x}_0 \in \partial\Omega_1$ in the middle points of the subintervals determined by the discretization. Taking the poles in the middle points we have well defined expressions for the integrands in the single and double layer potentials.

To calculate the unknown element values $\left(\frac{\partial u}{\partial \mathbf{n}}\right)_j$ we apply the discretized integral equation in the middle points of each boundary element denoted by $\mathbf{x}_i^M = (r_i^M, z_i^M)$, for $z_i^M = \frac{z_i+z_{i+1}}{2}$ the middle point of the subinterval i in z axis and $r_i^M = \frac{r_i+r_{i+1}}{2}$ a middle point of the ith subinterval determined by r, $i = 1,\ldots,n-1$

$$u\left(\mathbf{x}_i^M\right) = -\sum_{j=1}^{n-1}\left(\frac{\partial u}{\partial \mathbf{n}}\right)_j \int_{E_j} G\left(\mathbf{x},\mathbf{x}_i^M\right)dS(\mathbf{x}) + \sum_{j=1}^{n-1}\left(u_j - u\left(\mathbf{x}_i^M\right)\right)\int_{E_j}\frac{\partial G}{\partial \mathbf{n}}\left(\mathbf{x},\mathbf{x}_i^M\right)dS(\mathbf{x}).$$

If we denote $b_i = u\left(\mathbf{x}_i^M\right) - \sum_{j=1}^{n-1}\left(u_j - u\left(\mathbf{x}_i^M\right)\right)\int_{E_j}\frac{\partial G}{\partial \mathbf{n}}\left(\mathbf{x},\mathbf{x}_i^M\right)dS(\mathbf{x})$ and $A_{ij} = \int_{E_j} G\left(\mathbf{x},\mathbf{x}_i^M\right)dS(\mathbf{x})$ we obtain

$$b_i = \sum_{j=1}^{n-1} A_{ij}\left(-\frac{\partial u}{\partial \mathbf{n}}\right)_j. \tag{3.63}$$

Due to (3.61)

$$A_{ij} = A_{n-i,n-j},$$

and, if we suppose that u is symmetric in $\partial\Omega_1$ and using (3.62), we will also have

$$b_i = b_{n-i}.$$

Now we will proceed to obtain σ_0 and $\mathcal{N}(\ln(\sigma_0))$.

Obtaining σ_0

In the axisymmetric equation

$$\begin{aligned} \Delta u(\mathbf{x},0) &= 0 \text{ in } \mathbb{R}^3 \backslash \overline{\Omega(0)}, \\ u(\mathbf{x},0)|_{\partial\Omega} &= u_0(\mathbf{x},0), \\ u(\mathbf{x},0) &\longrightarrow O\left(|\mathbf{x}|^{-1}\right) \text{ for } |\mathbf{x}| \longrightarrow \infty, \end{aligned}$$

we assume $u_0 = C$ for a suitable constant associated with the total charge in the droplet, the integral equation is:

$$C = -\frac{1}{\pi}\int_a^b \frac{F(k)}{\sqrt{(z-z_0)^2+(r+r_0)^2}} \frac{\partial u}{\partial n}(r,z)\, r(z) \sqrt{1+r'(z)^2}\, dz,$$

which implies

$$C \simeq -\sum_{j=1}^{n-1} \left(\frac{\partial u}{\partial \mathbf{n}}\right)_j \int_{z_j}^{z_{j+1}} \frac{F\left(k\left(r(z), z, r_i^M, z_i^M\right)\right)}{\sqrt{(z-z_i^M)^2+(r+r_i^M)^2}} \sqrt{1+r'(z)^2}\, r(z)\, dz,$$

for $i = 1, \ldots, n-1$. Inverting numerically as in [26] and taking care with the subinterval that contains the pole (refining properly on it), we obtain an approximation to

$$\sigma_0(x_S) = -\left.\frac{\partial u}{\partial n}(r,z)\right|_{\partial\Omega(0)},$$

in the middle points (r_i^M, z_i^M) of each element. For the integration we used the trapezoidal rule, for the calculation of the inverse the GMRES method (an iterative gradient method for the solution of linear systems) and for approximate the derivative, central differences.

As we mentioned before, if we assume an initial shape $\Omega(0)$ symmetric, σ_0 will also be symmetric.

Obtaining $\mathcal{N}(\ln(\sigma_0))$

If now we assume that the boundary condition $u_0(\mathbf{x},0) = \ln(\sigma_0(r,z))$ in $\partial\Omega(0)$, we will have:

$$\ln(\sigma_0(r_0,z_0)) = -\frac{1}{\pi}\int_a^b \frac{F(k)}{\sqrt{(z-z_0)^2+(r+r_0)^2}}\frac{\partial u}{\partial n}(r,z)\, r(z)\sqrt{1+r'(z)^2}dz+$$
$$+\frac{1}{2\pi}\int_a^b \ln\left(\frac{\sigma_0(r,z)}{\sigma_0(r_0,z_0)}\right)\left(\frac{-F(k)}{\sqrt{(z-z_0)^2+(r+r_0)^2}}+\right.$$
$$\left.\frac{E(k)\left[(z-z_0)^2+2(z-z_0)\, r(z)\, r'(z)+(r_0-r)(r_0+r)\right]}{\sqrt{(z-z_0)^2+(r+r_0)^2}\left((z-z_0)^2+(r-r_0)^2\right)}\right)dz,$$

using $\sigma_0(r,z)$ calculated before. We are looking for $\frac{\partial u}{\partial n}(r,z)$ therefore we will use the discretized version:

$$\ln\left(\sigma_0(r_i^M,z_i^M)\right) - \frac{1}{2\pi}\sum_{j=1}^{n-1}\int_{z_j}^{z_{j+1}} \ln\left(\frac{\sigma_0(r,z)}{\sigma_0(r_i^M,z_i^M)}\right)\left(-\frac{F\left(k\left(r(z),z,r_i^M,z_i^M\right)\right)}{\sqrt{(z-z_i^M)^2+(r+r_i^M)^2}}+\right.$$
$$\left.\frac{E\left(k\left(r(z),z,z_i^M,r_i^M\right)\right)\left[\left(z-z_i^M\right)^2+2\left(z-z_i^M\right)r(z)\, r'(z)+\left(r_i^M-r\right)\left(r_i^M+r\right)\right]}{\sqrt{(z-z_i^M)^2+(r+r_i^M)^2}\left(\left(z-z_i^M\right)^2+\left(r-r_i^M\right)^2\right)}\right)dz$$
$$= -\frac{1}{\pi}\sum_{j=1}^{n-1}\left(\frac{\partial u}{\partial \mathbf{n}}\right)_j\int_{z_j}^{z_{j+1}}\frac{F\left(k\left(r(z),z,r_i^M,z_i^M\right)\right)}{\sqrt{(z-z_i^M)^2+(r+r_i^M)^2}}\sqrt{1+r'(z)^2}\, r(z)\, dz,$$

where $\left(\frac{\partial u}{\partial \mathbf{n}}\right)_j$ is an approximation of the normal derivative at the middle points. As before, we can invert numerically to obtain an approximate $\mathcal{N}(\ln(\sigma_0)) = \frac{\partial u}{\partial n}(r,z)$ using the same techniques than for σ_0 for the calculation of the integrals, inverting the matrix etc. For approximating $\ln\left(\frac{\sigma_0(r,z)}{\sigma_0(r_i^M,z_i^M)}\right)$ we interpolate linearly using the discretized version found previously.

Obtaining the boundary condition $F(V)$

We know

$$\sigma_1(x_S) = -\frac{2\int_{\partial\Omega}\mathcal{N}(\ln(\sigma_0))}{Q}\sigma_0(x_S) + 2\mathcal{N}(\ln(\sigma_0)) + O(\varepsilon),$$

and now we have the functions that we need to calculate it. Therefore we can obtain the values for the boundary conditions to be used in the Stokes system. Let us obtain the axisymmetric version and discuss the principal formulas used for the velocity field.

3.6.3 Boundary Element Method for the axisymmetric Stokes system

Now that we have the boundary conditions to calculate the velocity field, let us note that we can simplify the integral equations deduced before using axisymmetry as we did with Dirichlet problem, and the integral equation found for values $\mathbf{x}_0 \in \partial\Omega_1$ will be also in terms of elliptic integrals.

We already have an integral equation for the velocity at the surface of the drop. If $\mathbf{x}_0 \in \partial\Omega_1$

$$\begin{aligned} v_\alpha(\mathbf{x}_0) = & \frac{-1}{4\pi(\mu_1+\mu_2)} \int_C \Delta f_\alpha(\mathbf{x}) M_{\alpha\beta}(\mathbf{x},\mathbf{x}_0)\, dl \\ & + \frac{\mu_2-\mu_1}{4\pi(\mu_1+\mu_2)} \int_C q_{\alpha\beta\gamma}(\mathbf{x},\mathbf{x}_0) v_\beta(\mathbf{x}) n_\gamma(\mathbf{x})\, dl, \end{aligned}$$

discretizing and using as poles the middle points for finding the velocity on them, we have

$$\begin{aligned} & v_\alpha(r_i^M, z_i^M) - \frac{\mu_2-\mu_1}{4\pi(\mu_1+\mu_2)} \sum_{j=1}^{n-1} \left(v_\beta(r_i^M, z_i^M)\right)_j \int_{E_j} q_{\alpha\beta\gamma}\left(r(z), z, r_i^M, z_i^M\right) n_\gamma(r(z), z)\, dl \\ & = \frac{1}{4\pi(\mu_1+\mu_2)} \sum_{j=1}^{n-1} \int_{E_j} \Delta f_\alpha(r(z), z) M_{\alpha\beta}\left(r(z), z, r_i^M, z_i^M\right) dl. \end{aligned}$$

In the case of axisymmetric flux, the integrand of the integral of the double layer potential is not singular or weakly singular (see [56]), and the integral can be calculated by standard numerical methods (unlike the 3-D flux in which is necessary to remove the singularity (cf. [54], [56])).

3.6.4 Details on the numerical implementation

We will include the principal algorithm (with only the principal parameters) to illustrate the basic idea followed for generating the evolution of the drops.

Algorithm 12. ***Input parameters:***

μ_1 *viscosity of the drop.*

μ_2 *viscosity of the fluid surrounding the drop.*

Q *initial charge of the droplet.*

ε *dimensionless parameter associated with the Debye length.*

Configuration parameters:

n *number of nodes.*

e *eccentricity of the spherical harmonic for the initial mesh* $\Omega(0)$

1. $t \leftarrow t_0$
2. ***while*** $t < t_{max}$
3. *Calculate the surface charge density* σ_0 *at the midpoints of the mesh.*
4. *Calculate the correction* σ_1 *for the boundary condition* $F(V)$.
5. *Calculate the mean curvature at the midpoints of the mesh.*
6. *Calculate the velocity field at the midpoints of the mesh.*
7. *Interpolate the velocity to the nodes and project it to the normal.*
8. *Calculate an appropriate time step for determining the new mesh.*
9. *We move the mesh using the interpolated velocity to find the position of the nodes at the new time* $t + \Delta t$
10. *Smothing the grid, moving the nodes to the direction of maximum curvature.*
11. $t \leftarrow t + \Delta t$

Output: *The position of the nodes at a final time* t_{max}.

The most important details have been discussed before, therefore we just give few comments about the algorithm.

The initial mesh

We will take as initial data for the drop's shape a perturbed sphere by a spherical harmonic $Y_2^0(\theta, \phi) = \frac{1}{4}\sqrt{\frac{5}{\pi}}(3\cos^2\theta - 1)$ so that the eccentricity is $e \equiv \frac{r_{\max} - r_{\min}}{r_{\max} + r_{\min}}$

Steps 3 and 4: The surface charge density σ_0 and the correction σ_1

In the last section we already explained the kind of equations that we have to solve for them, and the methods involved. Basically are performed solving numerically the corresponding integral equation.

Step 5: The mean curvature at the midpoints

For the curvature of the generating curve we use the Frenet-Serret formula

$$\mathbf{t} \cdot \frac{d\mathbf{n}}{ds},$$

with derivative of arc length.

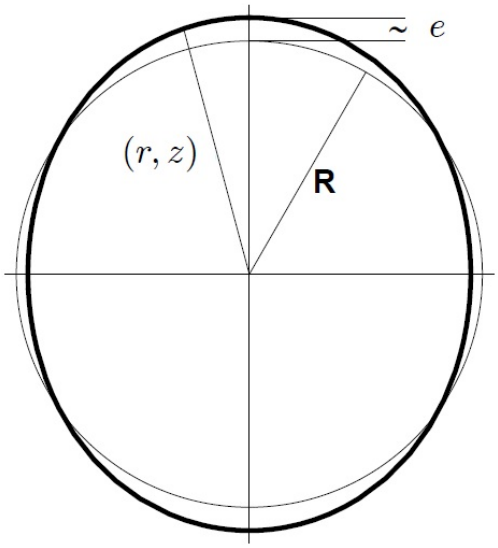

Steps 6 and 7: The velocity field.

Using the formulas afore mentioned for the axisymmetric velocity field in terms of elliptic integrals, and the trapezoidal rule for the integration in each element, we obtained the velocity field in the middle points, we interpolate to obtain the velocity at the nodes and finally project to the normal, because the normal direction determines the evolution of the drop, the tangential direction only redistributes the nodes.

Step 8: The time step

We obtain the time step from the equation that moves the drop:

$$\frac{d\mathbf{x}}{dt} \cdot \mathbf{n} = v \cdot \mathbf{n},$$

if we choose

$$\Delta t < \min_{i=1,\ldots,n-1} \frac{|\mathbf{x}_{i+1} - \mathbf{x}_i|}{|v_i|},$$

we have stability for the Euler explicit squeme that evolves the drop (CFL condition). From the nondimensionalization of the variables (for working with a dimensionless problem),

$$\tau = \frac{(\mu_1 + \mu_2) \min_{i=1,\ldots,n-1} ||\mathbf{x}_{i+1} - \mathbf{x}_i||}{\gamma},$$

and hence we choose

$$\Delta t < C\tau,$$

with C a sufficiently small (in order to guarantee stability) fixed constant. In this way we obtain an appropriate time step.

Steps 9 and 10: Moving and smoothing the mesh

We prepare the mesh for next iteration, but before of that, we calculate again the curvature for the new mesh and move the points in the direction of maximum curvature. In this way we obtain more resolution in the regions of high curvature of the droplet, where the experiments lead us to expect the formation of the jet.

3.7 Numerical results: the evolution of a droplet

We could obtain the flow using the boundary condition, the evolved droplet using

$$\frac{d\mathbf{x}}{dt} \cdot \mathbf{n} = \mathbf{v} \cdot \mathbf{n},$$

now we will find out the stability of the electrolitic droplet in terms of ε (that physically corresponds to the Debye Length).

3.7.1 Stability analysis

We start using an algorithm for the case $\varepsilon = 0$, i.e. assuming that the drop is a perfect conductor (and the corresponding equations for the potential) and using a similar argument to the bisection method we found that the critical charge to 3 decimals for dimensionless variables and equations, is $Q_{c,0} = 12.123$. Using the same bisection idea and the algorithm with the force term in the boundary using the correction σ_1 to the surface charge density, i.e. the case $\varepsilon \neq 0$, we found different values for the critical charge.

We found that the critical charge (to three decimals also) depends on ε and we used the perfect conductor case to express it relative to the critical charge for $\varepsilon = 0$:

ε	0	0.01	0.011	0.012	0.013	0.014	0.015	0.016
$Q_{c,\varepsilon}$	12.123	12.478	12.515	12.551	12.587	12.623	12.660	12.696
$\frac{Q_{c,\varepsilon}}{Q_{c,0}}$	1	1.0293	1.0323	1.0353	1.0382	1.0412	1.0442	1.0473
X_ε	1	1.0594	1.0656	1.0718	1.0778	1.0840	1.0903	1.0968

If we take a charge greater or equal than the critical charge for the respective case of ε, we have inestability. In the calculation of X_ε we are using that $X \sim Q^2$.

Fitting quadratically we obtained

$$\frac{Q_{c,\varepsilon}}{Q_{c,0}} = \frac{44.893}{12.123}\varepsilon^2 + \frac{35.108}{12.123}\varepsilon + 1,$$

with a norm of residuals 0.00086283.

Our conclusion is the following: The critical charge increases with ε. This fact agrees with the observation in [20] that water droplets, containing always a certain amount of ions, are able to hold an amount of charge slightly larger than Rayleigh's limit (that is, a charge corresponding to, $Q_{c,0}$).

3.7.2 The jets

If we take a value of charge that exceeds the critical charge we can see a deformation in the droplet, different than those observed in the numerical experiments in [26] and in [12], done considering the perfect conductor case

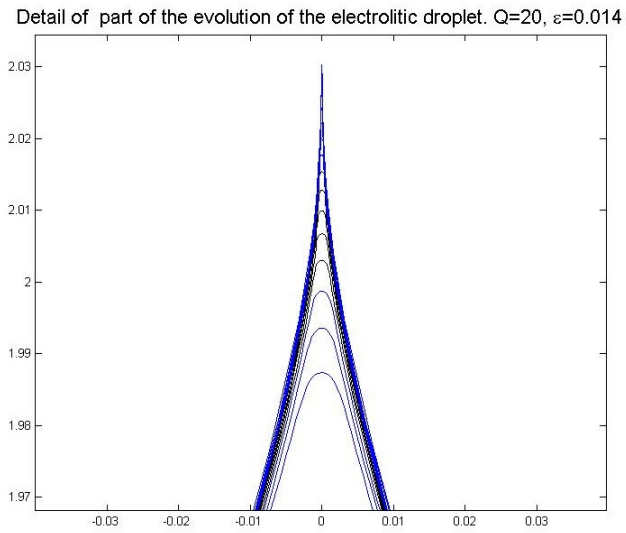

Figure 3.16: Some of the last profiles in the simulation.

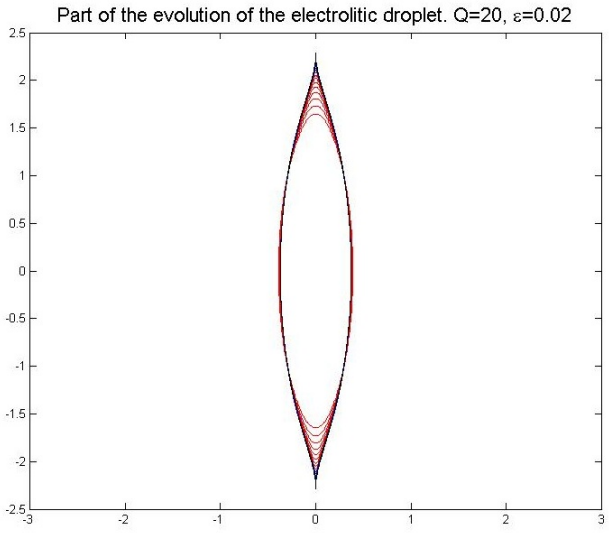

Figure 3.17: Part of the behavior of the electrolitic drop.

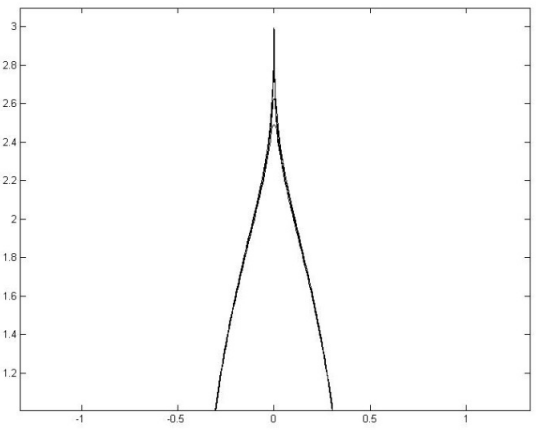

Figure 3.18: The formation of jet from an electrically charged viscous droplet. Numerical simulation from our model.

Figure 3.19: Experiment from Grimm and Beauchamp.

3.7.3 The velocity of the jet using dimensional arguments

We are interested in knowing the relation between the Debye-Length and the velocity of the jet, that is, the dependence in the distribution of the charges in the boundary with the jet.

Therefore, for a fixed charge, we will investigate the relation between ε and the component z of the velocity, i.e., v_z in the jet.

We have not defined what a jet is, and we will not define it but empirically, we will use an informal idea that comes from the observation of the experiments and comparing them with the evolution of the droplet in time with the simulations. For define it more properly we could use the evolution of the simulations and identifying the outputs for large times with small numerical error, the curvature in the apex, or also relate to the outputs the physical quantities associated to the drop, like for instance the charge in the "body" of the drop and comparing it with the charge in the part of the drop which we could call a "jet", since we know, due to the experiments, what should happen with the charge.

Some of the results obtained in the simulations about the the velocity are represented in Figures 3.20 and 3.21

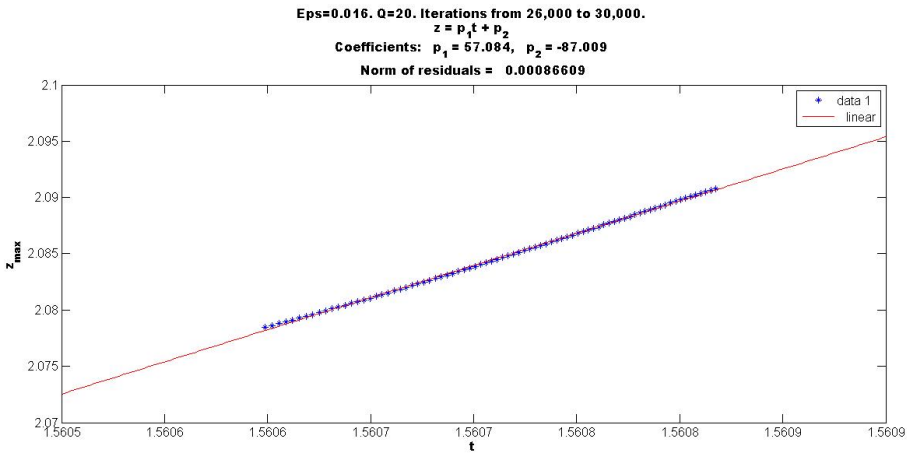

Figure 3.20: Possition of the apex of the drop as a function of time for $\varepsilon = 0.016, Q = 20$. Observe that the position grows linearly in time indicating the appearence of a jet with $V \simeq 57.084$

Observe in Figure 3.18 the presence of jets as observed in the experiments reported, for instance, in [20], [6].

We will analyse, based on the numerical simulations and asymptotic analysis, the main features of these jets as a function of ε (which is proportional to the absolute temperature) and ion concentration.

As we can observe, jets are emitted with a constant velocity (see Figures 3.21, 3.20). If we plot the velocity of the jet v_z as a function of ε (3.19), we can detect a scaling law

$$v_z \sim \frac{C}{\varepsilon}, \tag{3.64}$$

so that jets are emitted faster as ε decreases. Of course, very large velocities as $\varepsilon \to 0$ are not realistic, since inertial terms that have been neglected under Stokes approximation would then become dominant. Nevertheless, (3.64) provides an important qualitative result: the jet's velocity is inversely proportional to ε. Notice that in the limit $\varepsilon = 0$, which corresponds

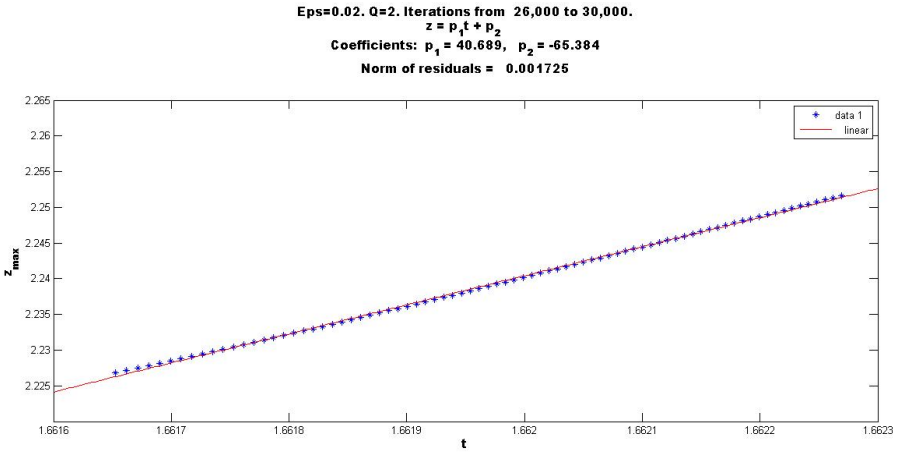

Figure 3.21: Possition of the apex of the drop as a function of time for $\varepsilon = 0.02, Q = 20$. Observe that the position grows linearly in time indicating the appearence of a jet with $V \simeq 40.689$

to the perfect conductor, the velocity becomes singular as shown in [26] with the formation of a conical tip. It is then expected that the radius of the jet collapses to zero as $\varepsilon \to 0$. This fact is observed numerically as represented in Fig. 3.18. A clear cone-jet structure can clearly be observed in Figures 3.16 and 3.18: a cone whose vertex connects with a thin jet. By mass conservation, the flux of mass across a cross-section of the cone (which is essentialy independent of ε as the jet develops) equals the flux of mass over a cross-section of the jet. Therefore, if the radius of the jet is r, then

$$\rho \pi r^2 v_z = Const,$$

which implies, by (3.64), a jet's radius

$$r \propto \varepsilon^{\frac{1}{2}}. \tag{3.65}$$

Since, for a given solution, ε is proportional to the absolute temperature, we can conclude that the jet's radius decreases with the absolute temperature or, in other words, decreases when the Debye layer's thickness decreases. This is a common experimental observation in the electrokinetic context.

The origin of the scaling law (3.64) for the velocity of the jet can be understood from the following simple heuristic argument: the jet appears when the correction due to the Debye layer becomes of the same order of magnitude than the capillary force. Since, for $\varepsilon = 0$, conical singularities develop as demonstrated in [12], [26] and they are such that

$$\mathcal{H} \propto \frac{1}{(t_0 - t)^{\frac{1}{2}}}, \ \sigma \propto \frac{1}{(t_0 - t)^{\frac{1}{2}}}, \ v_{z,tip} \propto \frac{1}{(t_0 - t)^{\frac{1}{2}}}$$

close to the singularity time t_0, we can now compare the terms

$$\gamma \mathcal{H} = O((t_0 - t)^{-\frac{1}{2}})$$
$$\varepsilon \sigma \mathcal{H} = \varepsilon O((t_0 - t)^{-1})$$

to conclude that jet starts to form when

$$\varepsilon = O((t_0 - t)^{\frac{1}{2}})$$

so that, the velocity is then

$$v_z \propto \frac{1}{(t_0 - t)^{\frac{1}{2}}} = O(\varepsilon^{-1})$$

Then it is reasonable to assume that the velocity of the jet behaves like:

$$v_z \sim C\varepsilon^{\alpha},$$

now if we use the simulations obtained with the algorithm, we would have

$$\ln(v_z) \sim \alpha \ln(\varepsilon) + \ln C,$$

therefore, if we use a linear fitting to the graph of $\ln(v_z)$ against $\ln(\varepsilon)$ we can obtain an approximate value of α using the values obtained from the simulations.

3.7.4 The velocity using the simulations

We will use now the simulations and an empiric definition of "jet" that includes using some of the last outputs and observing the change in the curvature in the apex. Considering outputs inside the formation that behaves like a jet, we use for all the ε cases, the times corresponding to iterations from $26,000$ to $30,000$, i.e., the same interval of time for all the analyzed cases. Using the respective height of the droplet, we can approximate the velocity for each case. Let us observe the iterations corresponding to the case of $\varepsilon = 0.016$ in Fig. 3.22.

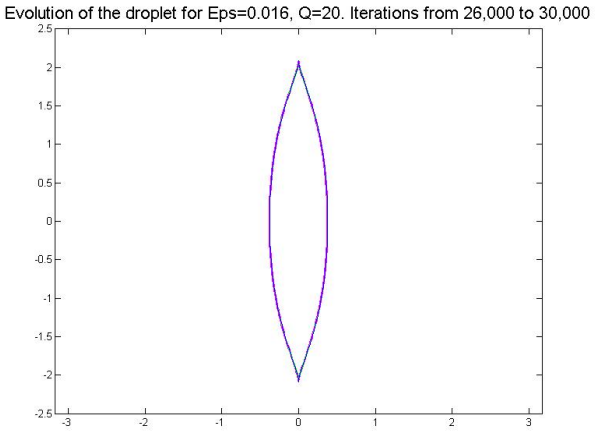

Figure 3.22: It seems to be a single drop, but it is a collection of droplets

If we zoom in some of the poles, we can see in the Fig. 3.23 that it is not a single drop but a collection of droplets with almost the same "body" but a different apex.

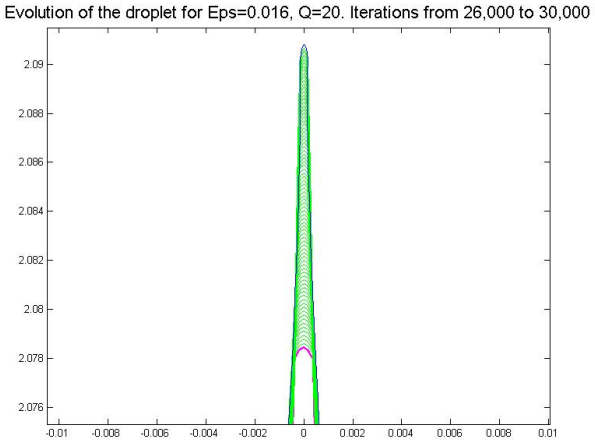

Figure 3.23: Zooming, we can see now how the droplet evolves, developing a jet

Considering the time against the height and fitting linearly, we can obtain an approximate velocity for each case considered, see for example in Fig.3.20 the graph for the case of $\varepsilon = 0.016$.

We obtained the velocity for physically relevant cases of ε, and the residual in the respective linear fitting:

ε	0.01	0.011	0.012	0.013	0.014	0.015	0.016
v_z	95.092	86.737	79.79	73.039	67.418	61.791	57.084
Residual	0.0002694	0.0003053	0.0003684	0.0004626	0.000572	0.000714	0.0008660

If we now consider the linear fitting of the logarithms of ε and v_z obtained before, we can see in Fig. 3.24 an approximate value to α using the coefficient of the independent variable.

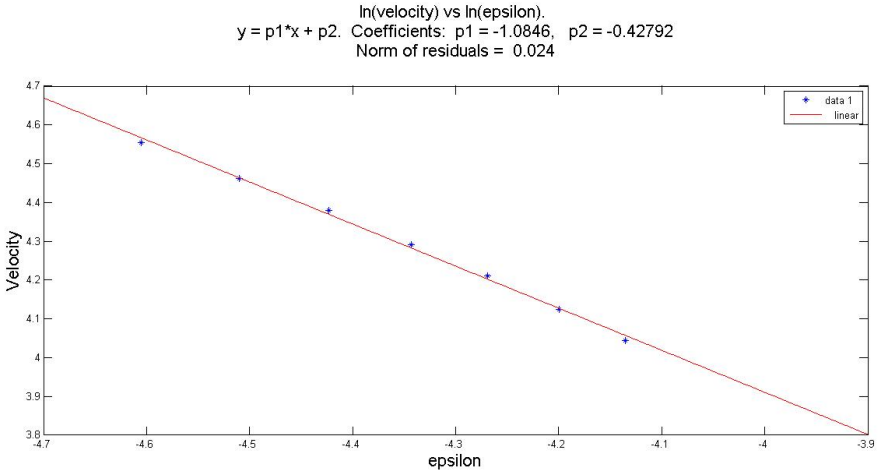

Figure 3.24: Approximating ε exponent considering cases with physical relevance

$$v_z \sim \frac{1}{\varepsilon},$$

we can strongly suspect then, that we already have a relation between the velocity and the Debye-Length, i.e, the velocity will grow with smaller values of ε.

3.7.5 The diluted case

Next, we discuss the effects of ion concentration on the jet's size and velocity. We can combine in dilute solutions the terms in $F(V)$ to obtain, up to constants that can be included in the pressure and corrections of $O(\varepsilon^2)$,

$$F(V) = \frac{\sigma^2}{2} e^{-\frac{2\varepsilon\kappa}{\sigma}}. \tag{3.66}$$

This expression coincides with the more general expression

$$F(V) = g_1\left(\frac{\chi}{\sigma}\right)\frac{\sigma^2}{2} e^{-g_2\left(\frac{\chi}{\sigma}\right)\frac{\varepsilon\kappa}{\sigma}}, \tag{3.67}$$

that was deduced for arbitrary (not necessarily diluted) ionic solutions. The parameter χ is proportional to the square root of the ion concentration. Notice that $g_2\varepsilon$ plays the same role in (3.67) as ε in (3.66). Hence, we expect a radius of the jet

$$r_j \propto g_2^{\frac{1}{2}}\varepsilon^{\frac{1}{2}}.$$

Since the function $g_2(s)$ is decreasing, we find that for a given value of ε, the jet's radius decreases with increasing, ion concentration. In fact, the graphical representation of $g_2(s)$ reveals an exponential decay, so that one can expect very strong decrease of the jet's radius when ion concentration experiences a significant increase. This fact can be seen in our figure 3.7.5.

In fact, it is well known by experimentalists interested in the production of micro and nanojets, that a method to produce extremely thin jets is to add salt to the liquid. Since

$$g_2(s) \simeq e^{-2s}, \text{ as } s \to \infty,$$

we can provide the following approximation for the jet's radius as a function of ion concentration μ and for a given value of ε:

$$r_j \propto e^{-C\mu^{\frac{1}{2}}}.$$

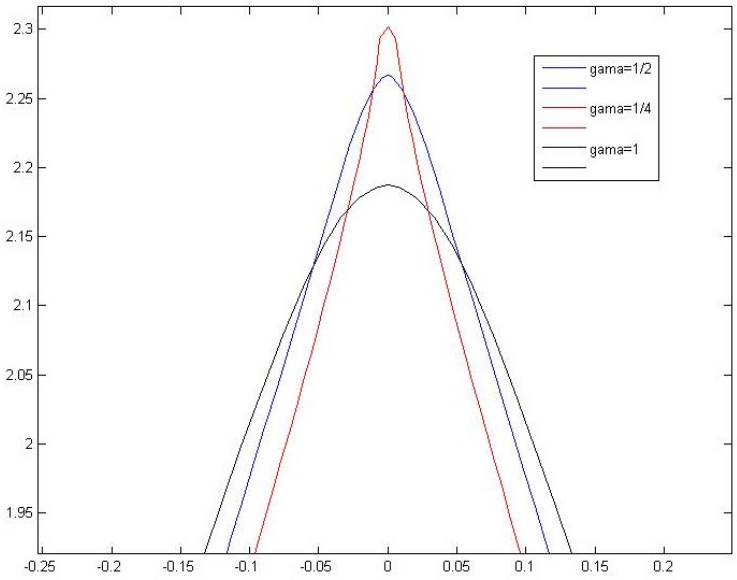

Figure 3.25: Iniciation of the jet for $\varepsilon = 0.03$ and $g_2 = 0.25, 0.5, 1$. Notice that the curvature increases as g_2 decreases

Chapter 4

The stability of drops with thick Debye layers: the Debye Hückel approximation

4.1 Introduction

In the previous chapters we considered the Poisson-Boltzmann model in order to describe the distribution of ions and free charges inside the drop. The main assumption was the smallness of a dimensionless parameter ε

$$\varepsilon = \frac{\varepsilon_0 \varepsilon_r k_B T l}{(ez)^2},$$

introduced in Chapter 2. If the positive ion concentration (number of ions per unit volume) times the characteristic length of the drop l is divided by this parameter, we get a quantity with dimensions the inverse of length square. If we compute a similar quantity with negative charge concentration and add to the previous one, we obtain a quantity with dimensions the inverse of length to the square: the inverse of the Debye length λ_D squared. More precisely: by denoting with M and N the amount of positive and negative charges respectively and with l a characteristic length scale of the drop (its volume to the $\frac{1}{3}$ power, for instance) we have

$$\lambda_D^{-2} = \frac{l\left(\frac{M}{l^3}\right)}{\varepsilon} + \frac{l\left(\frac{N}{l^3}\right)}{\varepsilon},$$

and we can construct the dimensionless quantity

$$\left(\frac{\lambda_D}{l}\right)^2 = \frac{\varepsilon}{M+N}. \tag{4.1}$$

Hence, for a drop of a given size and total number of ions, we were assuming a small Debye length as compared to drop's size. In this Chapter we will look at the opposite situation when the parameter ε is large and the Debye length is not necessarily small compared to the

radius of the drop. This allows to linearize the Poisson-Boltzmann equation under the, so called, Debye-Hückel approximation. One situation where Debye-Hückel approximation is valid is when dealing with very diluted ionic solutions, so that M and N in (4.1) are small.

We will perform the Debye-Hückel approximation from the Poisson-Boltzmann equation obtained in Chapter 2. Let us remember that assuming the presence of N electrolitic species, charge imbalance, negligible velocity and flux of charges in the drop, Poisson equation becomes

$$\Delta V = -\sum_{i=0}^{N-1} \frac{ez_i c_i}{\varepsilon_0 \varepsilon_r} e^{-\frac{ez_i}{k_b T} V}, \text{ in } \Omega, \tag{4.2}$$

last equation (4.2) is Poisson-Boltzmann equation and defines the electric potential distribution in the diffuse ionic layer adjacent to a charged surface. By writing

$$c_i = n_i^0 e^{\frac{ez_i}{k_b T} V_c}$$

with n_i^0 the bulk values (overall average) of the ith species. We obtain the equation

$$\Delta V = -\sum_{i=0}^{N-1} \frac{ez_i n_i^0}{\varepsilon_0 \varepsilon_r} e^{-\frac{ez_i}{k_b T}(V - V_c)}, \text{ in } \Omega. \tag{4.3}$$

where V_c is chosen such that $\sum_{i=0}^{N-1} \frac{ez_i c_i}{\varepsilon_0 \varepsilon_r} e^{-\frac{ez_i}{k_b T} V_c} = 0$. Hence, if the arguments of the exponentials in (4.3) are small then (4.3) can be linearized and yields the following homogeneous screened Poisson equation (a time-independent Klein-Gordon equation):

$$\Delta \widetilde{V} - (\lambda_D)^{-2} \widetilde{V} = 0, \quad \text{in } \Omega \tag{4.4}$$

where $\widetilde{V} = V - V_c$ and λ_D is, in the general case when there are multiple species, a parameter with dimension of length that is called the Debye screening length

$$(\lambda_D)^{-2} = \sum_{i=0}^{N-1} \frac{(ez_i)^2 n_i^0}{\varepsilon_0 \varepsilon_r k_b T}$$

If we rescale the space variable with the drop's length scale, $\mathbf{x}' = \frac{\mathbf{x}}{l}$ and we keep the notation Ω for the domain, we arrive at

$$\Delta \widetilde{V} - \kappa^2 \widetilde{V} = 0, \quad \text{in } \Omega \tag{4.5}$$

with κ a dimensionless parameter such that

$$\kappa^{-1} = \frac{\lambda_D}{l}$$

The approximation by which one arrives to (4.5) from (4.3) is called the Debye-Hückel approximation. In the case of a binary ionic solution whose ions have a valence one and in the presence of electrons, Poisson-Boltzmann equation can be written as (see Chapter 2)

$$\Delta u = \mu \sinh \frac{u - u_c}{\varepsilon}$$

with $V = \frac{ez}{\varepsilon_0 \varepsilon_r l} u$, $\varepsilon = \frac{\varepsilon_0 \varepsilon_r k_b T l}{(ez)^2}$ and $\varepsilon/\mu = \lambda_D/l$. It is then clear that Debye-Hückel approximation corresponds to the situation where $\varepsilon \gg 1$ so that $\widetilde{u} = u - u_c$ satisfies $\Delta\widetilde{u} - \kappa^2\widetilde{u} = 0$ at leading order in ε^{-1}.

Formally, when the nondimensionalized Debye length κ^{-1} tends to zero, one arrives from (4.5) to the equation $\widetilde{V} = 0$, that is to a constant potential V_c inside the drop just like in the case of a perfectly conducting medium. Outside the drop there is no charge and hence

$$\Delta V = 0, \text{ outside } \Omega \tag{4.6}$$

with V decaying to zero as $|\mathbf{x}| \to \infty$. At the boundary of the drop, the potential V must be continuous and differentiable. Finally, by Gauss' theorem, the net charge inside the drop is given by

$$Q = -\varepsilon_0 \int_{\partial\Omega} \frac{\partial V}{\partial n} dS \tag{4.7}$$

which serves as a relation to compute V_c given the net charge Q. The purpose of this chapter is to compute the correction introduced to Rayleigh stability criterion for stability already mentioned in previous chapters, i.e. $X < 1$ with X given by (3.1), when the potential is not constant inside the drop (we are not assuming a perfect conductor) but satisfies (4.5), (4.6), (4.7).

4.2 The linearized Stokes system

We have a drop that consists of a viscous incompressible fluid containing ions, which are electrically charged and produce stresses on the fluid through the so-called Maxwell stress tensor:

$$\tau_{ij} = E_i E_j - \frac{1}{2}\delta_{ij} |\mathbf{E}|^2 \tag{4.8}$$

As we mentioned in Chapter 3, its divergence is the force acting in the drop. Hence, the velocity and pressure field inside the drop satisfy the Stokes system

$$-\nabla p + \Delta \mathbf{v} + \mathbf{F}_e = 0 \text{ in } \Omega(t) \tag{4.9}$$

$$\nabla \cdot \mathbf{v} = 0 \text{ in } \Omega(t) \tag{4.10}$$

$$\mathbf{nTn} = -\gamma \mathcal{H} \text{ at } \partial\Omega(t) \tag{4.11}$$

$$\mathbf{tTn} = 0 \text{ at } \partial\Omega(t) \tag{4.12}$$

with $\mathbf{F}_e$ the electrical force $\mathbf{F}_e = \rho\mathbf{E}$, ρ the electric charge density and $\mathbf{E} = -\nabla V$ the local electric field with V the electric potential. The vectors $\mathbf{n}$, $\mathbf{t}$ are normal and tangent vectors respectively, $\mathcal{H}$ is the mean curvature (we can assume a change of variables for dropping off the factor 2 in the right hand side of (4.11)) of the drop's surface. Relation (4.11) expresses balance between viscous stresses and surface tension, and $\mathbf{T}$ is the viscous stress tensor

$$T_{ij} = -p\delta_{ij} + \left(\frac{\partial v_i}{\partial x_j} + \frac{\partial v_j}{\partial x_i} \right) \tag{4.13}$$

By Debye-Hückel approximation, $\rho = -\kappa^2 \widetilde{V}$ we have then

$$\rho \mathbf{E} = \kappa^2 \widetilde{V} \nabla \widetilde{V} = \frac{\kappa^2}{2} \nabla \widetilde{V}^2$$

If we assume that the domain $\Omega(t)$ is close to a ball of unit radius, we can assume also that

$$\partial\Omega(t) = \{\mathbf{r} : r(\theta, \varphi, t) = 1 + x(\theta, \varphi, t)\}$$

i,e., its boundary corresponds to a small perturbation of the unit sphere, where the perturbation is a function $x(\theta, \varphi, t) = \epsilon\lambda(\theta, \varphi, t)$. The variables (r, θ, φ) being a spherical coordinates system with $\theta \in [0, \pi], \varphi \in (0, 2\pi]$.

Let us define a Hanzawa transformation (cf. [38],[27])

$$\begin{aligned} r &= r' + \epsilon\lambda(\theta', \varphi', t)\chi(1 - r') \\ \theta &= \theta' \\ \varphi &= \varphi' \end{aligned} \tag{4.14}$$

with $\chi(z) \in C^\infty(\mathbb{R}), \chi(z) = \begin{cases} 0 \text{ if } |z| \geq \frac{3\delta_0}{4} \\ 1 \text{ if } |z| < \frac{\delta_0}{4} \end{cases}$, $0 < \chi(z) < 1$ in other case. $\left|\frac{d^k\chi}{dz^k}\right| \leq \frac{C}{\delta_0}$, $0 < \delta_0 < 1$ sufficiently small. This transforms the unit ball $B(0, 1)$ into $\Omega(t)$. Takes the ball of radius $1 - \frac{3\delta_0}{4}$ into itself and the unit sphere S^2 into $\partial\Omega(t)$.

The central idea is to express the system (4.9)-(4.12) in terms of functions in new variables and terms negligible at ϵ order coming from the Hanzawa transformation, to be solved in a more simple domain in which we can deal with functions in an appropriate and known base (spherical harmonics and vector spherical harmonics) and allows us to transform the pde system in an ode system. We will be using ideas and calculations from [32], [41] and [27].

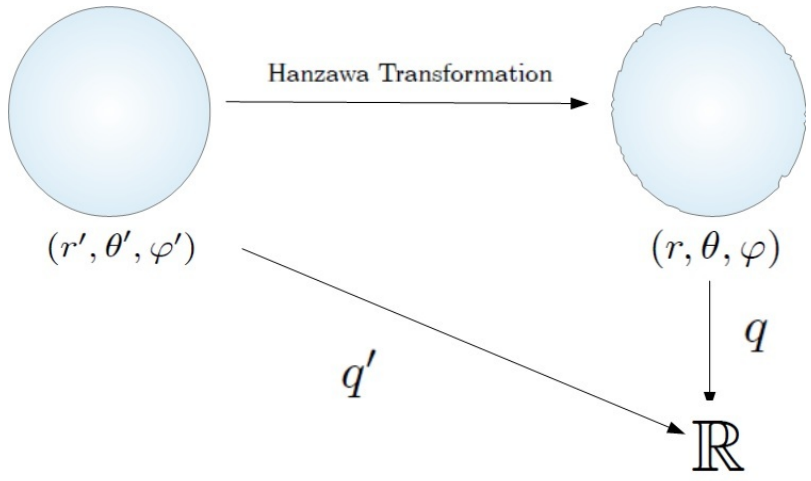

Figure 4.1: The Hanzawa transformation.

We have

$$\frac{\partial r'}{\partial r} = \frac{1}{1 - \epsilon\chi'\lambda} \tag{4.15}$$

if we denote $\omega = (\omega_1, \omega_2) = (\theta, \varphi)$ and $\omega' = (\omega_1', \omega_2') = (\theta', \varphi')$

$$\frac{\partial r'}{\partial \omega_i} = -\epsilon \frac{\chi\left(1 - r'\right)\lambda_{\omega_i'}}{1 - \chi'\lambda} \tag{4.16}$$

and

$$\frac{\partial^2 r'}{\partial r^2} = -\epsilon \frac{\chi''\lambda}{\left(1 - \epsilon\chi'\lambda\right)^3} \tag{4.17}$$

$$\frac{\partial^2 r'}{\partial \omega_i^2} = -\epsilon \frac{\chi\lambda_{\omega_i'\omega_i'}}{1 - \epsilon\chi'\lambda} - 2\epsilon^2 \frac{\chi'\chi\lambda_{\omega_i'}^2}{\left(1 - \epsilon\chi'\lambda\right)^2} - \epsilon^3 \frac{\chi''\chi^2\lambda\lambda_{\omega_i'}^2}{\left(1 - \epsilon\chi'\lambda\right)^3} \tag{4.18}$$

Denote

$$\begin{aligned} p' &= p(r' + \epsilon\lambda\chi\left(1 - r'\right), \theta', \varphi') \\ v_{r'}' &= v_r(r' + \epsilon\lambda\chi\left(1 - r'\right), \theta', \varphi') \\ v_{\omega_i'}' &= v_{\omega_i}(r' + \epsilon\lambda\chi\left(1 - r'\right), \theta', \varphi') \end{aligned}$$

Let us consider the base $\{\mathbf{e}_r, \mathbf{e}_\theta, \mathbf{e}_\varphi\}$, then for $q'\left(r', \omega'\right) = q(r' + \epsilon\lambda\chi\left(1 - r'\right), \omega)$,

$$\nabla_{(r',\omega')} q' = \frac{\partial q'}{\partial r'}\mathbf{e}_r + \frac{1}{r'}\frac{\partial q'}{\partial \theta'}\mathbf{e}_\theta + \frac{1}{r'\sin\theta'}\frac{\partial q'}{\partial \varphi'}\mathbf{e}_\varphi.$$

and we have

$$\begin{aligned} \frac{\partial q'}{\partial r'} &= \frac{\partial q}{\partial r} - \epsilon\frac{\partial q}{\partial r}\chi'\lambda \\ &= \frac{\partial q}{\partial r} + O\left(\epsilon\right) \end{aligned}$$

$$\begin{aligned} \frac{\partial q'}{\partial \omega_i'} &= \frac{\partial q}{\partial \omega_i} + \epsilon\frac{\partial q'}{\partial r'}\frac{\chi\lambda_{\omega_i}}{1 - \chi'\lambda} \\ &= \frac{\partial q}{\partial \omega_i} + O\left(\epsilon\right) \end{aligned}$$

$$\frac{1}{r} = \frac{1}{r' + \epsilon\lambda\chi} = \frac{1}{r'}\left[1 - \epsilon\frac{\lambda}{r'}\chi\left(1 - r'\right) + O\left(\epsilon^2\right)\right]$$

let us note that when r' is close to cero, $\chi\left(1 - r'\right) = 0$. Hence

$$\nabla_{(r',\omega')} q' = \nabla_{(r,\omega)} q + O\left(\epsilon\right)$$

analogously if we use now (4.17) and (4.18) and the chain rule for second order derivatives

$$\Delta_{(r',\omega')} q' = \Delta_{(r,\omega)} q + O\left(\epsilon\right)$$

see [27] for details.

Let us note that if $q = O(\epsilon)$

$$\nabla_{(r',\omega')} q' = \nabla_{(r,\omega)} q + O\left(\epsilon^2\right)$$
$$\Delta_{(r',\omega')} q' = \Delta_{(r,\omega)} q + O\left(\epsilon^2\right)$$

because the terms coming from the transformation involves q and q' (and bounded derivatives of χ).

We want to reduce (4.9), (4.10) to equivalent equations defined inside the sphere. Let us begin assuming that for $p, \mathbf{v} : \Omega(t) \longrightarrow \mathbb{R}$

$$p = p_0 + \epsilon p_1 + O\left(\epsilon^2\right) \tag{4.19}$$
$$v_r = v_{r0} + \epsilon v_{r1} + O\left(\epsilon^2\right) \tag{4.20}$$
$$v_{\omega_i} = v_{\omega_i,0} + \epsilon v_{\omega_i,1} + O\left(\epsilon^2\right) \tag{4.21}$$

$$\mathbf{v} = (v_r, v_\theta, v_\varphi)$$
$$\mathbf{v}_0 = (v_{r0}, v_{\theta 0}, v_{\varphi 0})$$
$$\mathbf{v}_1 = (v_{r1}, v_{\theta 1}, v_{\varphi 1})$$

etc., and the respective prime functions for the compositions with the transformation $p', \mathbf{v}' : B(\mathbf{0}, 1) \longrightarrow \mathbb{R}$

The normal vector exterior to the boundary can be approximated by (see [27])

$$\mathbf{n} = \mathbf{e}_r + O(\epsilon)$$

From now until we found an equation for the perturbation, we will use t as a parameter only, because the following equations does not involve time derivatives.

By [[31], Theorem 8.1] if $||x||_{C^2} \leq \epsilon$ with ϵ small, it is possible to linearize the mean curvature

$$\mathcal{H}(1 + \epsilon\lambda(\theta, \varphi, t)) = 1 - \epsilon\left(\lambda + \frac{1}{2}\Delta_\omega \lambda\right) + \tilde{x}, \quad ||\tilde{x}||_{C^1} \leq const\left(||x||_{C^2}\right)^2$$

Δ_ω is the Laplace operator on the surface of the unit sphere

$$\Delta_\omega = \frac{1}{\sin\theta}\frac{\partial}{\partial\theta}\left(\sin\theta\frac{\partial}{\partial\theta}\right) + \frac{1}{\sin^2\theta}\frac{\partial^2}{\partial\varphi^2}$$

Therefore the homogeneous problem (i.e. $\mathbf{F} = 0$) in the new variables becomes

$$\begin{aligned}
-\nabla p' + \Delta \mathbf{v}' &= O(\epsilon) \text{ in } B(\mathbf{0}, 1) \\
\nabla \cdot \mathbf{v}' &= O(\epsilon) \text{ in } B(\mathbf{0}, 1) \\
\mathbf{e}_r \mathbf{T}' \mathbf{e}_r &= -\gamma\left(1 - \epsilon\left(\lambda + \frac{1}{2}\Delta_\omega\lambda\right)\right) + O\left(\epsilon^2\right) \text{ at } r' = 1 \\
\mathbf{e}_\theta \mathbf{T}' \mathbf{e}_r &= \mathbf{e}_\varphi \mathbf{T}' \mathbf{e}_r = 0 \text{ at } r' = 1
\end{aligned}$$

$\mathbf{T}'$ the stress tensor in spherical variables and spherical base $\{\mathbf{e}_r, \mathbf{e}_\theta, \mathbf{e}_\varphi\}$ can be found in [46]. At $0th$ order we have

$$\begin{aligned} -\nabla p'_0 + \Delta \mathbf{v}'_0 &= 0 \text{ in } B(\mathbf{0}, 1) \\ \nabla \cdot \mathbf{v}'_0 &= 0 \text{ in } B(\mathbf{0}, 1) \\ \mathbf{e}_r \mathbf{T}'_0 \mathbf{e}_r &= -\gamma \text{ at } r' = 1 \\ \mathbf{e}_\theta \mathbf{T}'_0 \mathbf{e}_r &= \mathbf{e}_\varphi \mathbf{T}'_0 \mathbf{e}_r = 0 \text{ at } r' = 1 \end{aligned}$$

$$\mathbf{T}'_0 \mathbf{e}_r = \left(-p'_0 \delta_{ij} + 2 \frac{\partial v'_{r0}}{\partial r} \right) \mathbf{e}_r$$

In this case, the drop is moved by constant surface tension, its movement is constant then the displacement is constant, implying

$$\begin{aligned} \mathbf{v}'_0 &= 0 \\ p'_0 &= \gamma \end{aligned}$$

For the next order we have:

$$\begin{aligned} -\nabla \epsilon p'_1 + \Delta \epsilon \mathbf{v}'_1 &= O\left(\epsilon^2\right) \text{ in } B(\mathbf{0}, 1) \\ \nabla \cdot \epsilon \mathbf{v}'_1 &= O\left(\epsilon^2\right) \text{ in } B(\mathbf{0}, 1) \\ \mathbf{e}_r \mathbf{T}'_1 \mathbf{e}_r &= \epsilon\gamma \left(\lambda + \frac{1}{2} \Delta_\omega \lambda \right) \text{ at } r' = 1 \\ \mathbf{e}_\theta \mathbf{T}'_1 \mathbf{e}_r &= \mathbf{e}_\varphi \mathbf{T}'_1 \mathbf{e}_r = 0 \text{ at } r' = 1 \end{aligned}$$

where

$$\mathbf{e}_r \mathbf{T}'_1 \mathbf{e}_r = \epsilon \left(-p'_1 \delta_{ij} + 2 \frac{\partial v'_{r1}}{\partial r} \right)$$

the terms coming from the change of variables are $O(\epsilon^2)$ because of the $0th$ order results (assuming now a displacement by the constant γ in the pressure for simplifying calculations) and the functions involved in this approximation. Then we can cancell the ϵ to find the $1st$ order approximation. We will drop off the prime and subscripts in the functions and variables. Then we have to find simplified expressions for p and $\mathbf{v}$ (coming from p'_1 and $\mathbf{v}'_1$ respectively).

We have now the homogeneous version of (4.9), (4.10) to be solved inside the sphere

$$-\nabla p + \Delta \mathbf{v} = 0 \text{ in } B(\mathbf{0}, 1) \tag{4.22}$$

$$\nabla \cdot \mathbf{v} = 0 \text{ in } B(\mathbf{0}, 1) \tag{4.23}$$

with the linearized boundary conditions

$$-p + 2 \frac{\partial v_r}{\partial r} = \gamma \left(\lambda + \frac{1}{2} \Delta_\omega \lambda \right) \text{ at } r = 1 \tag{4.24}$$

$$\mathbf{e}_\theta T_{ij} \mathbf{e}_r = \mathbf{e}_\varphi T_{ij} \mathbf{e}_r = 0 \text{ at } r = 1 \tag{4.25}$$

The left hand side of (4.24) comes from the stress tensor in spherical variables and its right hand side from the linearized mean curvature.

Taking the divergence in (4.22) and using (4.23), this last equation (4.23) is equivalent to the system

$$\begin{aligned} \Delta p = 0 \text{ in } B(\mathbf{0},1) \\ \nabla \cdot \mathbf{v} = 0 \text{ on } \partial B(\mathbf{0},1) \end{aligned}$$

We have to solve then

$$\begin{aligned} -\nabla p + \Delta \mathbf{v} = 0 \text{ in } B(\mathbf{0},1) \\ \Delta p = 0 \text{ in } B(\mathbf{0},1) \\ \nabla \cdot \mathbf{v} = 0 \text{ at } r = 1 \\ \mathbf{e}_r \mathbf{T}\mathbf{e}_r = \gamma \left(\lambda + \frac{1}{2} \Delta_\omega \lambda \right) \text{ at } r = 1 \\ \mathbf{e}_\theta \mathbf{T}\mathbf{e}_r = \mathbf{e}_\varphi \mathbf{T}\mathbf{e}_r = 0 \text{ at } r = 1 \end{aligned}$$

Finally, we need to impose a kinematic equation for the motion of the interface. This is given by the equation

$$\mathbf{r}_t \cdot \mathbf{n} = \mathbf{v} \cdot \mathbf{n} \text{ at } \partial\Omega(t)$$

expressing the fact that the surface of the drop moves in the direction of its normal following the normal component of the velocity field. Its linearized version is

$$\lambda_t = v_r \tag{4.26}$$

In order to compute the linearized evolution of the drop's surface, we have to solve equation (4.22) added with the components of a suitable $\mathbf{F}_e$ related to (4.8), and equation (4.23), both inside the sphere with boundary conditions (4.24), (4.25). Then, by inserting the component v_r of the velocity, in terms of the perturbation λ, into (4.26) we obtain a linear evolution problem with solutions that may grow or decrease exponentially fast. If the solutions decay exponentially fast for any initial data, the drop's spherical shape will be stable. The drop will be unstable otherwise. The solution to the general system with $\mathbf{F}_e \neq 0$ will be the sum of the solution to the homogeneous problem (i.e. with $\mathbf{F}_e = 0$) with nonhomogeneous boundary conditions plus the solution to the nonhomogeneous problem with homogeneous boundary conditions.

In order to solve the linearized Stokes problem in the unit disk, the most suitable base is formed by vector spherical harmonics (see [1] for the definition of spherical harmonics and [41] for the properties of scalar and vector spherical harmonics):

$$p = \sum p_{lm}(r) Y_{lm}(\omega) \tag{4.27}$$

$$\mathbf{v} = \sum \alpha_{lm}(r) \overrightarrow{V}_{lm}(\omega) + \beta_{lm}(r) \overrightarrow{X}_{lm}(\omega) + \gamma_{lm}(r) \overrightarrow{W}_{lm}(\omega) \tag{4.28}$$

The spherical harmonics

$$Y_{lm}(\omega) \equiv \Theta_l^m(\theta) \frac{e^{im\varphi}}{(2\pi)^{1/2}}$$

where

$$\Theta_l^m(\theta) = (-1)^m \left[\frac{2l+1}{2}\frac{(l-m)!}{(l+m)!}\right]^{1/2} P_l^m(\cos\theta)$$

and

$$P_l^m(z) = \frac{1}{2^l l!}\left(1-z^2\right)^{m/2}\frac{d^{l+m}}{dz^{l+m}}\left(z^2-1\right)^l$$

Introducing the vector spherical harmonics [41]

$$\overrightarrow{V}_{lm}(\omega) \equiv \mathbf{e}_r\left\{-\left(\frac{l+1}{2l+1}\right)^{1/2} Y_{lm}\right\} + \mathbf{e}_\theta\left\{\frac{1}{[(l+1)(2l+1)]^{1/2}}\frac{\partial Y_{lm}}{\partial\theta}\right\} + \mathbf{e}_\varphi\left\{\frac{imY_{lm}}{[(l+1)(2l+1)]^{1/2}\sin\theta}\right\}$$

$$\overrightarrow{X}_{lm}(\omega) \equiv \mathbf{e}_\theta\left\{\frac{-mY_{lm}}{[l(l+1)]^{1/2}\sin\theta}\right\} + \mathbf{e}_\varphi\left\{\frac{-i}{[l(l+1)]^{1/2}}\frac{\partial Y_{lm}}{\partial\theta}\right\}$$

$$\overrightarrow{W}_{lm}(\omega) \equiv \mathbf{e}_r\left\{\left(\frac{l}{2l+1}\right)^{1/2} Y_{lm}\right\} + \mathbf{e}_\theta\left\{\frac{1}{[l(2l+1)]^{1/2}}\frac{\partial Y_{lm}}{\partial\theta}\right\} + \mathbf{e}_\varphi\left\{\frac{imY_{lm}}{[l(2l+1)]^{1/2}\sin\theta}\right\}$$

In terms of spherical harmonics and vector spherical harmonics:

$$\begin{aligned}\nabla p &= \sum \nabla\left(p_{lm}(r)Y_{lm}(\omega)\right)\\ &= \sum p_{lm}(r)\nabla Y_{lm}(\omega) + Y_{lm}(\omega)\nabla p_{lm}(r)\end{aligned}$$

using that

$$\nabla Y_{lm} = \frac{l}{r}\left(\frac{l+1}{2l+1}\right)^{1/2}\overrightarrow{V}_{lm}(\omega) + \frac{l+1}{r}\left(\frac{l}{2l+1}\right)^{1/2}\overrightarrow{W}_{lm}(\omega)$$

$$\nabla p_{lm}(r) = \frac{dp_{lm}}{dr}\mathbf{e}_r$$

and

$$\mathbf{e}_r Y_{lm} = -\left(\frac{l+1}{2l+1}\right)^{1/2}\overrightarrow{V}_{lm}(\omega) + \left(\frac{l}{2l+1}\right)^{1/2}\overrightarrow{W}_{lm}(\omega)$$

we obtain

$$\begin{aligned}\nabla p = \sum\Bigg[&p_{lm}(r)\left(\frac{l}{r}\left(\frac{l+1}{2l+1}\right)^{1/2}\overrightarrow{V}_{lm}(\omega) + \frac{l+1}{r}\left(\frac{l}{2l+1}\right)^{1/2}\overrightarrow{W}_{lm}(\omega)\right) +\\ &+\left(-\left(\frac{l+1}{2l+1}\right)^{1/2}\overrightarrow{V}_{lm}(\omega) + \left(\frac{l}{2l+1}\right)^{1/2}\overrightarrow{W}_{lm}(\omega)\frac{dp_{lm}}{dr}\right)\Bigg]\\ = \sum\Bigg[&\left(\frac{l+1}{2l+1}\right)^{1/2}\left(-\frac{d}{dr}p_{lm} + \frac{l}{r}p_{lm}\right)\overrightarrow{V}_{lm} +\\ &+\left(\frac{l}{2l+1}\right)^{1/2}\left(\frac{d}{dr}p_{lm} + \frac{l+1}{r}p_{lm}\right)\overrightarrow{W}_{lm}\Bigg]\end{aligned}$$

Let us note that if we use

$$\mathbf{e}_r \overrightarrow{V}_{lm} = -\left(\frac{l+1}{2l+1}\right)^{1/2} Y_{lm}$$

$$\mathbf{e}_r \overrightarrow{W}_{lm} \equiv \left(\frac{l}{2l+1}\right)^{1/2} Y_{lm}$$

we have

$$\begin{aligned}
\nabla p_{lm} \cdot \nabla Y_{lm} &= \frac{dp_{lm}}{dr}(r)\,\mathbf{e}_r \left[\frac{l}{r}\left(\frac{l+1}{2l+1}\right)^{1/2} \overrightarrow{V}_{lm}(\omega) + \frac{l+1}{r}\left(\frac{l}{2l+1}\right)^{1/2} \overrightarrow{W}_{lm}(\omega)\right] \\
&= \frac{dp_{lm}}{dr}(r)\,\frac{l}{r}\left(\frac{l+1}{2l+1}\right)^{1/2}\left(-\left(\frac{l+1}{2l+1}\right)^{1/2} Y_{lm}\right) + \\
&+ \frac{dp_{lm}}{dr}(r)\,\frac{l+1}{r}\left(\frac{l}{2l+1}\right)^{1/2}\left(\frac{l}{2l+1}\right)^{1/2} Y_{lm} \\
&= \left(-\frac{l}{r}\left(\frac{l+1}{2l+1}\right)\frac{dp_{lm}}{dr}(r) + \frac{l}{r}\left(\frac{l+1}{2l+1}\right)\frac{dp_{lm}}{dr}(r)\right) Y_{lm} = 0
\end{aligned}$$

and this implies

$$\begin{aligned}
\Delta p &= \sum \Delta\left(p_{lm}(r)\, Y_{lm}(\omega)\right) \\
&= \sum p_{lm}(r)\, \Delta Y_{lm}(\omega) + \sum Y_{lm}(\omega)\, \Delta p_{lm}(r) \\
&= \sum p_{lm}(r)\left(-\frac{l(l+1)}{r^2} Y_{lm}\right) + \sum\left(\frac{d^2 p_{lm}}{dr^2} + \frac{2}{r}\frac{dp_{lm}}{dr}\right) Y_{lm}(\omega) \\
&= \sum\left(\frac{d^2 p_{lm}}{dr^2} + \frac{2}{r}\frac{dp_{lm}}{dr} - \frac{l(l+1)}{r^2} p_{lm}\right) Y_{lm}(\omega)
\end{aligned}$$

By denoting

$$L_l = \frac{d^2}{dr^2} + \frac{2}{r}\frac{d}{dr} - \frac{l(l+1)}{r^2}$$

and using that [41] for an arbitrary radial function $R(r)$

$$\begin{aligned}
\Delta\left[R(r)\,\overrightarrow{V}_{lm}\right] &= L_{l+1}(R)\,\overrightarrow{V}_{lm} \\
\Delta\left[R(r)\,\overrightarrow{X}_{lm}\right] &= L_l(R)\,\overrightarrow{X}_{lm} \\
\Delta\left[R(r)\,\overrightarrow{W}_{lm}\right] &= L_{l-1}(R)\,\overrightarrow{W}_{lm}
\end{aligned}$$

$$\begin{aligned}
\Delta\mathbf{v} &= \sum\left[\Delta\left(\alpha_{lm}(r)\overrightarrow{V}_{lm}(\omega)\right) + \Delta\left(\beta_{lm}(r)\overrightarrow{X}_{lm}(\omega)\right) + \Delta\left(\gamma_{lm}(r)\overrightarrow{W}_{lm}(\omega)\right)\right] \\
&= \sum\left[L_{l+1}\left(\alpha_{lm}(r)\right)\overrightarrow{V}_{lm} + L_l\left(\beta_{lm}(r)\right)\overrightarrow{X}_{lm} + L_{l-1}\left(\gamma_{lm}(r)\right)\overrightarrow{W}_{lm}\right]
\end{aligned}$$

Using also

$$\nabla \cdot \left[R(r) \overrightarrow{V}_{lm} \right] = - \left(\frac{l+1}{2l+1} \right)^{1/2} \left[\frac{dR}{dr} + \frac{l+2}{r} R \right] Y_{lm}$$
$$\nabla \cdot \left[R(r) \overrightarrow{W}_{lm} \right] = \left(\frac{l}{2l+1} \right)^{1/2} \left[\frac{dR}{dr} - \frac{l-1}{r} R \right] Y_{lm}$$
$$\nabla \cdot \left[R(r) \overrightarrow{X}_{lm} \right] = 0$$

we have

$$\begin{aligned} \nabla \cdot \mathbf{v} &= \nabla \cdot \left[\alpha_{lm}(r) \overrightarrow{V}_{lm}(\omega) + \beta_{lm}(r) \overrightarrow{X}_{lm}(\omega) + \gamma_{lm}(r) \overrightarrow{W}_{lm}(\omega) \right] \\ &= \left\{ - \left(\frac{l+1}{2l+1} \right)^{1/2} \left(\frac{d\alpha_{lm}}{dr} + \frac{l+2}{r} \alpha_{lm} \right) + \left(\frac{l}{2l+1} \right)^{1/2} \left(\frac{d\gamma_{lm}}{dr} - \frac{l-1}{r} \gamma_{lm} \right) \right\} Y_{lm} \\ &= 0 \end{aligned}$$

then the Stokes system with the force term for (4.27) and (4.28) becomes

$$L_l p_{lm} = F_{lm,0} \tag{4.29}$$
$$L_{l+1} \alpha_{lm} - \left(\frac{l+1}{2l+1} \right)^{\frac{1}{2}} \left(-\frac{dp_{lm}}{dr} + \frac{l}{r} p_{lm} \right) = F_{lm,1} \tag{4.30}$$
$$L_l \beta_{lm} = F_{lm,2} \tag{4.31}$$
$$L_{l-1} \gamma_{lm} - \left(\frac{l}{2l+1} \right)^{\frac{1}{2}} \left(\frac{dp_{lm}}{dr} + \frac{l+1}{r} p_{lm} \right) = F_{lm,3} \tag{4.32}$$

with the equation

$$- \left(\frac{l+1}{2l+1} \right)^{\frac{1}{2}} \left(\frac{d\alpha_{lm}}{dr} + \frac{l+2}{r} \alpha_{lm} \right) + \left(\frac{l}{2l+1} \right)^{\frac{1}{2}} \left(\frac{d\gamma_{lm}}{dr} - \frac{l-1}{r} \gamma_{lm} \right) = 0$$

as a boundary condition.

Let us remember the linearized boundary conditions

$$-p + 2 \frac{\partial v_r}{\partial r} = \gamma \left(\lambda + \frac{1}{2} \Delta_\omega \lambda \right) \text{ at } r = 1$$
$$\mathbf{e}_\theta T_{ij} \mathbf{e}_r = \mathbf{e}_\varphi T_{ij} \mathbf{e}_r = 0 \text{ at } r = 1$$

If we have

$$\lambda(\omega, t) = \sum \lambda_{lm}(t) Y_{lm}(\omega)$$

$$\Delta_\omega \lambda = \sum \lambda_{lm}(t) \Delta_\omega (Y_{lm}(\omega)) = \sum \lambda_{lm}(t) (-l(l+1) Y_{lm}(\omega))$$

then

$$\lambda+\frac{1}{2}\Delta_{\omega}\lambda=\sum\lambda_{lm}\left(t\right)Y_{lm}\left(\omega\right)+\frac{1}{2}\sum\lambda_{lm}\left(t\right)\left(-l\left(l+1\right)Y_{lm}\left(\omega\right)\right)$$
$$=\sum\lambda_{lm}\left(t\right)\left(1-\frac{l\left(l+1\right)}{2}\right)Y_{lm}\left(\omega\right)$$

$$\gamma\left(\lambda+\frac{1}{2}\Delta_{\omega}\lambda\right)\mathbf{e}_{r}=\sum\lambda_{lm}\left(t\right)\left(1-\frac{l\left(l+1\right)}{2}\right)Y_{lm}\left(\omega\right)\mathbf{e}_{r}$$

Using

$$Y_{lm}\left(\omega\right)\mathbf{e}_{r}=-\left(\frac{l+1}{2l+1}\right)^{\frac{1}{2}}\overrightarrow{V}_{lm}+\left(\frac{l}{2l+1}\right)^{\frac{1}{2}}\overrightarrow{W}_{lm}$$

and some calculations from [32] , we can obtain

$$\left[\frac{3l+2}{2l+1}\frac{d\alpha_{lm}}{dr}-\frac{l(l+2)}{2l+1}\alpha_{lm}\right]-\frac{l^{\frac{1}{2}}(l+1)^{\frac{1}{2}}}{2l+1}\left[\frac{d\gamma_{lm}}{dr}-(l-1)\gamma_{lm}\right]$$

$$+\left(\frac{l+1}{2l+1}\right)^{\frac{1}{2}}p_{lm}+\gamma\left(\frac{l+1}{2l+1}\right)^{\frac{1}{2}}\left(1-\frac{l(l+1)}{2}\right)\lambda_{lm}=0 \tag{4.33}$$

$$\frac{d\beta_{lm}}{dr}-\beta_{lm}=0 \tag{4.34}$$

$$-\frac{l^{\frac{1}{2}}(l+1)^{\frac{1}{2}}}{2l+1}\left[\frac{d\alpha_{lm}}{dr}+(l+2)\alpha_{lm}\right]+\left[\frac{3l+1}{2l+1}\frac{d\gamma_{lm}}{dr}+\frac{(l-1)(l+1)}{2l+1}\gamma_{lm}\right]$$
$$-\left(\frac{l}{2l+1}\right)^{\frac{1}{2}}p_{lm}-\gamma\left(\frac{l}{2l+1}\right)^{\frac{1}{2}}\left(1-\frac{l(l+1)}{2}\right)\lambda_{lm}=0 \tag{4.35}$$

with the added condition mentioned above that comes from $\nabla\cdot\mathbf{u}=0$ on $\partial B\left(0,1\right)$.

$$-\left(\frac{l+1}{2l+1}\right)^{\frac{1}{2}}\left(\frac{d\alpha_{lm}}{dr}+\left(l+2\right)\alpha_{lm}\right)+\left(\frac{l}{2l+1}\right)^{\frac{1}{2}}\left(\frac{d\gamma_{lm}}{dr}-\left(l-1\right)\gamma_{lm}\right)=0 \tag{4.36}$$

The solution to the homogeneous problem (4.29)-(4.32) is

$$p_{lm}=P_{1}r^{l} \tag{4.37}$$
$$\alpha_{lm}=A_{1}r^{l+1} \tag{4.38}$$
$$\beta_{lm}=B_{1}r^{l} \tag{4.39}$$
$$\gamma_{lm}=C_{1}r^{l-1}+\frac{1}{2}\left(\frac{l}{2l+1}\right)^{\frac{1}{2}}P_{1}r^{l+1} \tag{4.40}$$

Substituting (4.37)-(4.40) into the boundary conditions (4.33)-(4.36) we get a linear system of equations for A_j, B_j, C_j, P_j:

$$
\begin{aligned}
-\left(\frac{l+1}{2l+1}\right)^{1/2}(2l+3)\,A_1+\left(\frac{l}{2l+1}\right)P_1&=0\\
\left(\frac{2l^2+3l+2}{2l+1}\right)A_1+\left(\frac{l+1}{2l+1}\right)^{3/2}P_1+S&=0\\
(l-1)\,B_1&=0\\
-\frac{l^{1/2}\,(l+1)^{1/2}\,(2l+3)}{2l+1}A_1+(2l-1)\,C_1+\frac{l^{1/2}\,(2l^2-1)}{(2l+1)^{3/2}}P_1-\frac{l^{1/2}}{(l+1)^{1/2}}S&=0
\end{aligned}
$$

with solutions

$$
\begin{aligned}
A_1&=-S\frac{l}{4l+2l^2+3}\\
B_1&=0\\
P_1&=-\frac{4l^2+8l+3}{2l^2+4l+3}\sqrt{\frac{l+1}{2l+1}}S\\
C_1&=\frac{1}{2}\frac{l\,(2l+1)\,(l+2)}{(l-1)\,(2l^2+4l+3)}\sqrt{\frac{l}{l+1}}S
\end{aligned}
$$

where

$$
S=\gamma\left(\frac{l+1}{2l+1}\right)^{\frac{1}{2}}\left(1-\frac{l(l+1)}{2}\right)\lambda_{lm}
$$

The radial velocity is then given in this case by

$$
\begin{aligned}
\overrightarrow{v}\cdot\overrightarrow{e_r}&=\sum\alpha_{lm}(1)\overrightarrow{V}_{lm}\cdot\overrightarrow{e_r}+\gamma_{lm}(1)\overrightarrow{W}_{lm}\cdot\overrightarrow{e_r}\\
&=\sum\left[-\left(\frac{l+1}{2l+1}\right)^{\frac{1}{2}}\alpha_{lm}(1)+\left(\frac{l}{2l+1}\right)^{\frac{1}{2}}\gamma_{lm}(1)\right]Y_{lm}\\
&=\gamma\sum\frac{1}{2}\frac{l\,(2l+1)}{(l-1)\,(2l^2+4l+3)}\left(1-\frac{l(l+1)}{2}\right)\lambda_{lm}Y_{lm}
\end{aligned}
\tag{4.41}
$$

The solution to the nonhomogeneous problem requires the calculation of $\mathbf{F}$ and its linearization.

4.2.1 Computation of the Potential, linearized Maxwell stress tensor and its divergence

The solution to (4.5), (4.6), (4.7) when Ω is a ball of center in 0 and radius 1is

$$
\begin{aligned}
V&=V_c+\frac{Q}{4\pi}\nu_{00}V_0(r),\ r<1\\
V&=\frac{Q}{4\pi}\frac{1}{r},\ r>1
\end{aligned}
$$

If we use the change of variables

$$x = \kappa r$$
$$y = \sqrt{r} V_0 (r)$$

they satisfies the modified Bessel differential equation

$$x^2 y'' + xy' - \left(x^2 + \frac{1}{4} \right) y = 0$$

Therefore

$$V_0(r) = \frac{I_{\frac{1}{2}}(\kappa r)}{r^{\frac{1}{2}}} = \sqrt{\frac{2}{\pi}} \frac{\sinh(\kappa r)}{\kappa^{\frac{1}{2}} r},$$

Continuity of V and its derivative at $r = 1$ yields the conditions

$$V_c + \nu_{00} \frac{Q}{4\pi} \sqrt{\frac{2}{\pi}} \frac{\sinh(\kappa)}{\kappa^{\frac{1}{2}}} = \frac{Q}{4\pi}$$
$$\sqrt{\frac{2}{\pi}} \frac{\sinh \kappa - \kappa \cosh \kappa}{\kappa^{\frac{1}{2}}} \nu_{00} = 1$$

from where it follows

$$V_c = -\frac{Q}{4\pi} \frac{\kappa \cosh \kappa}{\sinh \kappa - \kappa \cosh \kappa}$$
$$\nu_{00} = \sqrt{\frac{\pi}{2}} \frac{\kappa^{\frac{1}{2}}}{\sinh \kappa - \kappa \cosh \kappa}$$

We perturb now the sphere $r = r' + \epsilon \lambda (\theta', \varphi', t)$, for $(r', \theta', \varphi') \in \Omega$ or $(r', \theta', \varphi') \in \bar{\Omega}^c$ and using the regularity of the potential we can write

$$V(r) = V_c + \nu_{00} \frac{Q}{4\pi} V_0(r') + \epsilon \frac{Q}{4\pi} \sum_{l,m} \nu_{lm} g_{lm}(r') Y_{lm}(\theta', \varphi'),\ r' < 1$$
$$V(r) = \frac{Q}{4\pi} \frac{1}{r'} + \epsilon \frac{Q}{4\pi} \sum_{l,m} \frac{\mu_{lm}}{r'^{(l+1)}} Y_{lm}(\theta', \varphi'),\ r' > 1$$

where ν_{lm} and μ_{lm} have t as a parameter, and now

$$g_{lm}(r') = \frac{I_{l+\frac{1}{2}}(\kappa r')}{r'^{\frac{1}{2}}}$$

For simplicity we will drop the primes. Continuity of the potential and its derivative at the boundary, yield, at leading order

$$-\lambda_{lm} + \mu_{lm} = \nu_{00} V_0'(1) \lambda_{lm} + \nu_{lm} g_{lm}(1) \tag{4.42}$$
$$2\lambda_{lm} - (l+1)\mu_{lm} = \nu_{00} V_0''(1) \lambda_{lm} + \nu_{lm} g_{lm}'(1) \tag{4.43}$$

from where ν_{lm} follows as a linear function of λ_{lm}.

$$\mu_{lm} = \frac{2g_{lm} + g'_{lm} - \nu_{00}V_0''g_{lm} + \nu_{00}V_0'g'_{lm}}{g_{lm} + g'_{lm} + lg_{lm}}\lambda_{lm}$$

$$\nu_{lm} = -\frac{-1 + l + ((l+1)V_0' + V_0'')\,\nu_{00}}{g_{lm} + g'_{lm} + lg_{lm}}\lambda_{lm}.$$

In the case $l = 2$, which, analogously to [27] we expect to be the first one (as charge increases) to become unstabe, one has

$$\mu_{2m} = -\frac{(\sinh\kappa)\,(\kappa^2\sinh\kappa + 3\sinh\kappa - 3\kappa\cosh\kappa)}{\kappa\sinh(2\kappa) - \kappa^2\cosh^2\kappa - \sinh^2\kappa}\lambda_{lm} \tag{4.44}$$

$$\nu_{2m} = -\sqrt{\frac{\pi}{2}}\frac{\kappa^{\frac{5}{2}}\sinh\kappa}{\kappa\sinh(2\kappa) - \kappa^2\cosh^2\kappa - \sinh^2\kappa}\lambda_{lm}. \tag{4.45}$$

Let us remember that by Debye-Hückel approximation

$$\rho\mathbf{E} = \kappa^2\widetilde{V}\nabla\widetilde{V} = \frac{\kappa^2}{2}\nabla\widetilde{V}^2.$$

Then we can define a reduced pressure Π

$$\Pi = p - \frac{\kappa^2}{2}\widetilde{V}^2$$

so that equation (4.9) transforms into

$$-\nabla\Pi + \Delta\mathbf{v} = 0$$

At $\partial\Omega$, and at linear order in the perturbation, we have

$$\Pi = p - \kappa^2\left(\frac{Q}{4\pi}\right)^2\left(\frac{\nu_{00}^2V_0^2(1)}{2} + \nu_{00}V_0(1)\sum_{l,m}\left(\nu_{00}V_0'(1)\lambda_{lm} + \epsilon\nu_{lm}g_{lm}(1)\right)Y_{lm}(\theta,\varphi)\right) + O(\lambda^2)$$

4.2.2 Solution of the linear system

By expanding Π in spherical harmonics as in (4.27) with coefficients $\Pi_{lm}(r)$ and the velocity as in (4.28), we obtain $\beta_{lm} = 0$ and the linear system for $(\alpha_{lm}, \gamma_{lm}, \Pi_{lm})$:

$$L_{l+1}\alpha_{lm} - \left(\frac{l+1}{2l+1}\right)^{\frac{1}{2}}\left(-\frac{d\Pi_{lm}}{dr} + \frac{l}{r}\Pi_{lm}\right) = 0 \tag{4.46}$$

$$L_{l-1}\gamma_{lm} - \left(\frac{l}{2l+1}\right)^{\frac{1}{2}}\left(\frac{d\Pi_{lm}}{dr} + \frac{l+1}{r}\Pi_{lm}\right) = 0 \tag{4.47}$$

$$-\left(\frac{l+1}{2l+1}\right)^{\frac{1}{2}}\left(\frac{d\alpha_{lm}}{dr} + \frac{l+2}{r}\alpha_{lm}\right) + \left(\frac{l}{2l+1}\right)^{\frac{1}{2}}\left(\frac{d\gamma_{lm}}{dr} - \frac{l-1}{r}\gamma_{lm}\right) = 0 \tag{4.48}$$

together with the following boundary conditions (at $r = 1$):

$$-\left(\frac{l+1}{2l+1}\right)^{\frac{1}{2}}\left(\frac{d\alpha_{lm}}{dr}+(l+2)\alpha_{lm}\right)+\left(\frac{l}{2l+1}\right)^{\frac{1}{2}}\left(\frac{d\gamma_{lm}}{dr}-(l-1)\gamma_{lm}\right)=0 \tag{4.49}$$

$$\begin{aligned}&\left[\frac{3l+2}{2l+1}\frac{d\alpha_{lm}}{dr}-\frac{l(l+2)}{2l+1}\alpha_{lm}\right]-\frac{l^{\frac{1}{2}}(l+1)^{\frac{1}{2}}}{2l+1}\left[\frac{d\gamma_{lm}}{dr}-(l-1)\gamma_{lm}\right]+\left(\frac{l+1}{2l+1}\right)^{\frac{1}{2}}\Pi_{lm}\\&=-\left(\frac{l+1}{2l+1}\right)^{\frac{1}{2}}\left(\nu_{00}V_0(1)\left(\nu_{00}V_0'(1)\lambda_{lm}+\nu_{lm}g_{lm}(1)\right)\right)\end{aligned} \tag{4.50}$$

$$\begin{aligned}&-\frac{l^{\frac{1}{2}}(l+1)^{\frac{1}{2}}}{2l+1}\left[\frac{d\alpha_{lm}}{dr}+(l+2)\alpha_{lm}\right]+\left[\frac{3l+1}{2l+1}\frac{d\gamma_{lm}}{dr}+\frac{(l-1)(l+1)}{2l+1}\gamma_{lm}\right]-\left(\frac{l}{2l+1}\right)^{\frac{1}{2}}\Pi_{lm}\\&=\left(\frac{l}{2l+1}\right)^{\frac{1}{2}}\left(\nu_{00}V_0(1)\left(\nu_{00}V_0'(1)\lambda_{lm}+\nu_{lm}g_{lm}(1)\right)\right)\end{aligned} \tag{4.51}$$

From the solution of the linear system (4.46)-(4.48) with boundary conditions (4.49)-(4.51), we find $\alpha_{lm}(1)$ and $\gamma_{lm}(1)$ and hence

$$\begin{aligned}\overrightarrow{v}\cdot\overrightarrow{e_r}&=\sum\alpha_{lm}(1)\overrightarrow{V}_{lm}\cdot\overrightarrow{e_r}+\gamma_{lm}(1)\overrightarrow{W}_{lm}\cdot\overrightarrow{e_r}\\&=\sum\left[-\left(\frac{l+1}{2l+1}\right)^{\frac{1}{2}}\alpha_{lm}(1)+\left(\frac{l}{2l+1}\right)^{\frac{1}{2}}\gamma_{lm}(1)\right]Y_{lm}\end{aligned} \tag{4.52}$$

The $l = 2$ mode for the radial velocity is, using (4.52), identity (4.42) and (4.44):

$$\frac{5}{19}\left(\frac{Q}{4\pi}\right)^2\kappa^2\frac{\kappa\sinh 2\kappa-2\cosh 2\kappa+2\kappa^2+2}{\cosh 2\kappa+\kappa^2\cosh 2\kappa-2\kappa\sinh 2\kappa+\kappa^2-1}\frac{\sinh(\kappa)}{\kappa\cosh\kappa-\sinh\kappa}\lambda_{2m}Y_{2m}=:AY_{2m}$$

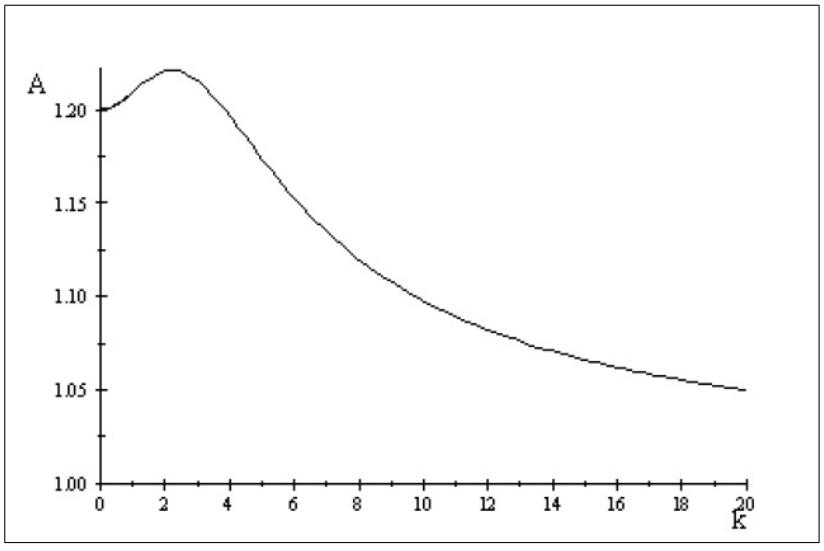

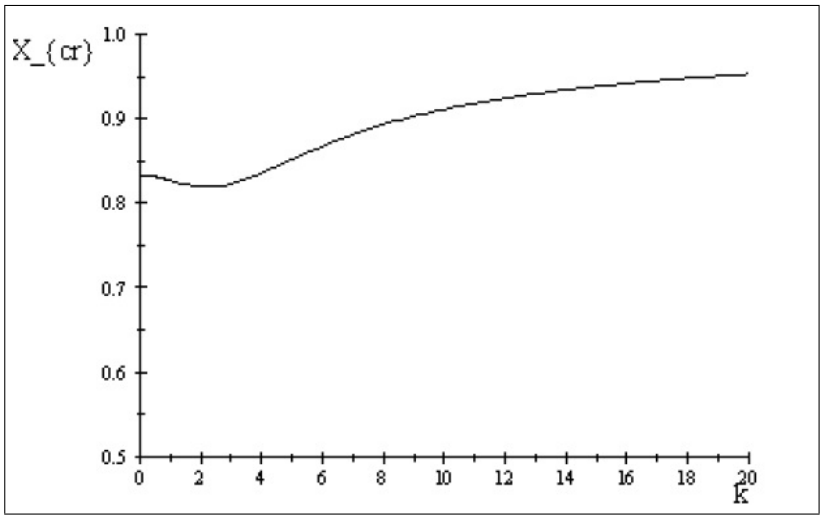

4.3 Stability vs Instability

Using (4.26), (4.41) and (4.52) we obtain, for the $l = 2$ mode:

$$\lambda_{2m,t} = \left[-\frac{10}{19}\gamma + \frac{5}{19}\kappa^2 \left(\frac{Q}{4\pi}\right)^2 \frac{\kappa \sinh 2\kappa - 2\cosh 2\kappa + 2\kappa^2 + 2}{\cosh 2\kappa + \kappa^2 \cosh 2\kappa - 2\kappa \sinh 2\kappa + \kappa^2 - 1} \frac{\sinh(\kappa)}{\kappa \cosh \kappa - \sinh \kappa} \right] \lambda_{2m} \tag{4.53}$$

which is the linearized evolution problem for the $l = 2$ mode. The term in brackets can be positive or negative: in the first case, the amplitude $\lambda_{2m}(t)$ will grow exponentially fast, while in the second it will decrease exponentially fast. When increasing exponentially fast from an initial value $\lambda_{2m}(0)$, the growth will deviate the drop's shape from the spherical equilibrium shape and, eventually, nonlinearities will come into play. When the λ_{2m} modes undergo exponential drecease, the nonlinearities will decrease even faster and it is straighforward to show (see [32], [27] for the technical details) that all them can be controlled to yield asymptotic stability towards the spherical shape.

Hence, the condition for instability driven by the λ_{2m} mode is that the term in brackets in (4.53) is positive. This yields instability when

$$\frac{1}{2\gamma}\left(\frac{Q}{4\pi}\right)^2 > \frac{\cosh 2\kappa + \kappa^2 \cosh 2\kappa - 2\kappa \sinh 2\kappa + \kappa^2 - 1}{\kappa \sinh 2\kappa - 2\cosh 2\kappa + 2\kappa^2 + 2} \frac{\kappa \cosh \kappa - \sinh \kappa}{\kappa^2 \sinh(\kappa)} \tag{4.54}$$

Since we are taking, for the sake of simplicity, a drop with radius $R_0 = 1$ and a system of units such that $\varepsilon_0 = 1$, we can recognize at the left hand side (4.54) the Rayleigh's fissibility parameter

$$X = \frac{1}{2\gamma\varepsilon_0 R_0^3}\left(\frac{Q}{4\pi}\right)^2$$

Hence, the condition for instability given by (4.54) is just the condition that $X > X_{cr}$ where

$$X_{cr} = \frac{\cosh 2\kappa + \kappa^2 \cosh 2\kappa - 2\kappa \sinh 2\kappa + \kappa^2 - 1}{\kappa \sinh 2\kappa - 2\cosh 2\kappa + 2\kappa^2 + 2} \frac{\kappa \cosh \kappa - \sinh \kappa}{\kappa^2 \sinh(\kappa)} \tag{4.55}$$

We conclude then that the fact of having an electrolyte solution lowers down the critical value of Rayleigh fissibility parameter which is, in any case, larger than 0.818.

This result is in contrast with the result obtained in the previous chapter: when coupling Stokes with Poisson-Boltzmann equation in the asymptotic limit when $\kappa \to \infty$, we obtained that the critical Rayleigh fissibility parameter is increased. The result in this chapter, which is only valid for κ small (this is the condition of validity of Debye-Hückel approximation), goes in the opposite direction.

We have discussed stability based on the λ_{2m} mode. The other modes, by continuity in the parameter κ, will be stable if λ_{2m} is stable provided κ is sufficiently large (the limit of the perfect conductor is $\kappa \to \infty$ and the fact that the first unstable mode is λ_{2m} was proved in [27]). We cannot exclude that a higher mode than λ_{2m} becomes unstable, for κ sufficiently small, before λ_{2m} does. This would only lower down X_{cr} from the value given in (4.55), but the drop is still unstable for lower values than $X = 1$, which is the unstability threshold for the perfect conductor.

Bibliography

[1] Abramowitz, M. and Stegun, I. A., Handbook of mathematical functions with formulas, graphs, and mathematical tables. National Bureau of Standards Applied Mathematics Series 55. Washington, D.C. 1964.

[2] Aneshansley D., Eisner T., Spray aiming in the bombardier beetle: Photographic evidence,*Proc. Natl. Acad. Sci. USA* (1999) 97059709.

[3] Assi F, Zabow G, Jenks R, Prentiss M. Guided microfluidics by electromagnetic capillary focusing. *Appl. Phys. Lett.*80:1483-85.

[4] Atkinson, K. E., The Numerical Solution of Integral Equations of the Second Kind, Cambridge University Press (1997)

[5] Batchelor GK. Developments in microhydrodynamics. In Theoretical and Applied Mechanics, ed. W Koiter. pp. 33–55. The Netherlands: Elsevier North Holland. (1977)

[6] Beauchamp J. L., Grimm R. L.; Field-induced droplet ionization mass spectrometry,*J. Phys. Chem. B* 2003, 107, 14161.

[7] Beauchamp J. L., Grimm R. L., Dynamics of field induced droplet ionization: Time-resolved studies of distortion, jetting, and progeny formation from charged and neutral methanol droplets exposed to strong electric fields, *J. Phys. Chem. B* 2005, 109, 8244-8250

[8] Beauchamp J., Exploding Nanodroplets: Applications to Frontier Studies in Mass Spectrometry, Ion Solvation, and the Chemistry of molecular Clusters., Presentation.

[9] Beebe DJ, Mensing GA, Walker GM. Physics and applications of microfluidics in biology. *Annu. Rev. Biomed. Eng.* 4:261–86 (2002).

[10] Berge B. , Quillet C., Electrowetting: A Recent Outbreak, *Current Opinion in Colloid & Interface Science*, **6**(1):34-39 (2001).

[11] Berge B. and Peseux J., Variable focal lens controlled by an external voltage: An application of electrowetting, *Eur. Phys. J.* E 3, 159 (2000).

[12] Betelú S. I., Fontelos M. A., Kindelán U. and Vantzos O., Sigularities on charged drops, *Phys. Fluids* 18, 051706 (2006).

[13] Blake T. D. , Clarke A. and Stattersfield E. H., An Investigation of Electrostatic Assist in Dynamic Wetting, *Langmuir* 16, 2928 (2000).

[14] Blyth M., Boundary Element and Finite Element Methods Notes. University of East Anglia. Norwich, UK (2012).

[15] Brézis H., Functional Analysis, Sobolev Spaces and Partial Differential Equations. Springer, 2010.

[16] Bush J., Hu D., Walking on water: Biolocomotion at the interface, *Annu. Rev. Fluid Mech.* 11 (2005) 207-228.

[17] Canny MJ. Flow and transport in plants. *Annu. Rev. Fluid Mech.* 9:275–96 (1977)

[18] Cho S. K., Moon H., Kim C.-J, Creating, Transporting, Cutting, and Merging Liquid Droplets by Electrowetting-Based Actuation for Digital Microfluidic Circuits, *Journal of Microelectromechanical Systems*, Vol. 12, No. 1, Feb 2003.

[19] Chorin A. J. and Marsden J.E., A mathematical introduction to fluid mechanics, 3d Edition. Springer, 1980.

[20] Duft D. , Achtzehn T., Müller R., Huber B. A. andLeisner T. , Rayleigh jets from levitated microdroplets,*Nature*, vol. 421, 9 January 2003, pg. 128.

[21] Dvorak P., Labs-On-A Chip Spur multiphysics Simulations, *Medical Design*, Oct 2005.

[22] Eggers J. and Fontelos M., Singularities: Formation, Structure and Evolution preprint.

[23] Evans L. C., Partial Differential Equations (Graduate Studies in Mathematics, V. 19) GSM/19, American Mathematical Society 1998.

[24] Fernández de la Mora J., The Fluid Dynamics of Taylor Cones, *Annual Review of Fluid Mechanics*, Vol. 39 (2007), 217-243.

[25] Fontelos M. A. , Garcia-Garrido V. J., and Kindelan U., Evolution and breakup of viscous rotating drops. *SIAM J. Appl. Math.*, 71(6):1941-1964, 2011.

[26] Fontelos M. A., Kindelán U. and Vantzos O., Evolution of neutral and charged droplets in an electric field, *Phys. Fluids* 20 (2008), 092110.

[27] Fontelos M. A.,Friedman A. , Symmetry-breaking bifurcations of charged drops, *Arch. Ration. Mech. Anal.* 172,2 (2004), 267-294.

[28] Fontelos M. A., Gamboa L. B., On the structure of double layers in Poisson-Boltzmann equation, Discrete Contin. *Dyn. Syst., Ser. B* 17, No. 6, 1939-1967 (2012).

[29] Fortner N. , Shapiro B., Equilibrium and Dynamic Behavior of Micro Flows under Electrically Induced Surface Tension Actuation Forces, Proceedings of the International Conference on MEMS, NANO and Smart Systems (ICMENS'03).

[30] Friedman A., Tintarev K., Boundary asymptotics for solutions of the Poisson-Boltzmann equation, *J. Diff. Eq.* 69 (1) (1987), 15-38.

[31] Friedman A. and Reitich F., Nonlinear stability of quasi-static Stefan problem with surface tension: a continuation approach, *Ann. Scu. Norm. Super. Pisa* (4), 30 (2001), 341-403.

[32] Friedman A., Reitich F., Quasi-static motion of a capillary drop, II: the three-dimensional case, *J. Differential Equations* 186 (2002) 509–557.

[33] Garcia-Garrido V. J., The mathematical models of rotating droplets with charge or subject to electric fields Analysis and Numerical Simulation. PhD Thesis, Universidad Autónoma de Madrid, Madrid Spain (2013).

[34] Garzon M., Gray L. J., and Sethian J. A.. Numerical simulations of electrostatically driven jets from nonviscous droplets *Phys. Rev. E* 89 (2014), 033011

[35] Gheber L. A.,Ghosal S. , Glawdell T. et al. Encyclopedia of Microfluidics and Nanofluidics Vol. 1. Springer, 2008.

[36] Gilbarg D., Trudinger N. S., Elliptic Partial Differential Equations of Second Order (2nd Edition), Springer-Verlag, 2001.

[37] Griffiths D. J., Introduction to Electrodynamics. Prentice Hall, 1999.

[38] Hanzawa, E.I.: Classical solutions of the Stefan problem. *Tohoko Math. J.* (2) 33, 297–335 (1981)

[39] Happel J, Brenner H. 1965. Low Reynolds Number Hydrodynamics. Englewood Cliffs, NJ: Prentice-Hall. 553 pp.

[40] Hayes R. A. and Feenstra B. j., Video speed electronic paper based on electrowetting, *Nature*, 425, pp. 383-385 (2003)

[41] Hill E.L., The theory of vector spherical harmonics, *Amer. J. Phys.* 222 (1954) 211-214.

[42] Ho C-M, Tai Y-C., Micro-electro-mechanical systems (MEMS) and fluid flows. *Annu. Rev. Fluid Mech.* 30:579–612 (1998)

[43] Jackson J. D., Classical Electrodynamics, John Wiley & Sons, New York; 3rd edition,1999.

[44] Jain KK. Biochips and microarrays: Technology and commercial potential. Informa Pharm. Ind. Rep. London: Informa Pharmaceuticals (2000).

[45] Kuiper S. and Hendriks B. H. W., Variable-focus liquid lens for miniature cameras, *Appl. Phys. Lett.* 85, 1128 (2004).

[46] Landau L. D. and Lifshitz E. M., Fluid Mechanics. Pergamon Press, 1987.

[47] Lippmann G., Relations entre les phénomènes électriques et capillaries, *Ann. Chim. Phys.* 5, 494 (1875).

[48] Loscertales I.G. , Barrero A., Guerrero I., Cortijo R., Marquez M., Gañan-Calvo A. M., Micro/Nano Encapsulation Via Electrified Coaxial Liquid Jets, *Science*, Vol. 295, 5560 (2002), 1695-1698.

[49] MacGorman D. R., Rust W. D., The Electrical Nature of Storms, Oxford University Press, (1998)

[50] Masliyah J. H., Bhattacharjee S., Electrokinetic and Colloid Transport Phenomena, Wiley 2006.

[51] Mugele F. , Baret J. C., Electrowetting: From Basics to Applications, *J. Phys.: Condens. Matter* **17**:R705-R774 (2005).

[52] Parker A. R., Lawrence C. R., Water capture by a desert beetle, *Nature* 414 (2001) 33-34.

[53] Percin G., Khuri-Yakubb B. T., Piezoelectric droplet ejector for ink-jet printing of fluids and solid particles *American Institute of Physics.* Vol. 74,2: 1120-1127 (2003).

[54] Pozrikidis C., Boundary integral and Singularity methods for linearized viscous flow. Cambridge texts in Applied Mathematics, Cambridge University Press, 1992.

[55] Pozrikidis C., Fluid Dynamics: Theory, Computation, and Numerical Simulation 2nd. Edition, Springer, 2009.

[56] Pozrikidis C., A Practical Guide to Boundary Element Methods with the Software Library BEMLIB, Chapman & Hall, 2002.

[57] Prins M. W. J., Welters W. J. J. and Weekamp W., Fluid Control in Multichannel Structures by Electrocapillary Pressure, *Science* 291, 277 (2001)

[58] Lord Rayleigh, On the equilibrium of liquid conducting masses charged with electricity, *Philos. Mag.* 14, 184 (1882).

[59] Rubinstein I., Electro-diffusion of ions, Studies in Applied and Numerical Mathematics, *SIAM* 1987.

[60] Russel WB, Saville DA, Schowalter WR. Colloidal Dispersions. Cambridge, UK: Cambridge Univ. Press. 525 pp. (1989)

[61] Ryham R. J., Existence, uniqueness, regularity and long-term behavior for dissipative systems modeling electro-hydrodinamics, preprint.

[62] Saville D. A., Electrohydrodynamics: The Taylor-Melcher Leaky Dielectric Model, *Annual Review of Fluid Mechanics* **29**:27-64 (1997).

[63] Sethian J. A. Level Set Methods and Fast Marching Methods: Evolving Interfaces In Computational Geometry, Fluid Mechanics, Computer Vision and Materials Science. Cambridge University Press (1999)

[64] Stone HA, Kim S. Microfluidics: Basic issues, applications, and challenges. *AIChE J.* 47:1250–54 (2001)

[65] Stone H.A., Stroock A.D., Ajdari A., Engineering Flows in Small Devices: Microfluidics Toward a Lab-on-a-Chip, *Annu. Rev. Fluid Mech.* **36**:381-411 (2004).

[66] Stroock AD., Whitesides GM 2001. Flexible methods for microfluidics. *Phys. Today* 54:42–48

[67] Taylor G. I., Disintegration of water drops in an electric field, *Proc. Roy. Soc. London A* 280 (1964), 383-397.

[68] VanderWyst A.,Christlieb A., Sussman M., Boyd I. D., Level Set Simulations of Charged Droplets Using a Boundary Element Method, IEPC-2005-019 Presented at the 29-th International Electric Propulsion Conference, November 2005, Princeton University.

[69] Vantzos O., Mathematical modeling of charged liquid droplets: numerical simulation and stability analysis. MA Thesis, University of North Texas, Denton TX (2006).

[70] Voldman J, Gray ML, Schmidt MA. Microfabrication in biology and medicine. *Annu. Rev. Biomed. Eng.* 1:401–25 Jain (2000).